NTNU
Norwegian University of
Science and Technology

Assessment of Necessary Air Gap of Semi-Submersible Accounting for Simultaneous Occurrence of Wind, Wind Sea and Swell Sea

Ole Kristian Vikenes

Marine Technology
Submission date: June 2018
Supervisor: Sverre Kristian Haver, IMT

Norwegian University of Science and Technology
Department of Marine Technology

NTNU

Department of Marine Technology

Master thesis

Ole Kristian Vikenes

Trondheim, 2018

Assessment of Necessary Air Gap of Semi-Submersible Accounting for Simultaneous Occurrence of Wind, Wind Sea and Swell Sea

Background

Sufficient still water air gap is important both for fixed and floating platforms. What is a sufficient air gap according to the rules depends on the rule regime under which the platform is planned to be operating. All fixed platforms and floating platforms operating at one site for its design life time, platform design will follow the regulations provided by the Petroleum Safety Authority Norway. For floating platforms operating as drilling rigs, there is an opening in the regulations to design platform according to the maritime regulation.

In the MSc focus shall be on a given semi-submersible platform. The rigid body transfer functions are made available. The aim of the MSc is to estimate q-probability air gap, q = 10^{-2}/year and q = 10^{-4}/year, for the worst location under platform deck accounting for joint occurrence of wind, wind-sea and swell sea. A consistent estimation of q-probability air gap requires that a long term analysis is performed. The platform is to be operating in the Northern North Sea. NORA10 data for the years from September 1957 - September 2017 will be made available.

Long term response analysis can be carried out using an all sea state approach or a peak-over-threshold approach. In this master thesis focus is to be given to various interpretations of the all sea state approach. The difference between the various approaches are basically how many of all sea states that needs to be accounted for in order to obtain reasonable results. All observed sea states or merely all sea states above some threshold set for the governing weather characteristic.

Accounting for weather conditions beyond what is observed may be a challenge, the candidate should establish an approach for correcting for this if necessary. A linear response analysis can be utilized, but non-linearities in the wave crest heights shall be included in the analyses. A possibility is to utilize the approach proposed by DNVGL. The analysis can at first be done by neglecting wind speed. If time permits, one may consider to include wind in the joint modelling. As a minimum effect of wind speed shall be discussed for some few important sea states in order to indicate the error in results due to neglecting wind.

Below a possible division into sub-tasks is given.

1. Demonstrate how a short term air gap analysis is to be done accounting for simultaneous occurrence of wind sea and swell sea propagating in different directions. This should include a demonstration of how the transfer function for the air gap variable is determined. Use a JONSWAP type of wave spectrum both for wind sea and swell sea.

2. Present and discuss how the all sea states method and the all storms method can be formulated for the given problem. For the all sea states method discuss the various approaches planned to be included and demonstrate how q-probability air gap can be estimated by the various approaches.

3. For an example problem, for which an "exact" all sea states approach can be done, compare the q-probability values obtained using the various approaches suggested in point above compared to the "exact" all sea states method.

4. Do the long term analyses for the air gap variable. For one of the approaches do the long term analysis using merely total significant wave height and dominating spectral peak period as sea state characteristics. Do the analysis both for JONSWAP spectrum and Torsethaugen spectrum.

5. Investigate the effect of neglecting the direct effect wind on the air gap variable.
6. Discuss the results of various analyses of the air gap variable for q = 10^{-2}/year and q = 10^{-4}/year.
7. Present the work in a scientific report and present conclusions regarding your main findings.

The candidate may of course select another scheme as the preferred approach for solving the requested problem. He may also involve other subjects than those mentioned above if found to be important for answering the overall problem; air gap requirement for semi-submersibles.

The work may show to be more extensive than anticipated. Some topics may therefore be left out after discussion with the supervisor without any negative influence on the grading.

The candidate should in his report give a personal contribution to the solution of the problem formulated in this text. All assumptions and conclusions must be supported by mathematical models and/or references to physical effects in a logical manner. The candidate should apply all available sources to find relevant literature and information on the actual problem.

The report should be well organised and give a clear presentation of the work and all conclusions. It is important that the text is well written and that tables and figures are used to support the verbal presentation. The report should be complete, but still as short as possible.

The final report must contain this text, an acknowledgement, summary, main body, conclusions, suggestions for further work, symbol list, references and appendices. All figures, tables and equations must be identified by numbers. References should be given by author and year in the text, and presented alphabetically in the reference list. The report must be submitted in two copies unless otherwise has been agreed with the supervisor.

The candidate should give a written plan that describes the progress of the work mid-way through the MSc period. The plan can be limited to give a table of content for the MSc thesis, status regarding completion for the various chapters and what is considered the main remaining challenges. As an indication such a plan should be available by mid-April.

From the report it should be possible to identify the work carried out by the

candidate and what has been found in the available literature. It is important to give references to the original source for theories and experimental results.

The report must be signed by the candidate, include this text, appear as a paperback, and - if needed - have a separate enclosure (binder, diskette or CD-ROM) with additional material.

Supervisor: Sverre Haver

Acknowledgement

I would like to thank my supervisor, Sverre Haver, for his support during the work on this assignment. The passion for the subject and the availability for discussions, has made the work highly interesting and educational. Aker Solutions is acknowledged through Anne Katrine Bratland for providing the WAMIT output files containing the transfer functions for the semi-submersible. In addition, I am grateful that Anne Katrine has answered my questions regarding the WAMIT output files and the questions dealing with air gap analysis in general.

A special thanks goes to my wife, Iselin, for her unlimited support and understanding throughout the spring. In addition, the waiting of the arrival of our little boy the upcoming summer, has given me loads of motivation and been a healthy reminder that the master thesis is not the only thing in life.

Finally, I would express my gratitude to my fellow students at the Department of Marine Technology for their assistance and friendship. This is especially true for my comrades at the office, Anders Juul Weiby and Lars Gellein Halvorsen. Thanks for an extraordinary final year as a student in Trondheim.

Abstract

The objective of this thesis is to estimate the necessary air gap of a semi-submersible in the Northern North Sea accounting for simultaneous occurrence of wind, wind sea and swell sea. This is done by performing a linear analysis following the simplified procedure for calculating air gap as found in DNVGL-OTG-13. The non-linearities are accounted for by applying an α-factor of 1.2 in the analysis. Long term estimates for the ULS and ALS air gap are predicted using the all sea state approach (ASS) and the peak-over-threshold method (POT).

ASS considers the contributions to the extreme values from all observed sea states. Hence, the long term analysis is performed by combining the short term variability of the 3-hour maximum response described conditionally on all possible sea states with the long term joint distribution of the significant wave height, H_s, and the spectral peak period, T_p. Since the traditional all sea state approach (TASS) is highly time-consuming for more complex response problems, a modified version of the all sea state approach (MASS) is proposed as an equally accurate alternative to the traditional approach. Similar to the POT approach, the modified version only considers events above a set threshold for the most important weather characteristic, H_s. However, each sea state above the threshold is considered separately to follow the methodology of the TASS approach.

POT considers the storms above a selected threshold in the long term analysis. The extreme values are found from the established long term distribution of the largest response within an arbitrary storm. Non-observed events are accounted for by merging the conditional distribution of the largest response given the most probable largest response with the long term distribution of the most probable largest response. Inverse First Order Reliability Method (IFORM) is used to create response contours, where the maximum along the contours is taken as the q-probability response. This methodology is also proposed as a way of accounting for non-observed events for the MASS approach.

Several cases for the wave conditions are investigated: combined sea, total sea, wind sea, $\alpha = 1.2$ and 1.3, JONSWAP and Torsethaugen wave spectrum. Torsethaugen gives more conservative results than JONSWAP for the air gap problem. Combined sea, total sea and wind sea give the same results, which suggests that the swell contribution can be neglected in the analysis for the air gap problem.

The platform considered in the thesis is found to have a negative air gap in both ULS and ALS for the most critical point under the platform. Hence, the platform must be designed to withstand horizontal wave loads in deck. The MASS approach gives more conservative results than the POT approach, because statistical independence between adjacent sea states is assumed for the MASS approach.

Sammendrag

Hensikten med denne masteroppgaven er å estimere nødvendig air gap for en flytende plattform i Nordsjøen, der man tar hensyn til den samtidige påvirkningen av vind, vindsjø og dønning. Dette blir gjort ved å gjennomføre en lineær analyse som følger den forenklede prosedyren for å beregne air gap beskrevet i DNVGL-OTG-13. Ulineæriteter blir tatt hensyn til ved å benytte en α-faktor på 1.2 i analysen. Langtidsestimater for ULS og ALS air gap blir beregnet ved bruk av alle sjøtilstanders metode (ASS) og terskelmetoden (POT).

ASS tar hensyn til bidragene til ekstremverdiene fra alle observerte sjøtilstander. Dette betyr at langtidsanalysen blir gjennomført ved å kombinere korttidsvariabiliteten av 3-timers maksimal respons gitt alle mulige sjøtilstander med den koblede langtidsfordelingen av H_s og T_p. Siden den tradisjonelle alle sjøtilstanders metode (TASS) er veldig tidskrevende for komplekse responsproblemer, vil en modifisert variant av alle sjøtilstanders metode (MASS) bli foreslått som et like nøyaktig og godt alternativ som den tradisjonelle tilnærmingen. På samme måte som POT tar den modifiserte varianten bare hensyn til hendelser over en bestemt grense satt for den viktigste værkarakteristikken, H_s. Likevel vil alle sjøtilstander over grensen bli sett på hver for seg for å opprettholde fremgangsmåten i den tradisjonelle metoden.

POT ser på stormer over en bestemt grense i langtidsanalysen. Ekstremverdiene blir bestemt fra langtidsfordelingen av den største responsen i en tilfeldig storm. Ikke-observerte hendelser blir tatt hensyn til ved å sette sammen den betingede fordelingen av den største responsen gitt den mest sannsynlig største responsen med langtidsfordelingen av den mest sannsynlig største responsen. IFORM blir benyttet til å lage respons konturer, der maksimalverdiene til konturene blir satt til q-sannsynlighet responsen. Denne metoden blir også foreslått som en måte å ta hensyn til ikke-observerte hendelser for MASS metoden.

Flere tilfeller for havforholdene blir utforsket: kombinert sjø, total sjø, vin-

dsjø, $\alpha = 1.2$ and 1.3, JONSWAP og Torsethaugen bølgespekter. Torsethaugen gir mer konservative resultater enn JONSWAP for air gap problemet. Kombinert sjø, total sjø og vindsjø gir samme resultater, noe som antyder at bidragene fra dønning kan bli neglisjert i langtidsanalysen for air gap problemet.

Plattformen som blir benyttet i denne oppgaven har negativt air gap i både ULS og ALS for det mest kritiske punktet under plattformen. Derfor må plattformen designes for å kunne tåle horisontale bølgekrefter i dekket. MASS metoden gir mer konservative resultater enn POT, fordi statistisk uavhengighet mellom sammenhengende sjøtilstander er antatt for MASS metoden.

Contents

List of Figures

List of Tables

Abbreviations

ALS	Accidental limit state
ASS	All sea states approach
cdf	Cumulative density function
dof	Degree of freedom
IFORM	Inverse first-order reliability method
JONSWAP	Joint north sea wave project
LF	Low frequency
MASS	Modified all sea states approach
NCS	Norwegian continental shelf
POT	Peak over threshold
PSA	Petroleum safety authority Norway
QTF	Quadratic transfer function
RAO	Response amplitude operator
SWL	Short time average sea-level in storm
TASS	Traditional all sea states approach
ULS	Ultimate limit state
WAMIT	Computer program used to calculate transfer functions
WF	Wave frequency

Nomenclature

A	Wave amplitude
A_γ	Spectral normalizing factor
a	Air gap
a_{ALS}	Air gap in ALS
a_{ULS}	Air gap in ULS
a_0	Still water air gap
C_{3h}	3-hour maximum crest height
$C_{3hmax,mean}$	3-hour maximum crest height found at $F_{C_{3h}}(c) = 0.5$
$C_{3h,ULS}$	3-hour maximum crest height in ULS
$C_{3h,ALS}$	3-hour maximum crest height in ALS
c	Crest height
d	Water depth
d_{hor}	Horizontal distance from the center of the rotational axis out to the considered point on the semi-submersible
e	Euler number
F	Cumulative density function
$F_{C_{3h}}(c)$	cdf of the 3-hour maximum crest height
$F_{C_{3h}\|H_sT_p}(c\|h,t)$	cdf of the 3-hour maximum crest height given weather characteristics
$F_{H_s}(h)$	cdf of the marginal distribution for H_s
$F_{T_p-\epsilon\|H_s}(t-\epsilon\|h)$	cdf of the conditional distribution of $T_p - \epsilon$ given H_s

$F_U(u)$	cdf of the storm maximum upwell
$F_{U_{annualmax}}(u)$	cdf of the annual 3-hour maximum upwell
$F_{U_k\|k}(u\|k)$	cdf of the conditional distribution of the storm maximum upwell in a given storm
$F_{U_m\|k}(u\|k)$	cdf of the conditional distribution of the step maximum upwell in a given storm
$F_{U_{max}}(u)$	cdf of the 3-hour maximum upwell in an arbitrary storm
$F_{U_s\|storm}(u\|storm)$	cdf of the Gumbel distribution approximated to the exact distribution of the storm maximum upwell
$F_{U_{ss}\|seastate}(u\|seastate)$	cdf of the Gumbel distribution approximated to the exact distribution of the sea state maximum upwell
$F_{U\|\tilde{U}}(u\|\tilde{u})$	cdf of the conditional distribution of storm maximum upwell given the most probable largest storm upwell
$F_{\tilde{U}}(\tilde{u})d\tilde{u}$	cdf of the most probable largest storm upwell
$F_{X_{3h}}(x)$	cdf of the 3-hour maximum response
$F_{X_{3h}\|H_sT_p}(x\|h,t)$	cdf of the 3-hour maximum response given weather characteristics
$f_{H_s}(h)$	pdf of the marginal distribution for H_s
$f_{H_s\|T_p}(h\|t)$	pdf of the conditional distribution of T_p given H_s
$f_{H_sT_p}(h,t)$	pdf of the joint distribution of weather characteristics
$f_{\tilde{U}}(\tilde{u})d\tilde{u}$	pdf of the most probable largest storm upwell
g	Acceleration of gravity
g()	Failure boundary
H_s	Significant wave height
$H_{s,sw}$	Significant wave height for swell sea
$H_{s,tot}$	Significant wave height for total sea
$H_{s,w}$	Significant wave height for wind sea
$H_{s,3h}$	3-hour maximum significant wave height

$H(\omega;\beta)$	Transfer function
$H(\omega;\beta)_{Im}$	Imaginary part of transfer function
$H(\omega;\beta)_{Re}$	Real part of transfer function
$\|H(\omega;\beta)\|$	Response amplitude operator
K	Total number of observed storms
$K(h_i,t_j)$	Contribution to the extreme crest height from sea state i,j in the scatter diagram
k_1	Wave number
M	Number of steps in a storm
M_n	n^{th} sample moment
m_n	n^{th} spectral moment
N_s	Expected number of storms above the selected threshold per year
n_{3h}	Number of events within 3 hours
$p_f(u)$	Probability of failure
$p_{i,j}$	Probability of the sea state in row i and column j in the scatter diagram to occur
p_r	Probability of exceedance for a given return period
$p_S(s)$	Probability mass function for the Poisson distribution
$Q_{C_{3h}}(c)$	Probability of exceeding the 3-hour maximum crest height value
$Q_{C_{3h}\|H_sT_p}(c\|h,t)$	Probability of exceeding the 3-hour maximum crest height value given weather characteristics
$Q_{U_{3h}}(u)$	Probability of exceeding the 3-hour maximum upwell value
$Q_{U_{3h}\|H_sT_p}(u\|h,t)$	Probability of exceeding the 3-hour maximum upwell value given weather characteristics
q	Annual probability of exceedance
r	radius of circles in standard Gaussian space

S	Random variable of how many storms that occur within a year
$S_J(\omega)$	JONSWAP wave spectrum
$S_{PM}(\omega)$	Pierson-Moskowitz wave spectrum
S_{RR}	Total response spectrum
S_{RS}	Response spectrum for the swell sea
S_{RW}	Response spectrum for the wind sea
$S_T(\omega)$	Torsethaugen wave spectrum
$S_{\eta\eta}(\omega;\beta)$	Wave spectrum
s_1	Steepness parameter
T	Wave period
T_f	Torsethaugen boundary limit period
T_p	Spectral peak period
$T_{p,sw}$	Spectral peak period for swell sea
$T_{p,tot}$	Spectral peak period for total sea
$T_{p,w}$	Spectral peak period for wind sea
T_R	Return period
T_2	Zero up-crossing period
t_1	Mean wave period
U	Upwell - relative wave elevation
U_{ALS}	Storm maximum upwell in ALS
U_{ALS}^{WF}	Maximum wave frequency upwell in ALS
U_{LF}	Low frequency upwell
U_{mean}	Upwell due to a static mean heel angle
U_{ULS}	Storm maximum upwell in ULS
U_{ULS}^{WF}	Maximum wave frequency upwell in ULS
U_{WF}	Wave frequency upwell
U_{3h}	3-hour maximum upwell obtained from Monte Carlo Simulation

$U_{3h,mean}$	3-hour maximum upwell obtained from $F_{U_{3h}}(u) = 0.5$
$U_{3h,ULS}$	3-hour maximum upwell in ULS
$U_{3h,ULSmean}$	Mean of the 100 3-hour maximum upwell long term analysis in ULS
$U_{3h,ALS}$	3-hour maximum upwell in ALS
$\tilde{U}$	Most probable largest storm upwell
u_{crit}	Critical upwell value
u_R	Ursell number
$u_{1,2}$	Variables in the standard Gaussian space
W	Wind velocity
x,y	Horizontal coordinates
z_p	Vertical motion of the semi-submersible
α	Asymmetry factor accounting for non-Gaussian effects
α_F	Parameter in the Forristall distribution
α_{H_s}	Parameter for the 3-parameter Weibull distribution for H_s
$\alpha_{m,k}$	Gumbel parameter for step number m and storm number k
$\alpha_{T_p-\epsilon\|H_s}$	Parameter for the 2-parameter Weibull distribution for $T_p - \epsilon$ given H_s
$\alpha_{\tilde{u}}$	Parameter for the 3-parameter Weibull distribution for $\tilde{u}$
β	Incoming wave direction
β_F	Parameter in the Forristall distribution
β_{H_s}	Parameter for the 3-parameter Weibull distribution for H_s
$\beta_{m,k}$	Gumbel scale parameter for step number m and storm number k
β_s	Gumbel scale parameter in distribution of storm maximum response
$\beta_{T_p-\epsilon\|H_s}$	Parameter for the 2-parameter Weibull distribution for $T_p - \epsilon$ given H_s
$\beta_{\tilde{u}}$	Parameter for the 3-parameter Weibull distribution for $\tilde{u}$

β_v	Normalized β_s with respect to the storm most probable largest response
$\beta_{v,5\%}$	5-percentile of β_v
$\beta_{v,95\%}$	95-percentile of β_v
$\bar{\beta_v}$	Mean value of β_v
γ	Spectral peak enhancement factor
γ_{Hs}	Skewness for the sample of H_s
ϵ	Lower limit for T_p
ζ	Wave elevation
η_{3h}	Events occurring in a 3-hour period
θ	Incoming wind heading
λ_{H_s}	Parameter for the 3-parameter Weibull distribution for H_s
$\lambda_{\tilde{u}}$	Parameter for the 3-parameter Weibull distribution for $\tilde{u}$
μ_{H_s}	Mean value for the sample of H_s
$\mu_{m,k}$	Mean value of the 3-hour maximum upwell for step number m in storm number k
ρ	Poisson parameter describing the annual expected number of storms
$\sigma_{a,b}$	Spectral width parameters for the JONSWAP spectrum
σ_{H_s}	Standard deviation of the sample of H_s
$\sigma_{m,k}$	Standard deviation of the 3-hour maximum upwell for step number m in storm number k
σ_s	Spectral width parameter
σ^2	Variance
$\phi(\omega;\beta)$	Phase difference
ϕ_{LF}	Maximum angle from LF contributions
ϕ_{mean}	Maximum static mean heel angle
ω	Angular frequency
ω_p	Spectral peak frequency

Chapter 1

Introduction

1.1 Background

In December 2015 the semi-submersible, COSL Innovator, was operating at the Troll field on the Norwegian Continental Shelf (NCS). In what can be characterised as a normal winter storm, the semi-submersible was hit by a huge wave, leading to many crushed windows on the residential floor and one fatality. After this accident both class societies and engineering companies have increased the focus on the air gap in order to ensure that the platforms operating on the NCS have a sufficient air gap. In Norway there are two rule regimes deciding how the air gap shall be determined. For all fixed and floating platforms operating at one site for its design life, platform design will follow the regulations provided by the Petroleum Safety Authority Norway (PSA). However, for floating platforms operating as drilling rigs, there is an opening in the regulations to design platforms according to the maritime regulation. The rule regimes give different requirements to what is a sufficient air gap, where the PSA provides the most conservative alternative.

Air gap is defined as the distance from the water surface to the underside of the deck of the platform. This means that positive air gap ensures that the waves do not hit the the upper structure of the platform. For fixed structures the air gap can be decided single-handedly based on the extreme crest heights calculated for the given operation area. Floating platforms, on the other hand, will move along with the waves. The motion of the platform will have a positive effect on the air gap, but it is more difficult to decide what is a sufficient air gap.

The characteristic response for an offshore structure is defined by an annual

probability, q-probability, of exceedance. In the design of offshore structures there are mainly two limit states, ultimate limit state (ULS) and accidental limit state (ALS), which are used as checkpoints for the robustness of the structure related to the response problem at hand. ULS corresponds to a 100-year return period, which is the same as an annual probability of exceedance of $q = 10^{-2}$. ALS corresponds to a 10000-year return period, hence an annual probability of exceedance of $q = 10^{-4}$. To estimate ULS and ALS values that yields reliable results for the air gap, some sort of long term analysis has to be performed that takes into account all sources of inherent randomness.

1.2 Objective

The aim of the master thesis is to estimate q-probability air gap in ULS and ALS for the most critical location under the platform deck accounting for joint occurrence of wind, wind sea and swell sea. A consistent estimation of q-probability air gap requires that a long term analysis is performed. Two methods, the all sea states approach (ASS) and the peak-over-threshold approach (POT), will be used to estimate the necessary air gap. As the traditional all sea states approach (TASS) is highly time consuming for complicated response problems, modified variants of the all sea states approach (MASS) will be established and utilised in the long term analysis.

Model tests carried out on platforms operating on the NCS has been performed in total sea, where irregular waves come from one direction. The real sea system is of a combined nature, consisting of a wind sea component and one or several swell sea components. Therefore, another objective of the thesis is to see if utilising combined sea in the analysis has a significant impact on the estimated air gap. The transfer functions used to estimate the air gap are provided from earlier calculations in WAMIT, while the post-processing and long term analysis are performed in MATLAB.

1.3 Outline of thesis

Chapter 2 gives a presentation of the structure and the coordinate systems used for the semi-submersible. The environmental data from NORA10 used in the assignment are presented, including a brief look at the incoming direction of the most severe weather conditions. The definition of the polar coordinate systems in NORA10 and WAMIT is reviewed, and a storm event is defined to give input to the long term analysis using POT.

Chapter 3 goes through the procedure of calculating the air gap (upwell) as given by the simplified analysis in DNVGL-OTG-13, DNVGL (2017). An explanation of the establishment of the relevant transfer functions from WAMIT is given, with the transfer function for the relative wave elevation as the final objective. An introduction to the JONSWAP and Torsethaugen wave spectra is given, along with the process of establishing the response spectrum. In addition a short term analysis is explained and exemplified for the upwell problem. Finally, an introduction to the two main methods used in the the long term analysis is provided.

Chapter 4 gives an introduction to the all sea states approach. Both the methodology of the TASS approach and the MASS approach are reviewed step by step . For a simple response problem, the crest height, both methods are performed. The results are compared and the validity of the MASS approach is evaluated. In addition, a threshold sensitivity study for the modified method is performed.

Chapter 5 is where the MASS approach and the POT approach is used to perform long term analyses accounting for observed events. A closer introduction to the POT approach is given. Finally, a threshold sensitivity study is performed for the upwell problem.

Chapter 6 accounts for non-observed events in the long term analysis of the MASS approach and the POT approach. A similar approach as used in the POT analysis is suggested for the MASS approach.

Chapter 7 covers the Metocean contour line approach. The methodology is presented, and estimates for the ULS and ALS upwell are found. In the end, the results found from the MASS approach and the POT approach are used to decide what percentile levels they correspond to for ULS and ALS.

Chapter 8 includes the contribution from low frequency motions and the static mean heel angle.

Chapter 9 is devoted to comparison of the results obtained for the different methods. Air gap estimates for ULS and ALS are given.

Chapter 10 and 11 give some concluding remarks and proposes suggestions for further work.

Chapter 2

Structure and environmental data

2.1 Description of structure

The semi-submersible considered in this assignment is the Midgard platform. Even though the platform was never built, model tests were performed in order to evaluate the motion characteristics. Together with the results obtained from analyzes performed in WAMIT, this builds a solid foundation for investigating different aspects of the platform. The main dimensions are shown in Table 2.1.

Table 2.1: Main dimensions of the platform

Length Platform	$L_{platform}$	80.65m
Width Platform	$W_{platform}$	80.65m
Width Column	W_{column}	17.2m
Operating displacement	M_{op}	50216t
Still water air gap	a_0	20m

The platform has four quadratic columns supporting the deck. They are placed in each corner as shown in Figure 2.1. The pontoons combine all the columns and form a quadratic ring.

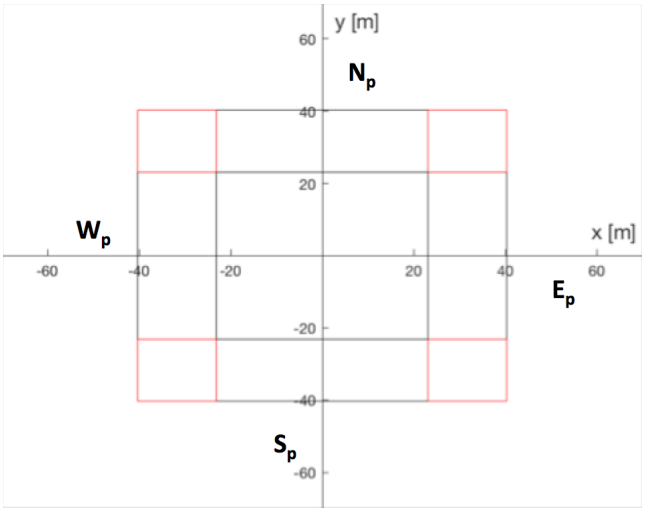

Figure 2.1: Dimensions and definition of the internal coordinate system of the semi-submersible

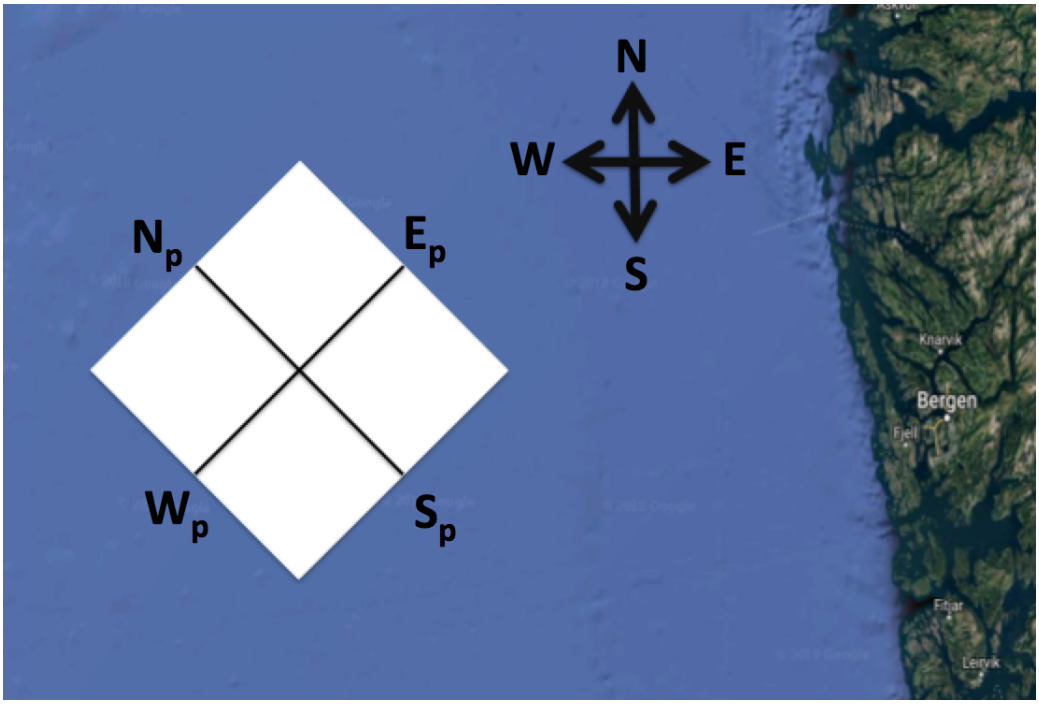

Figure 2.2: Heading of the semi-submersible compared to the geographic coordinate system

The platform's internal coordinate system is defined in Figure 2.1, while the assumed operating heading compared to the earth-fixed coordinate system is visualized in Figure 2.2. This means that the geographic north corresponds to the platforms northeastern corner.

2.2 Environmental data

The importance of good quality data is essential in the design of offshore structures in order to estimate reliable extreme loads and responses. In this assignment the NORA10 hindcast provides the governing environmental data given for the location (60°79'N,3°56'E) at the Troll field on the NCS, (Reistad et al., 2007). The hindcast contains weather characteristics for every 3-hour sea state from 1957-2017. For each sea state the significant wave height, H_s, the spectral peak period, T_p, and the incoming direction of the weather, β, are given for total-, wind- and swell sea. In addition, the wind velocity, W, for different heights above sea level are given together with the corresponding wind heading, θ.

2.2.1 Total- and combined sea

The waves in the ocean are of a combined nature. They consist of a wind sea component and one or several swell sea components. In NORA10 the different swell contributions are merged to one main swell sea component. The swell sea is a result of old storms that have happened at locations far away. It is characterised by relatively low sea states with long wave periods. The wind generated sea is created by the wind from the storm at the actual location. This sea state is characterised by steeper and higher sea states. The term combined sea is in this thesis defined as when swell sea and wind sea are considered separately with regard to H_s, T_p and β. This means that for a given response problem the response is calculated for the swell and wind case separately, before the total response is found by superposition of the two solutions (given linear analysis).

Total sea on the other hand, considers both swell and wind sea as one unit propagating in the same direction, with $T_{p,tot} = T_{p,w}$ and $H_{s,tot} = \sqrt{H_{s,w}^2 + H_{s,sw}^2}$. As $T_{p,w}$ is considered for total sea, it is obvious that it is assumed that wind sea is the dominating contribution to the total sea, even though swell sea might be dominating in some sea states.

2.2.2 Randomize T_p

A closer look at the hindcast data reveals that T_p is given in discrete classes. The reason for this is that T_p is archived as a logarithmic value with one decimal in order to save storage space. As an example the T_p values in the range 15,64 - 17,12, which corresponds to the logarithmic numbers 2,75 - 2,84, are stored as the discrete $\ln(T_p)$ value 2,8. In reality T_p is of a random nature. Hence, gathering T_p into discrete classes gives a wrong picture of the real situation. Therefore, in order to have data that are consistent with reality, T_p has to be randomized. A correction procedure is proposed by Statoil, (Andersen, 2009). The original and the randomized observations are shown in Figure 2.3.

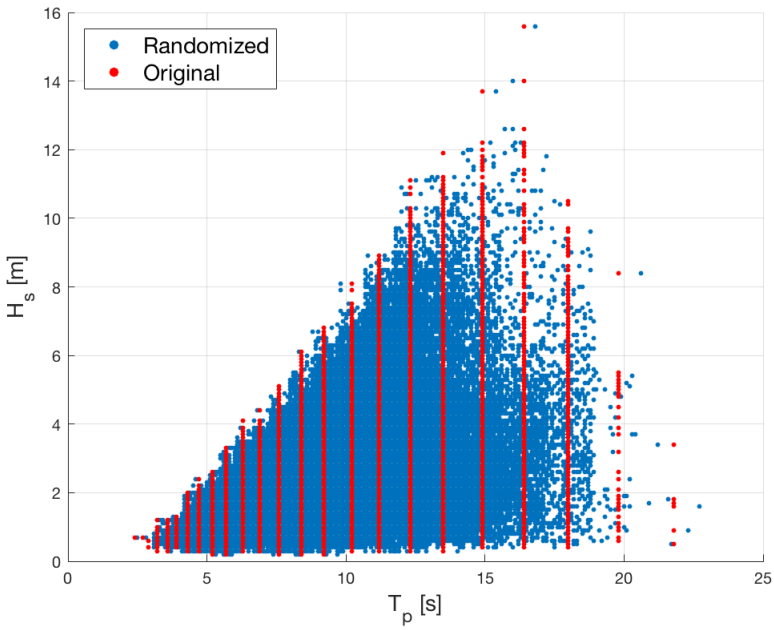

Figure 2.3: Original vs randomized observations

The new randomized T_p values are used together with the corresponding H_s values to create a scatter diagram that contains information on how many sea states that have occurred within a specific class of H_s and T_p. The increments used are $\delta_{H_s} = 0.5m$ and $\delta_{T_p} = 1s$. The scatter diagram is found in Appendix A.

2.2.3 Definition of incoming direction of waves

The definition of the polar coordinate systems used in NORA10 and WAMIT are shown in Figure 2.4. NORA10 relates to the earth-fixed coordinate system, while WAMIT uses the internal coordinate system of the platform. NORA10 follows the meteorological definition with 0 in the geographical north and increasing degrees in the clockwise direction. WAMIT defines 0 for the platform east with increasing degrees in the counter clockwise direction. Another difference is that the wave direction given in the NORA10 hindcast is the direction that the incoming wave comes from, while the data provided by WAMIT are given for the direction the wave propagates towards. As shown in Figure 2.4 a wave heading of $\beta_{NORA10} = 195°$ given in NORA10 should be connected to the data for $\beta_{WAMIT} = 30°$ in WAMIT. Unless specified, β corresponds to β_{NORA10} in the thesis.

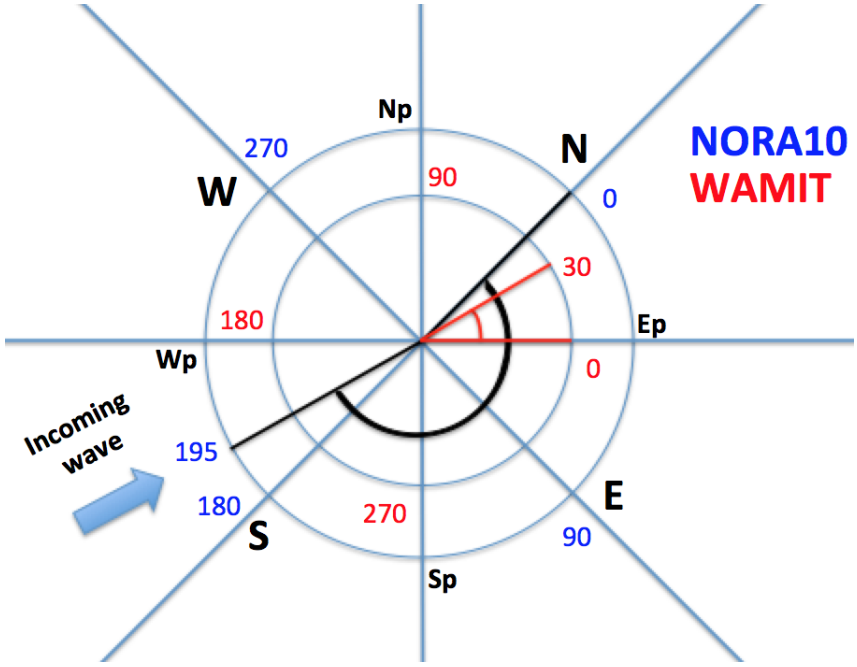

Figure 2.4: Definition of wave direction in NORA10 and WAMIT

2.2.4 Direction of the most critical sea states

The incoming direction of the highest sea states for total sea, where only sea states with H_s larger than 8m are included, are shown in Figure 2.5. The sea states are separated into 8 corridors of 45° each. The highest sea states come from the west, while there are most sea states with an incoming direction from the south.

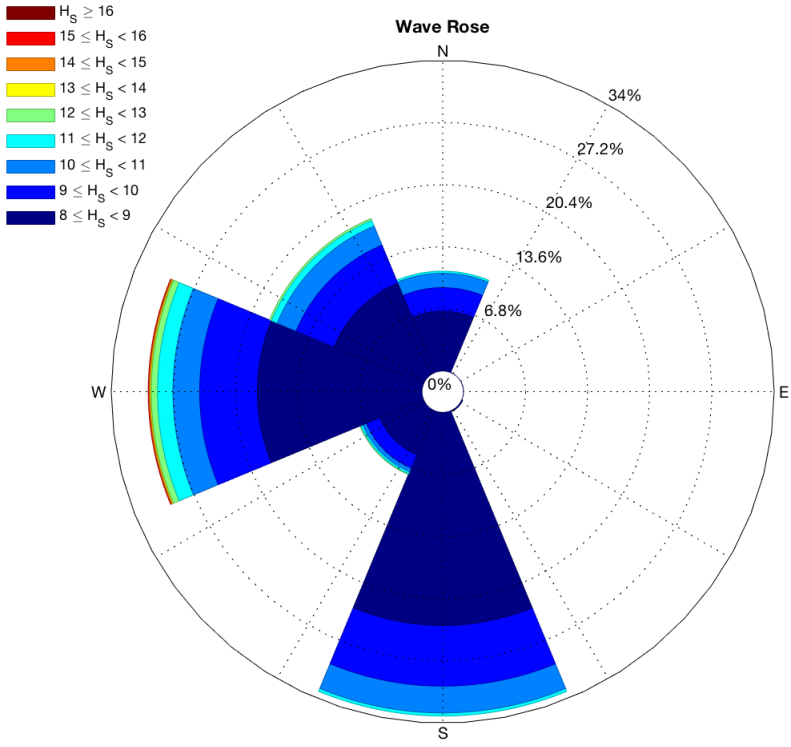

Figure 2.5: Direction of incoming total sea for sea states with $H_{s,tot} \geq 8$m.

Figure 2.6 and 2.7 show the incoming direction for the wind and swell sea, respectively, for the same sea states as considered for total sea in Figure 2.5. The wind sea mainly comes from the south and the west. The largest wind generated sea states comes from the west, while smaller and steeper sea states dominate from the south. Most of the swell sea comes from a southwestern direction. Still, the largest swell contributions come from the west, from storms in the Atlantic Ocean. As expected there are negligible

contributions from the east, due to the short open water distance from shore.

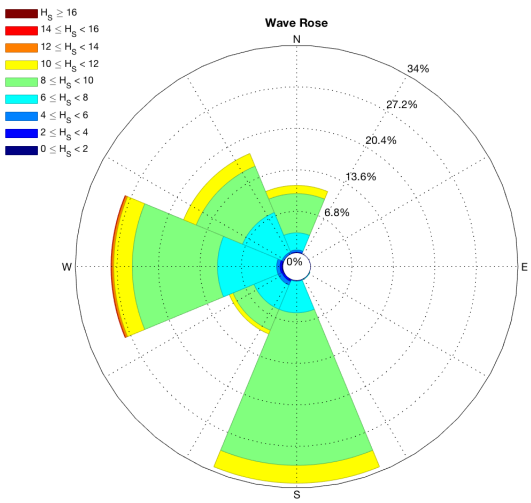

Figure 2.6: Direction of incoming wind sea for sea states with $H_{s,tot} \geq 8$m.

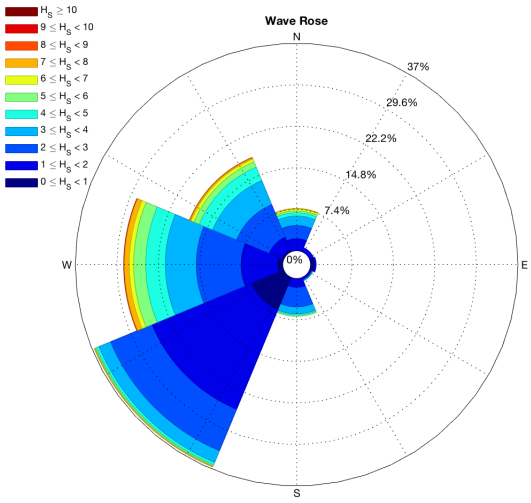

Figure 2.7: Direction of incoming swell sea for sea states with $H_{s,tot} \geq 8$m.

2.2.5 Definition of storm event

The POT approach deals with storms, hence a storm event has to be defined. A storm consists of one or several adjacent sea states that exceed a given threshold set for the most important weather characteristic considered, which in this assignment is assumed to be H_s. Normally this threshold is set quite high to only include the most severe storms in the estimation of the extreme design conditions. A storm can last for several days with varying intensity. A consequence of this is that some 3-hour sea states might fall under the threshold for H_s. Even though the storm should be considered as one ongoing event, the sea states below the threshold separates the storm into several smaller storm events. These shorter storm events are naturally highly correlated. As one of the main assumptions used in the POT approach is statistical independence between storms, adjacent shorter storm events should be merged to form one large storm event. Sandbakken (2016) suggests that two consecutive storms with a time window less than 24 hours between them should be merged to one storm event. An example of this is shown in Figure 2.8.

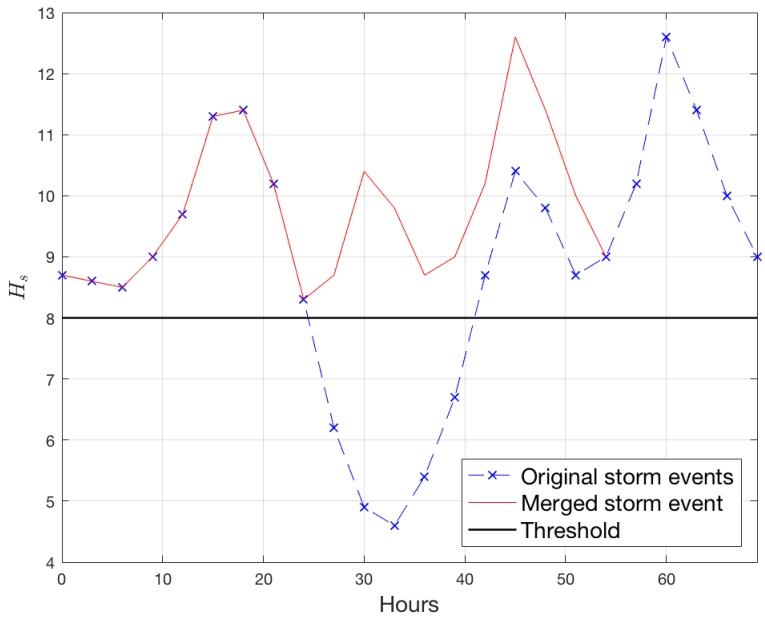

Figure 2.8: Two consecutive storms are merged into one storm event by erasing the sea states between the two events that are lower than the threshold at $H_s = 8$m.

The hindcast provided from NORA10 defines 280 storm events when a threshold at $H_s = 8$m is used. Merging the consecutive storms reduces the number of storm events to 262, which will be used in the POT analysis when the threshold is set to $H_s = 8$m.

Chapter 3

Calculation of upwell and air gap

The platform considered in this thesis is a semi-submersible, which is also known as a column stabilised unit. The method used for the calculation of air gap is based on the simplified analysis procedure for column stabilised units, described in DNVGL-OTG-13, (DNVGL, 2017).

When the semi-submersible floats in still water (no waves), the distance from the SWL to the underside of the deck is called the still water air gap, a_0. This is the air gap that has to be designed sufficiently large for the semi-submersible to avoid wave impact. Introducing waves causes vertical motions, z_p, for the semi-submersible. The difference between the wave surface and the semi submersible's mean water line, the relative wave elevation, is called upwell, as given in Eq. (3.1).

$$U(x, y, t) = \zeta(x, y, t) - z_p(x, y, t) \tag{3.1}$$

Air gap is the vertical distance from the underside of the deck, $a_0 + z_p$, to the wave surface elevation ζ, as per Eq. (3.2). The definition of the relevant quantities for the air gap calculation is shown in Figure 3.1.

$$a(x, y, t) = (a_0(x, y) + z_p(x, y, t)) - \zeta(x, y, t) = a_0(x, y) - U(x, y, t) \tag{3.2}$$

As seen from Eq. (3.2), both z_p and ζ has to be known for a given point under the platform at a given time in order to calculate the instantaneous air

gap at the given point. As a_0 is given from weight/buoyancy considerations and is independent of time, the emphasis in the air gap calculations is given to U. Since the objective is to find the minimum air gap for different limit states, a corresponding approach will be to find the maximum upwell for the equivalent limit states. Therefore the procedure in DNVGL-OTG-13 considers U in the analysis instead of a.

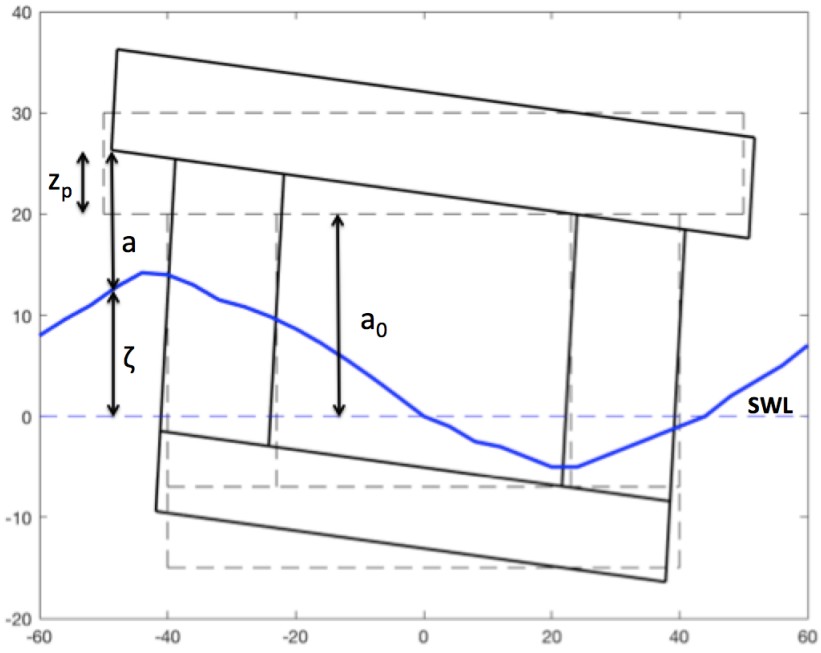

Figure 3.1: Definition of quantities used in the air gap calculation

In the simplified analysis three important contributions to U are considered:

- wave frequency (WF) upwell U_{WF}
- low frequency (LF) upwell U_{LF}
- mean upwell due to a static mean inclination of the floater U_{mean}

The WF upwell is the most important contribution to the total upwell, and is therefore the main focus in both this chapter and the following long term analyses. If not specified, U will in the following chapters correspond to U_{WF}. The LF contributions, especially from wind, will be discussed and quantified later in the thesis. The reason that LF wind is not included as

part of the main analysis, is that the transfer functions provided by WAMIT only deals with the WF range. The mean upwell due to a static mean heel angle is also accounted for in the end when the estimated upwell results are presented. The effect of current is assumed to be of little importance for the air gap problem and has been neglected. Run-up is not considered for this analysis, hence the results for locations closer than 0.2 W_{column} from vertical column walls, will not be representative estimates for the upwell, (DNVGL, 2017).

3.1 Relative wave elevation - U_{WF}

The undisturbed incoming wave field is changed due to the presence of the platform. For a column stabilised unit this is mainly due to diffraction and radiation. As a consequence of the large area of the columns, especially diffraction plays an important role for the wave field which occurs around and under the platform. To account for the diffraction effect, transfer functions for the diffracted wave field are provided from WAMIT for different locations around and under the platform. However, these only contain the linear diffraction contribution to the wave surface elevation. In addition the real wave elevation has non-Gaussian contributions with a steeper and higher crest, and a wider trough. To account for important non-linear diffraction contributions and non-linearities in the wave process, an asymmetry factor, α, is introduced. In DNVGL-OTG-13 it is recommended that α is set to 1.2 for the whole platform, while it might be necessary in some cases to raise it to 1.3 along the outer edge of the deck box in the up-wave direction, (DNVGL, 2017). The asymmetry factor is introduced for the wave elevation as shown in Eq. (3.3).

$$\zeta = \zeta^{(L)} + \zeta^{(NL)} = \alpha\zeta^{(L)} \tag{3.3}$$

The asymmetry factor is used to account for non-linear effects for total and wind sea. Due to the long periods, swell sea is assumed to have negligible non-linear effects. Therefore, the asymmetry factor is not utilised in the swell sea case. **It is important to notice that including the α-factor will only give correct results for the extreme values**. Since the main objective of the assignment is to establish ULS and ALS estimates, this demand is fulfilled.

The vertical motion of the platform in a given horizontal position is described by the combined heave, roll and pitch motion as given in Eq. (3.4).

$$z_p(x, y, t) = \xi_3(t) + y\xi_4(t) - x\xi_5(t) \tag{3.4}$$

This is the combined vertical motion excited in the WF range for a given horizontal position on the platform at a given time. When the wave elevation and the vertical motion is found, U_{WF} can be calculated from Eq. (3.1).

3.2 Transfer functions from WAMIT

A transfer function describes how the response behaves given an input with unit amplitude. In a frequency domain analysis, spectra are often used to describe both the input acting on the system and the response of the system, accounting for the irregularity of the process. The transfer function, $H(\omega;\beta)$, for a given wave period and wave heading, can be found from the complex components as shown in Eq. (3.5).

$$H(\omega;\beta) = H(\omega;\beta)_{Re} + iH(\omega;\beta)_{Im} \tag{3.5}$$

From Eq. (3.6) the magnitude (RAO) and the phase can be found.

$$\begin{aligned} |H(\omega;\beta)| &= \sqrt{H(\omega;\beta)_{Re}^2 + H(\omega;\beta)_{Im}^2} \\ \phi(\omega;\beta) &= atan\left[\frac{H(\omega;\beta)_{Im}}{H(\omega;\beta)_{Re}}\right] \end{aligned} \tag{3.6}$$

The main objective is to establish the transfer functions describing the relation between the undisturbed incoming waves and the upwell. However, to obtain these transfer functions several steps have to be accounted for to form the final transfer function. These steps are described in detail in the following.

3.2.1 Diffracted wave field

When the waves approach the semi-submersible, the semi-submersibles presence will disturb the incoming waves. This interaction is called diffraction, and leads to a diffracted wave field where the waves may be larger or smaller than the incoming undisturbed waves. The magnification differs for the locations under the semi-submersible, and has to be accounted for in the further analysis. Therefore a linear diffraction/radiation analysis has been

performed in WAMIT by Aker, and the results are provided to be used in this analysis, (Aker Solutions, 2018). Transfer functions for the diffracted wave field for 612 field points around and under the platform are calculated. For each field point 16 different wave headings with a difference 22.5° are considered. In addition, for each field point and each wave heading, the transfer functions are calculated for 57 wave periods between 2 and 40 seconds. Each output includes the quantities given in Table 3.1, (WAMIT, 2016).

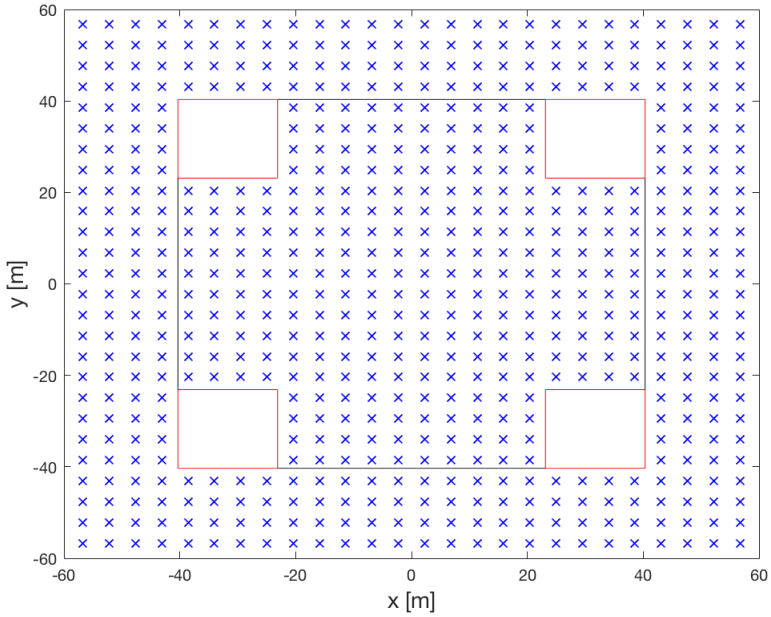

Figure 3.2: The grid used in the WAMIT analysis is shown together with the semi-submersible's dimensions.

Table 3.1: Quantities given in the WAMIT output file for the diffracted wave field

Wave period	Wave heading	Field Point
0.825000E+01	0.202500E+03	208

Magnitude	Phase	Real	Imaginary
9.318252E-01	-7.698200E+01	2.099002E-01	-9.078767E-01

Field point is the point number considered in the grid system in WAMIT.

Magnitude and Phase are the quantities given in Eq. (3.6), Real and Imaginary are the complex parts of the transfer function, as shown in Eq. (3.5). Figure 3.2 shows that each field point is connected with a x- and y-coordinate, covering the important areas around and under the semi-submersible. The relevant field points considered in the long term analysis and the most critical location under the platform with regard to air gap are shown in Figure 3.3.

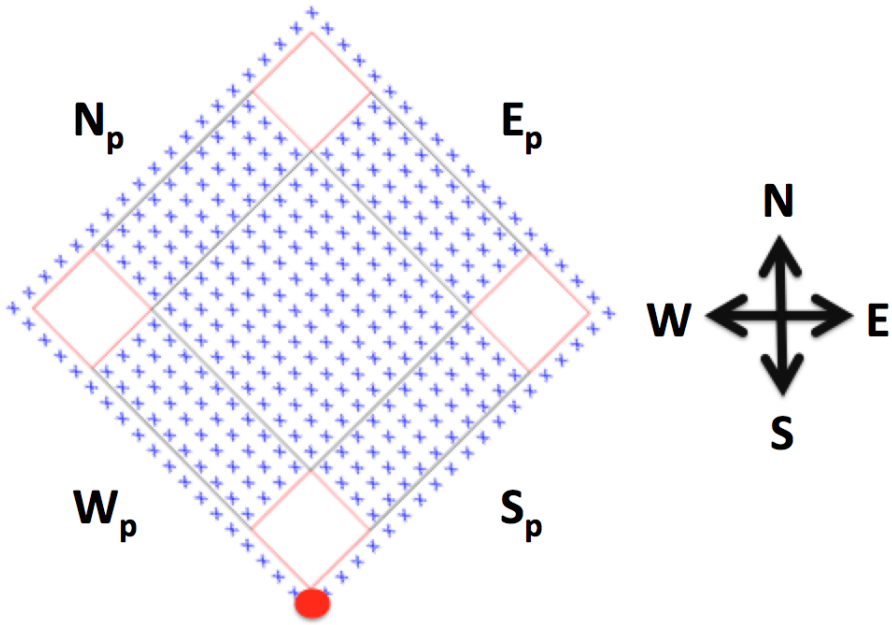

Figure 3.3: The field points considered in the upwell analysis are visualized together with the heading of the platform in the geographical coordinate system. The most critical location with regard to upwell is located in the southwestern corner of the platform, corresponding to the geographical south.

The transfer function $H(\omega;\beta)^{(LDiffWave)}$ describe the connection between the undisturbed incoming wave and the diffracted wave field. However, the transfer functions produced by WAMIT only take into account the linear diffraction contribution, neglecting the non-linear diffraction contributions. In order to include the non-linear diffraction contribution and the asymmetry of the real non-linear waves, an asymmetry factor, α, is introduced. α is multiplied with the real and imaginary parts of the transfer function separately, as shown in Eq. (3.7). As mentioned earlier, α is set to 1.2 for

total and wind sea, while α is set to 1.0 for swell sea.

$$\begin{aligned} H(\omega;\beta)_{Re}^{(NLDiffWave)} &= \alpha H(\omega;\beta)_{Re}^{(LDiffWave)} \\ H(\omega;\beta)_{Im}^{(NLDiffWave)} &= \alpha H(\omega;\beta)_{Im}^{(LDiffWave)} \end{aligned} \tag{3.7}$$

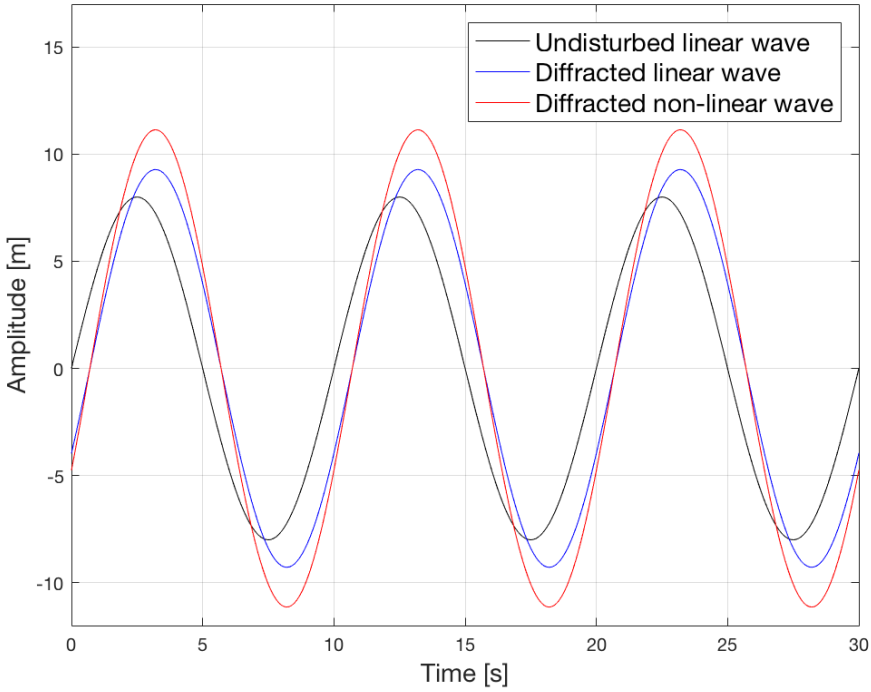

Figure 3.4: The undisturbed linear wave is shown together with the linear and non-linear diffracted waves for a regular wave with T = 10s, $\beta = 180°$ and A = 8m. The southwest corner of the semi-submersible is considered.

The wave elevation accounting for diffraction and non-linear effects can be calculated as $\zeta^{NL} = |H(\omega;\beta)^{(NLDiffWave)}|\ \zeta^{L}$, where ζ^{L} is the undisturbed incoming long-crested wave. This can be done for different locations around and under the semi-submersible. An example is shown in Figure 3.4 where a regular wave shows the difference between the linear undisturbed wave, the linear and the non-linear diffracted wave. The non-linear diffracted wave is steeper and higher in this case. It is also noticed that the non-linear asymmetry of real waves, a wider trough and a steeper crest, is not represented. However, the steeper crest that dominates in the estimation

of extreme response is well captured. Therefore, as discussed in section 3.1, including α only gives correct results for the extreme values.

3.2.2 Vertical motion of the semi-submersible

The output file from WAMIT describing the transfer functions for the motions in the 6 degrees of freedoms, dofs, includes the quantities given in Table 3.2, (WAMIT, 2016). The transfer functions are given for the COG of the semi-submersible, covering the same wave periods and wave headings as for the diffracted wave field.

Table 3.2: Quantities given in the WAMIT output file for the motions in the 6 dofs.

Wave period	Wave heading	dof
0.120000E+02	0.180000E+03	3

Magnitude	Phase	Real	Imaginary
5.583491E-01	-7.330601E+00	5.537854E-01	-7.124218E-02

The vertical motion of an arbitrary point on the semi-submersible is dependent on the heave, roll and pitch motion as given in Eq. (3.4). When the transfer functions for the motions are given in complex quantities, the combined transfer function for the vertical motion is simply found by adding the real part and the imaginary part separately as given in Eq. (3.8).

$$\begin{aligned} H(\omega;\beta)_{Re}^{(Motion)} &= H(\omega;\beta)_{Re,3} + yH(\omega;\beta)_{Re,4} - xH(\omega;\beta)_{Re,5} \\ H(\omega;\beta)_{Im}^{(Motion)} &= H(\omega;\beta)_{Im,3} + yH(\omega;\beta)_{Im,4} - xH(\omega;\beta)_{Im,5} \end{aligned} \tag{3.8}$$

The heave motion and the total vertical motion accounting for roll and pitch are compared to the undisturbed incoming wave in Figure 3.5. When only heave is considered, the vertical motion of the platform is relatively small compared to the incoming wave. Keeping in mind that a location at the southwestern corner of the platform is considered, the roll and pitch contributions should have a considerable effect on the vertical motion. This is also the case, as the total vertical motion almost has the same amplitude as the undisturbed incoming wave. The phase difference is somewhat increased.

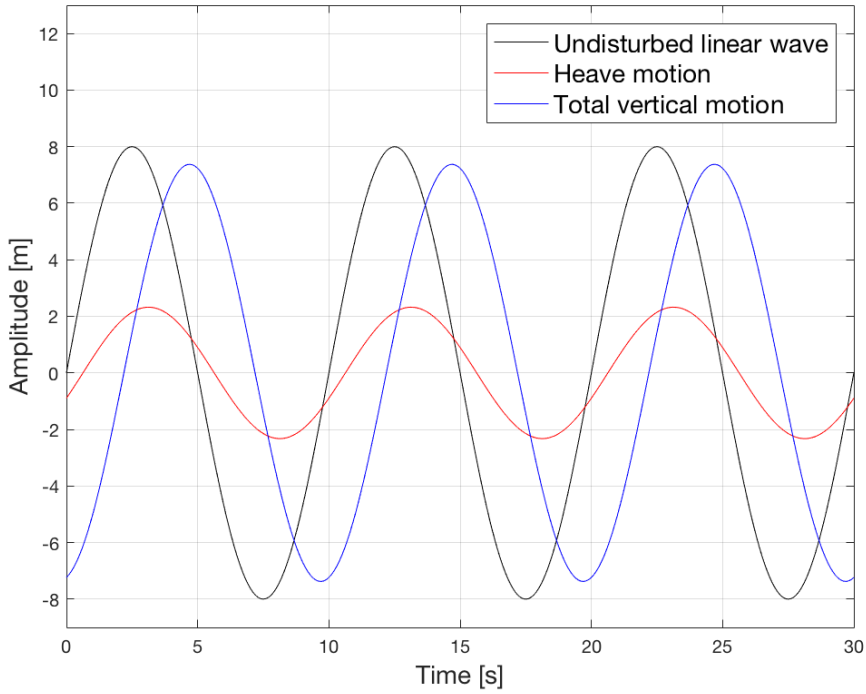

Figure 3.5: The incoming wave is shown together with the heave motion and the total vertical motion for a regular wave with T = 10s, $\beta = 180°$ and A = 8m. The southwestern corner of the semi-submersible is considered.

The positive effect that the vertical motion of the platform has on the air gap is visualized in Figure 3.6. For an incoming wave along the positive x-axis, the platform in position (a) takes advantage of the heave motion to rise with the wave, avoiding wave impact under the center of the platform. As the wave propagates towards the last column in position (b), the platform lowers the front and lifts the back. As a new wave approaches in position (c), the platform starts to rise at the front. Therefore, the platform is capable of lifting the front in position (d) to avoid horizontal wave impact in the front of the upper deck. This simple example shows that the motions of the floating platforms have a positive effect, since they are able to follow the waves. This means that they in principle can have smaller air gap than fixed platforms.

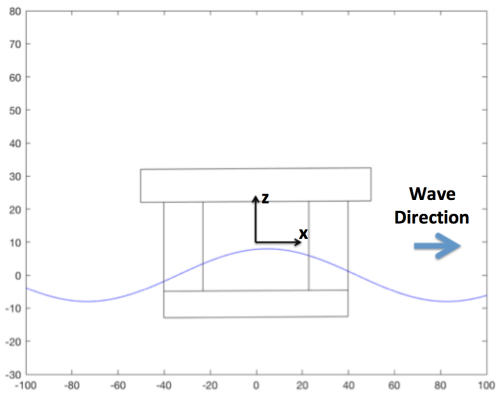

(a)

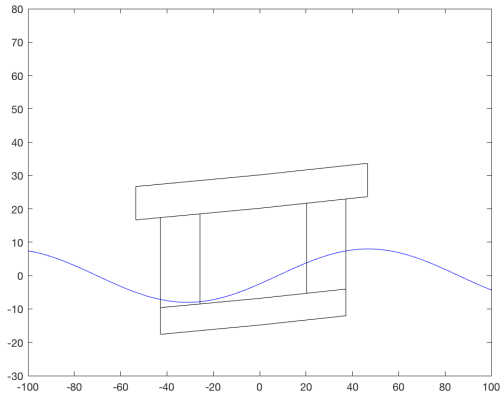

(b)

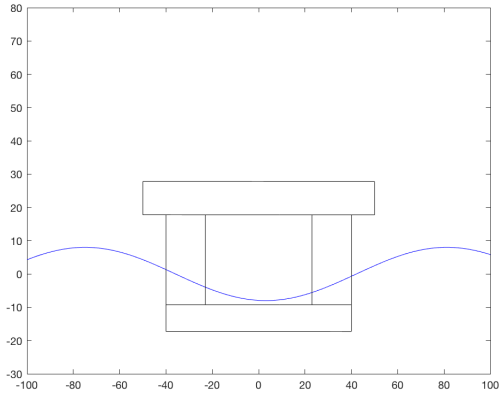

(c)

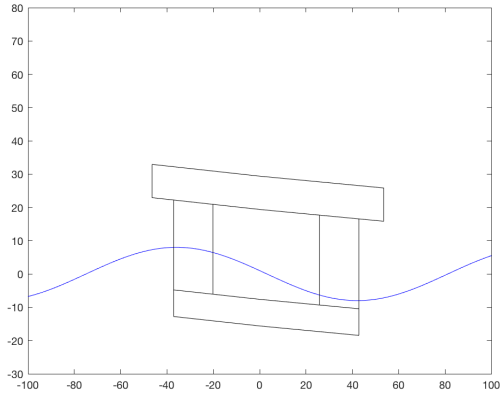

(d)

Figure 3.6: Vertical motion (combined heave and pitch) of the semi-submersible with an incoming wave propagating in the positive x-axis, T = 10s and A = 8m.

3.2.3 Relative wave elevation - upwell

The transfer function for the relative wave elevation, upwell, is found by subtracting the vertical motion from the diffracted wave elevation for the real and imaginary part separately, as given in Eq. (3.9).

$$\begin{aligned} H_{\zeta R}(\omega;\beta)_{Re}^{(Relative)} &= H(\omega;\beta)_{Re}^{(NLDiffWave)} - H(\omega;\beta)_{Re}^{(Motion)} \\ H_{\zeta R}(\omega;\beta)_{Im}^{(Relative)} &= H(\omega;\beta)_{Im}^{(NLDiffWave)} - H(\omega;\beta)_{Im}^{(Motion)} \end{aligned} \tag{3.9}$$

The magnitude and phase of the transfer function for the relative wave elevation can then be found from Eq. (3.6). In Figure 3.7 a steep wave with T = 10s and A = 8m is shown with the diffracted wave, the vertical motion and the relative motion. The vertical motion is large, almost following the amplitude of the diffracted non-linear wave. However, the short wave period leads to a phase shift for the vertical motion, because the platform are not able to react fast enough to the incoming waves. Therefore, the relative wave elevation becomes large.

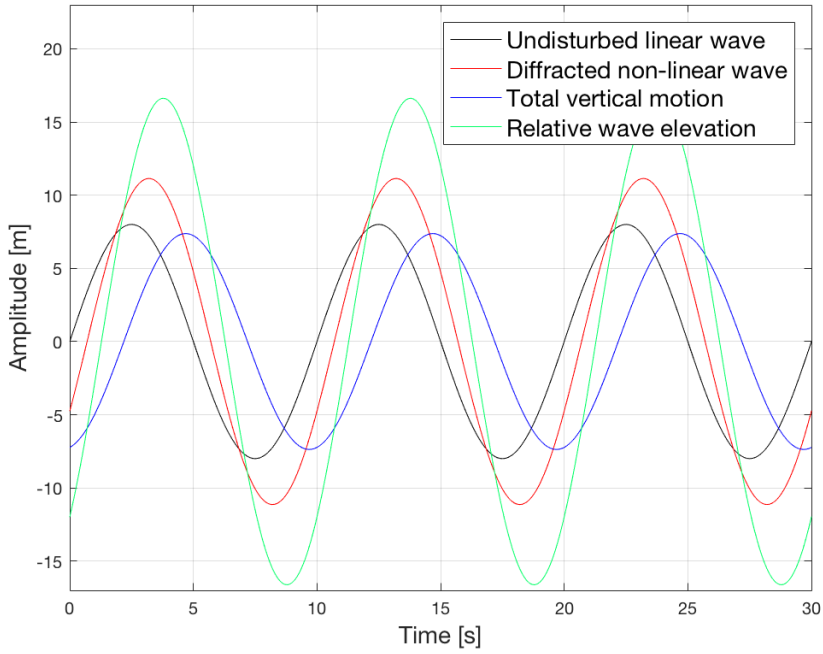

Figure 3.7: The incoming wave is shown together with the diffracted non-linear wave, the total vertical motion and the relative wave elevation (up-well) for a regular wave with T = 10s, $\beta = 180°$ and A = 8m at the southwest corner of the semi-submersible.

The transfer functions for the diffracted wave field ($\alpha = 1.2$), the vertical motion and the relative wave elevation are shown for the southwestern corner of the platform in Figure 3.8. For lower periods the relative wave elevation has large variations, which might be unphysical and give larger results than obtained in reality, because model tests will tend to flat out the response in this area, (Haver, 2018). However, further investigations of this subject is not considered in this assignment.

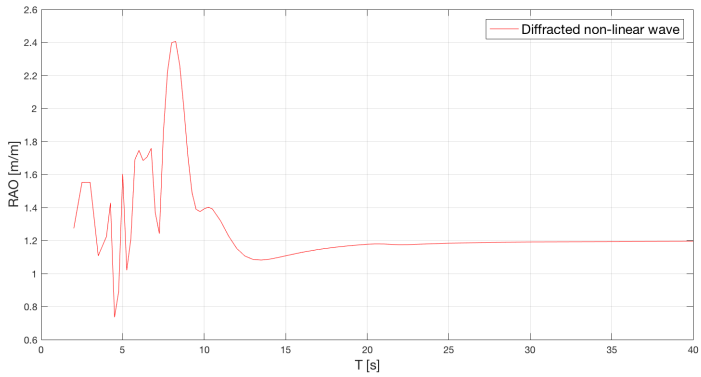

(a) Diffracted non-linear wave

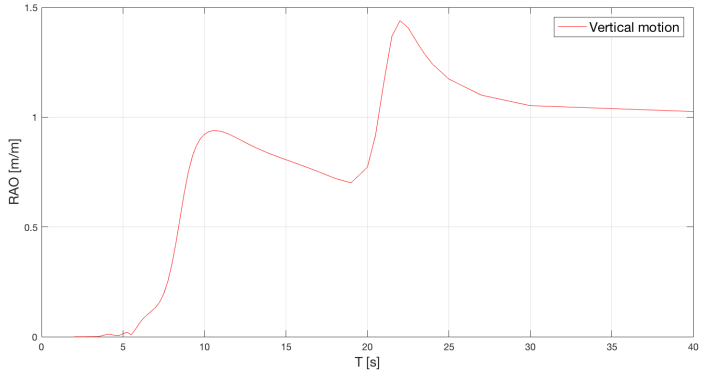

(b) Vertical motion

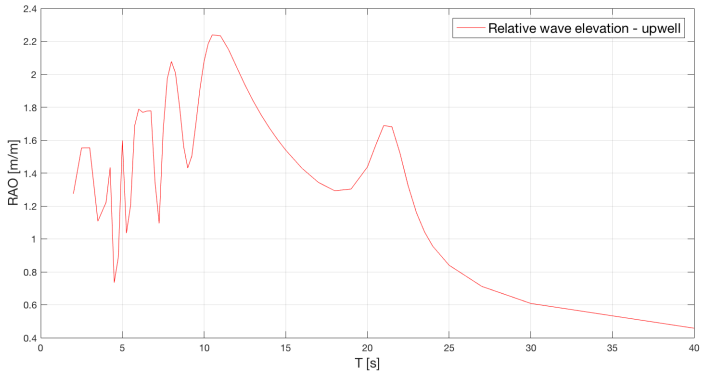

(c) Relative wave elevation - upwell

Figure 3.8: Transfer functions are provided for the most critical location under the platform with incoming sea from the geographic south.

3.3 Wave spectrum

A sea state is normally described by the statistical properties H_s and T_p. The sea surface elevation process is of an irregular nature, conveniently described by a wave spectrum. A wave spectrum contains information on how much energy that is distributed on the different wave frequencies in the sea state. In order to perform a stochastic response analysis, a proper wave spectrum is needed to describe the wave conditions. On the NCS there are mainly three spectra used, Pierson-Moskowitz, JONSWAP and Torsethaugen. The two latter spectra are outlined in the following.

3.3.1 JONSWAP

Through the Joint North Sea WAve Project, Hasselmann et al. (1973) established a one-peaked wave spectrum called JONSWAP. Utilising the variant given in DNVGL-RP-C205, the spectrum has five parameters, γ, σ_a, σ_b, A_γ and ωp. The formulation of the spectrum is given in Eq. (3.10), (DNVGL, 2014).

$$S_J(\omega) = \frac{5}{16} H_s^2 \omega_p^4 \omega^{-5} exp\left(-\frac{5}{4}\left(\frac{\omega}{\omega_p}\right)^{-4}\right) A_\gamma \gamma^{exp\left(-0.5\left(\frac{\omega-\omega_p}{\sigma_s \cdot \omega_p}\right)^2\right)} \tag{3.10}$$

The spectral width parameter, σ_s, is given as σ_a or σ_b dependent on whether the considered frequency is smaller or higher than the spectral peak frequency, ω_p. The respective values for σ_s are found from Eq. (3.11).

$$\begin{aligned} \sigma_s &= \sigma_a = 0.07, \quad \omega \leq \omega_p \\ \sigma_s &= \sigma_b = 0.09, \quad \omega > \omega_p \end{aligned} \tag{3.11}$$

The normalizing factor is given by $A_\gamma = 1 - 0.287ln(\gamma)$, while the peak enhancement factor, γ, can be computed from Eq. (3.12), (Torsethaugen et al., 2004).

$$\gamma = 42.2\left(\frac{2\pi H_s}{g T_p}\right)^{\frac{6}{7}} \tag{3.12}$$

Where γ has a value from 1 to 7. Eq. (3.12) is devoted to wind sea. Therefore, the swell sea is in this thesis assumed to have $\gamma = 1$, which

means that the JONSWAP spectrum reduces to the well known Pierson-Moskowitz spectrum as shown in Eq. (3.13). The importance of varying γ for swell sea should be investigated further.

$$S_{PM}(\omega) = \frac{5}{16} H_s^2 \omega_p^4 \omega^{-5} exp\left(-\frac{5}{4}\left(\frac{\omega}{\omega_p}\right)^{-4}\right) \tag{3.13}$$

Since the JONSWAP spectrum is based on experiments in growing wind seas, the spectrum is considered to be a good model for the wind generated sea in the JONSWAP area, defined by Eq. 3.14.

$$3.6\sqrt{H_s} \leq T_p \leq 5\sqrt{H_s} \tag{3.14}$$

Typical JONSWAP spectra for the wind sea and swell sea are plotted together in Figure 3.9. As expected the energy is distributed on different wave periods for the two cases. The wave spectrum for the wind sea contains more energy than the swell sea spectrum.

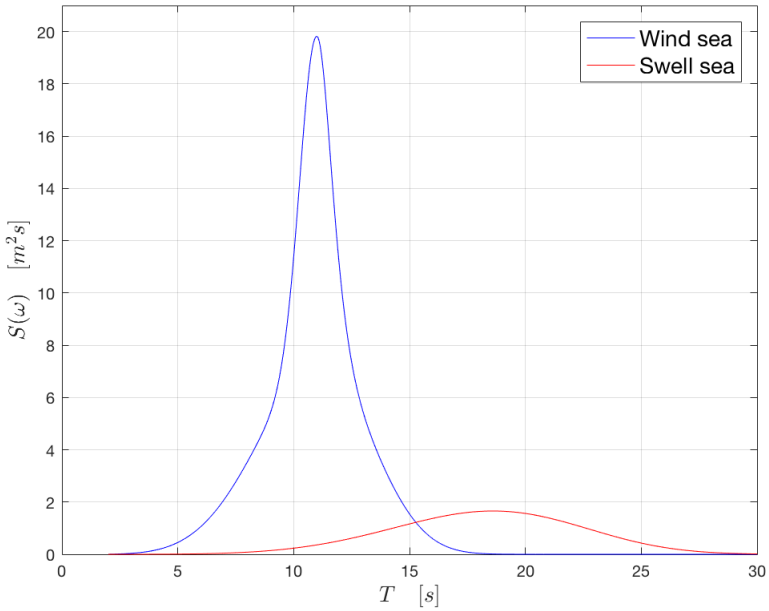

Figure 3.9: Typical JONSWAP spectra for swell sea with $H_{s,sw} = 2.5m$ and $T_{p,sw} = 18.6s$, and wind sea with $H_{s,w} = 8m$ and $T_{p,w} = 11s$.

3.3.2 Torsethaugen

The sea system in reality is generally of a combined nature, with contributions from wind sea and swell sea separately. As an attempt to model both wind and swell sea contributions in a common wave spectrum, Torsethaugen et al. (2004) have established a two-peaked spectrum based on empirical observations in the Norwegian sea. This spectrum is a sum of two JONSWAP like spectra, representing the wind and swell sea, respectively. Still, it should be noticed that Torsethaugen utilises a high frequency decay proportional to ω^{-4} instead of ω^{-5} which is utilised in JONSWAP, (Haver, 2017). Torsethaugen spectrum do not account for the fact that wind and swell sea in general come from different directions. This means that total sea characterised by $H_{s,tot}$ and $T_{p,tot}$ is the input to the spectrum. In most cases this means that use of Torsethaugen spectrum will give conservative results.

Torsethaugen differs between a wind dominated region and a swell dominated region. The boundary limit, T_f, separating the two regions is defined in Eq. (3.15).

$$T_f = 6.6H_s^{1/3} \tag{3.15}$$

A given sea state is associated with growing wind sea if $T_p < T_f$, and associated with swell sea or decaying wind sea if $T_p > T_f$, (Haver, 2017). Dependent on which region that governs the sea state, the total spectrum can be calculated based on the simplified form given in DNVGL-RP-C205, (DNVGL, 2014). To follow the procedure the calculations are performed with the frequency, f [Hz], while the final spectrum is transformed to ω by using the transformation $S(\omega) = \frac{1}{2\pi}S(f)$. The Torsethaugen spectrum is given as per Eq. (3.16).

$$S_T(\omega) = \frac{1}{2\pi}S_T(f) = \frac{1}{2\pi}\sum_{j=1}^{2} E_j S_{nj}(f_{nj}) \tag{3.16}$$

Where $E_j = \frac{1}{16}H_{sj}^2 T_{pj}$ and $f_{nj} = f \cdot T_{pj}$ is non-dimensional frequency used as input to the non-dimensional spectral density given in Eq. (3.17).

$$S(f_{nj}) = G_0 A \gamma_j \Gamma_{Sj} \gamma_{Fj} \tag{3.17}$$

Where $G_0 = 3.26$. The rest of the parameters are calculated based on which sea system that has the primary peak, according to Eq. (3.15). The char-

acteristics for the primary peak correspond to j = 1, and the characteristics for the secondary peak corresponds to j = 2. Γ_{Sj}, $A_{\gamma j}$ and γ_{Fj} are then given from Eq. (3.18).

$$\begin{aligned}
\Gamma_{Sj} &= f_{nj}^{-4} exp[f_{nj}^{-4}] \\
A_{\gamma 1} &= \frac{(1 + 1.1[ln(\gamma)]^{1.19})}{\gamma} \\
A_{\gamma 2} &= 1 \\
\gamma_{F1} &= \gamma^{exp[-\frac{1}{2\sigma^2}(f_{n1}-1)^2]} \\
\gamma_{F2} &= 1
\end{aligned} \tag{3.18}$$

In addition there are different procedures to calculate H_{sj}, T_{pj} and γ_j for the primary and secondary peak, dependent on which sea system that dominates the sea state. For wind dominated sea, $T_p < T_f$, the procedures in Eq. (3.19) and (3.20) are used to find the three parameters for the primary and secondary peak, corresponding to wind and swell respectively.

$$\begin{aligned}
H_{s1} &= r_{pw} H_s \\
T_{p1} &= T_p \\
\gamma_1 &= 35\left[\frac{2\pi H_{s1}}{g T_p^2}\right]^{0.857}
\end{aligned} \tag{3.19}$$

$$\begin{aligned}
H_{s2} &= \sqrt{1 - r_{pw}^2} H_s \\
T_{p2} &= T_f + 2.0 \\
\gamma_2 &= 1
\end{aligned} \tag{3.20}$$

Where $r_{pw} = 0.7 + 0.3exp\left(-\left(2\frac{T_f - T_p}{T_f - 2\sqrt{H_s}}\right)^2\right)$. For swell dominated sea, $T_p > T_f$, the procedures in Eq. (3.21) and (3.22) are used to find the three parameters for the primary and secondary peak, corresponding to swell and wind respectively.

$$
\begin{aligned}
H_{s1} &= r_{ps} H_s \\
T_{p1} &= T_p \\
\gamma_1 &= 35 \left[\frac{2\pi H_s}{g T_f^2} \right]^{0.857} \left(1 + 6 \left(\frac{T_p - T_f}{25 - T_f} \right) \right)
\end{aligned}
\tag{3.21}
$$

$$
\begin{aligned}
H_{s2} &= \sqrt{1 - r_{ps}^2} H_s \\
T_{p2} &= 6.6 H_{s2}^{1/3} \\
\gamma_2 &= 1
\end{aligned}
\tag{3.22}
$$

Where $r_{ps} = 0.6 + 0.4 exp\left(-\left(\frac{T_f - T_p}{0.3(25 - T_f)} \right)^2 \right)$. The total spectrum as found from Eq. (3.16) are shown for wind dominated sea in Figure 3.10 and for swell dominated sea in Figure 3.11. A comparison of the JONSWAP and Torsethaugen spectrum is shown in Figure 3.12 for the most severe sea state in the NORA10 hindcast.

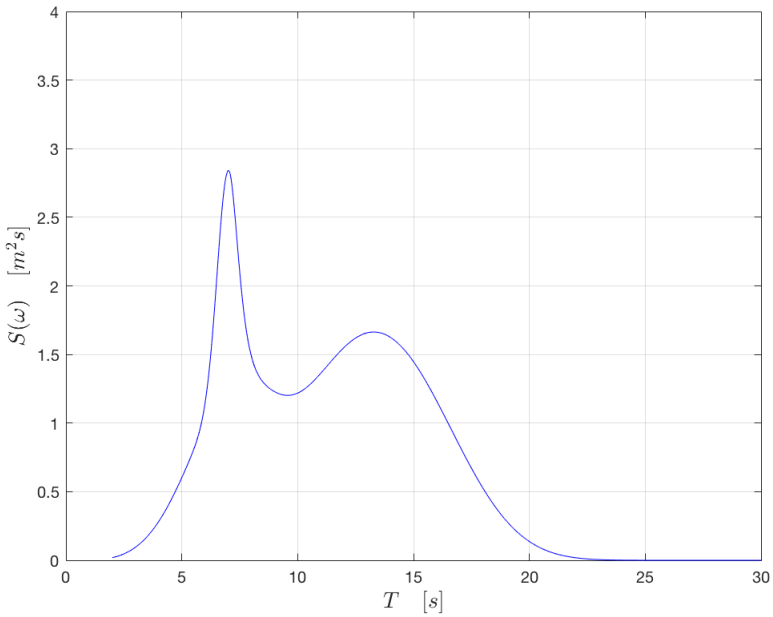

Figure 3.10: A typical Torsethaugen spectrum for wind dominated sea, $H_{s,tot} = 5m$ and $T_{p,tot} = 7s$.

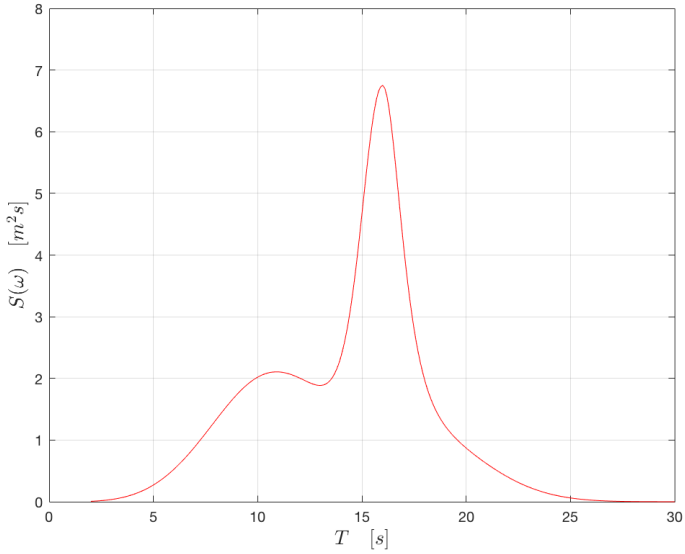

Figure 3.11: A typical Torsethaugen spectrum for swell dominated sea, $H_{s,tot} = 5m$ and $T_{p,tot} = 16s$.

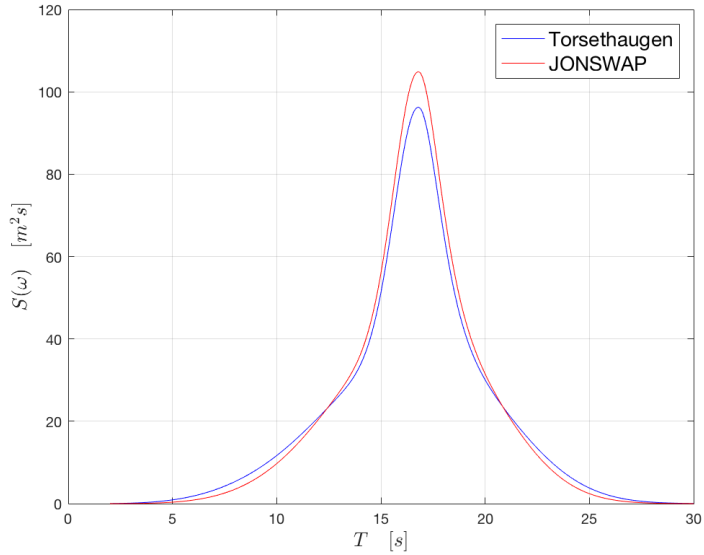

Figure 3.12: The JONSWAP and Torsethaugen spectra are plotted for the most severe sea state in the NORA10 hindcast, $H_{s,tot} = 15.6m$ and $T_{p,tot} = 16.8s$.

3.4 Response spectrum for upwell in combined sea

The response spectrum of a process is given by the squared RAO multiplied with the wave spectrum for the sea state, as shown in Eq. (3.23), (Price and Bishop, 1974).

$$S_{RR}(\omega) = |H_{\zeta R}(\omega)|^2 S_{\zeta\zeta}(\omega) \tag{3.23}$$

If the wave spectrum is given by total sea, the response spectrum is found directly from Eq. (3.23). However, if combined sea is considered, the response spectrum for the upwell has to be calculated for both wind and swell sea separately, as given in Eq. (3.24).

$$\begin{aligned} S_{RW}(\omega;\beta_1) &= |H_{\zeta RW}(\omega;\beta_1)^{(Relative)}|^2 S_{\zeta\zeta}(\omega;\beta_1) \\ S_{RS}(\omega;\beta_2) &= |H_{\zeta RS}(\omega;\beta_2)^{(Relative)}|^2 S_{\zeta\zeta}(\omega;\beta_2) \end{aligned} \tag{3.24}$$

As mentioned earlier α is used to correct the wave elevation for the wind sea, but not for the swell sea. Hence, the transfer function obtained in Eq. (3.7) is not multiplied with α in the process of establishing the transfer function for the upwell in the swell sea case.

As shown by Vestbøstad et al. (2002) in Eq. (3.25), the total response spectrum for the upwell can be taken as the sum of the response spectra due to swell and wind sea. This is valid in a linear analysis.

$$S_{RR}(\omega) = S_{RW}(\omega) + S_{RS}(\omega) \tag{3.25}$$

Typical response spectrum, wave spectrum and squared RAOs are shown for wind sea and swell sea in Figure 3.13 and 3.14, respectively.

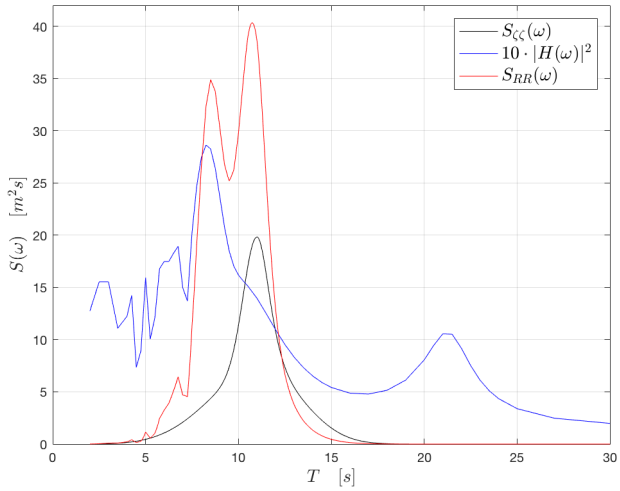

Figure 3.13: The response spectrum, $S_{RR}(\omega)$, the JONSWAP spectrum, $S_{\zeta\zeta}(\omega)$, and the magnified squared RAO, $10 \cdot |H(\omega)|^2$ are plotted for wind sea, $H_{s,w} = 8m$ and $T_{p,w} = 11$. The field point in the southwestern corner of the semi-submersible is considered.

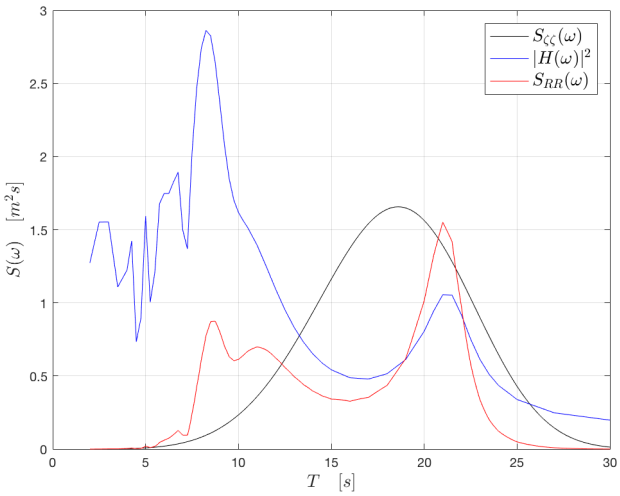

Figure 3.14: The response spectrum, $S_{RR}(\omega)$, the JONSWAP spectrum, $S_{\zeta\zeta}(\omega)$, and the squared RAO, $|H(\omega)|^2$ are plotted for swell sea, $H_{s,sw} = 2.5m$ and $T_{p,sw} = 18.6$. The field point in the southwestern corner of the semi-submersible is considered.

A typical total response spectrum is shown in Figure 3.15 together with the underlying response spectrum contributions from wind and swell.

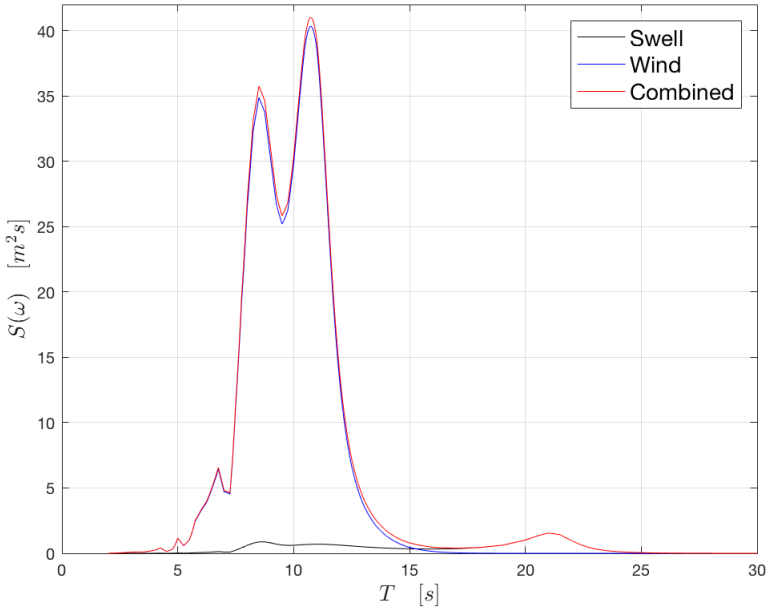

Figure 3.15: The total response spectrum plotted together with the wind and swell response spectra at the field point in the southwestern corner of the semi-submersible.

3.5 Short term analysis

In order to perform a short term upwell analysis the variance, σ^2, and the zero up-crossing period, T_2, have to be calculated.

$$\sigma^2 = m_0 = \int_0^\infty S_{RR}(\omega) d\omega \tag{3.26}$$

$$T_2 = 2\pi \sqrt{\frac{m_0}{m_2}} \tag{3.27}$$

Where the n^{th} moment of the response spectrum can be determined from Eq. (3.28).

$$m_n = \int_0^\infty \omega^n S_{RR}(\omega) d\omega \tag{3.28}$$

It is assumed that the wave elevation is a Gaussian stochastic process. As a simplified linear analysis is performed, the upwell response will also be Gaussian distributed. It can be shown that for a general stationary, narrow banded, Gaussian process with E[u(t)] = 0, the distribution of maxima is given by the Rayleigh distribution, (Price and Bishop, 1974). By assuming that all maxima obtained for a given period are statistically independent and identically Rayleigh distributed, the distribution for the largest of the maximum within the period can be determined. For a 3-hour period the cdf of the largest maxima can be found from Eq. (3.29).

$$F_{U_{3h,max}}(u) = (1 - exp(-(\frac{u^2}{2m_0})))^{n_{3h}} \tag{3.29}$$

Where the number of events within 3-hours, n_{3h}, is given by Eq. (3.30).

$$n_{3h} = \frac{10800}{T_2} \tag{3.30}$$

A normal approach to create samples of random 3-hour extremes is to use Monte Carlo simulations. This technique is used when real world observations are not available, but the statistical distribution function, $F_{U_{3h,max}}(u)$, is known. In this case, u can be solved from Eq. 3.29 to form Eq. 3.31.

$$u = \sqrt{-2m_0 ln(1 - F_{U_{3h,max}}(u)^{\frac{1}{n_{3h}}})} \tag{3.31}$$

Possible realizations of the 3-hour maximum upwell can be established by drawing a random number from a uniform distribution between 0-1 to decide $F_{U_{3h,max}}(u)$. As the value for $F_{U_{3h,max}}$ is known, it possible to decide a realization of u from Eq. 3.31. This is continued until a large enough sample of possible realizations is established. The procedure is visualized in Figure 3.16.

Another important quantity to consider is the most probable largest value, $\tilde{u}$. This can be found by considering the total number of observations within the given 3-hour period as per Eq. 3.32.

$$\begin{aligned} P[U_{3h,max} > \tilde{u}_{3h}] &= 1 - F_{U_{3h,max}}(\tilde{u}) \\ &= 1 - (1 - exp(-(\frac{\tilde{u}^2}{2m_0})))^{n_{3h}} = \frac{1}{n_{3h}} \end{aligned} \tag{3.32}$$

Solving Eq. 3.32 for $\tilde{u}$ leads to Eq. 3.33.

$$\tilde{u} = \sqrt{-2m_0 ln(1 - (1 - \frac{1}{n_{3h}})^{n_{3h}}} \tag{3.33}$$

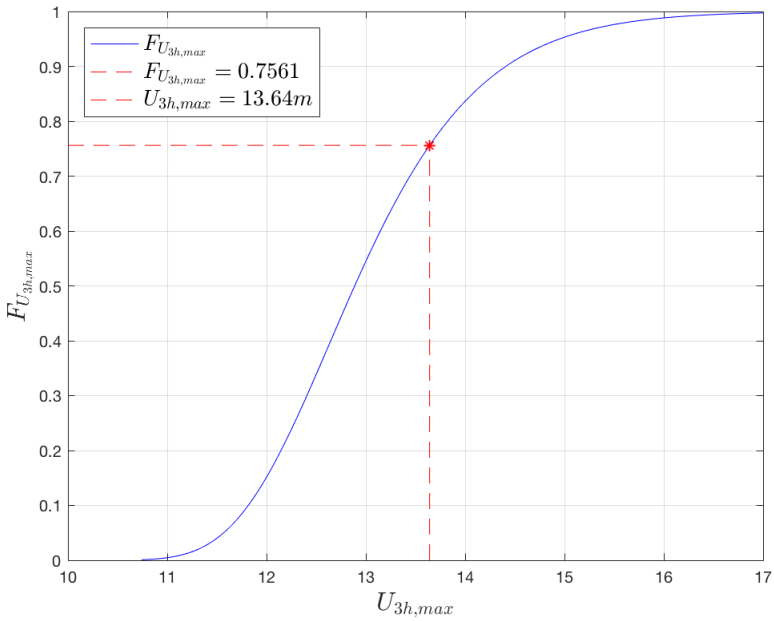

Figure 3.16: A random 3-hour maximum upwell is created using Monte Carlo simulation.

3.6 Long term analysis

The air gap of a semi-submersible is a result of relative platform motions occurring while exposed to wind and waves. The environmental forces are of a random nature, and can be considered as a stochastic process. Hence, the response is also a stochastic process. This means that given the same weather characteristics (H_s, T_p and W) in a sea state, the response will not

give the same result for two observations in the same sea state. Therefore, a distribution is needed to describe how the process behaves given some weather characteristics.

To estimate a q-probability response it is required that all sources of inherent randomness are accounted for. There are two sources: short term variability and long term variability. The long term variability tells how the weather characteristics change between the sea states, and is typically the most important contribution to the randomness. This is because a large critical response is most likely to occur in a severe sea state which has low probability of occurring. The short term variability can also be of importance, often dependent on the response problem at hand. An extreme response might occur in an ordinary sea state together with an uncommon realisation of the response quantity. To properly account for the randomness, the short term variability must be included.

A long term analysis must be performed in order to estimate reliable q-probability response results. In the marine field several methods are used; all sea states approach (ASS), all storms approach (POT), metocean contour line approach, annual maximum method (AMM) and different approaches using extreme value distributions. In this thesis two methods will mainly be discussed, ASS and POT.

The all sea states approach, Jasper (1956), Battjes (1972) and Nordenstrøm (1971), uses all available data in order to estimate the extreme values from a long term analysis. For each sea state the short term variability is made conditionally on the governing weather characteristics for the problem at hand. For the upwell problem the most important weather characteristics are H_s, T_p and W. However, in the simplified analysis the wind contribution is found separately, meaning that only H_s and T_p decide the weather conditions. The long term variability is represented by the joint distribution of H_s and T_p. The resulting expression for the long term distribution of the 3-hour maximum upwell is given in Eq. (3.34).

$$F_{U_{3h}}(u) = \int_h \int_t F_{U_{3h}|H_sT_p}(u|h,t) f_{H_sT_p}(h,t) dh dt \tag{3.34}$$

Where $F_{U_{3h}|H_sT_p}(u)$ represents the short term variability and $f_{H_sT_p}(h,t)$ is the joint distribution representing the long term variability.

The all storm approach, Jahns et al. (1972), Haring et al. (1978) and Tromans et al. (1995), more often referred to as peak-over threshold (POT), only considers the data above a selected threshold. Hence, storm conditions

are the governing data used to estimate the extreme upwell. The methodology outlined in Haver (2017) will be the basis for the POT approach in this thesis.

Accounting for non-observed events is important, especially when ALS estimates are found. Therefore the procedure found in Haver (2017) and Sandbakken (2017) will be used to include the contributions from non-observed events in the long term analysis. In POT, the short term variability is made conditional on the most probable largest maximum upwell, $\tilde{u}$, within an arbitrary storm. By fitting a useful probability model to the observations of $\tilde{u}$, the long term variability of $\tilde{u}$ can be found. Together this forms the long term distribution of the storm maximum upwell as shown in Eq. (6.1).

$$F_U(u) = \int_{\tilde{U}} F_{U|\tilde{U}}(u|\tilde{u}) f_{\tilde{U}}(\tilde{u}) d\tilde{u} \tag{3.35}$$

Where $F_{U|\tilde{U}}(u|\tilde{u})$ represents the short term variability and $f_{\tilde{U}}(\tilde{u})$ is the long term variability. An analogue procedure will also be proposed as a solution to account for non-observed events in the ASS approach.

Chapter 4

Introduction to the All sea states approach - Crest height problem

In order to find the ULS and ALS response, a long term analysis have to be performed. As the meteorologists and marine engineers have produced hindcast data all the way back to the mid 50s for the North Sea, a large amount of good quality environmental data are available, (Reistad et al., 2007). The ASS approach takes advantage of this by considering the contributions to the extreme values from all observed sea states. Hence, the long term analysis is performed by combining the short term variability of the 3-hour maximum response described conditionally on all possible sea states with the long term joint distribution of H_s and T_p. The long term distribution of the 3-hour maximum response is then given by Eq. (4.1).

$$F_{X_{3h}}(x) = \int_h \int_t F_{X_{3h}|H_sT_p}(x|h,t) f_{H_sT_p}(h,t) dhdt \tag{4.1}$$

It is assumed that all sea states are statistically independent, which is not exactly true in reality. Each sea state will to some extent be correlated with the adjacent sea states. However, this assumption gives conservative results, which has shown to be 3-5 % on the safe side, (Haver, 2017).

In this chapter both the traditional all sea states approach (TASS) and a modified version of the all sea states approach (MASS) will be introduced. As the name suggests, TASS considers all observed sea states in the long term analysis. This may be highly time consuming for more complex

response problems, where spectra and transfer functions are needed to calculate the response quantity. As the aim of the assignment is to establish extreme 3-hour responses for ULS and ALS, it is assumed that higher sea states are of most concern. Therefore, a threshold for H_s will be set for the MASS, excluding the sea states that are lower than the given threshold. This methodology looks similar to the POT approach, where storms over a chosen threshold are used to decide the ULS and ALS response characteristics. However, for MASS, all sea states above the threshold are assumed independent and not part of a common storm.

In order to exemplify and describe both methods, the crest height is chosen as a proper response problem to consider. As the crest height is a relatively simple response quantity, well described by a statistical model like the Forristall 2^{nd} order model, it can quite accurately quantify the goodness of the MASS approach. Omnidirectional long-crested total sea is considered for the crest height problem. Since the crest height is described by a statistical distribution, it is convenient with regard to time to use the TASS approach to find extreme responses. It is then the objective to investigate if MASS will be a reasonable alternative to TASS for this response problem. The results obtained for the extreme crest heights from the MASS and TASS approach will be compared. This is important in order to verify how well the modified version behaves, before it is used on more complex response problems, e.g. upwell. A thorough presentation of the TASS approach is performed in this section, since it is considered important to show the differences from the MASS approach.

4.1 Traditional all sea state approach

The all sea state approach, in this thesis referred to as the traditional all sea states approach - TASS, performs the integration in Eq. (4.1) directly in order to establish the long term probability distribution of the 3-hour maximum crest height. It is of importance for the results to find probability models that can represent the short term variability, $F_{C_{3h}|H_sT_p}(c|h,t)$, and the long term variability, $f_{H_sT_p}(h,t)$, in a satisfactory way, based on the hindcast data available.

4.1.1 Short term variability - $F_{C_{3h}|H_sT_p}(c|h,t)$

The short term conditional distribution for the 3-hour maximum crest height can according to Forristall (2000) be given as in Eq. (4.2).

$$F_{C_{3h}|H_sT_p}(c|h,t) = \left[1 - exp(-(\frac{c}{\alpha_F h_s})^{\beta_F})\right]^{n_{3h}} \tag{4.2}$$

Eq. (4.2) is an empirical model for the global crest height, valid for second order irregular wave theory. It can be used both for long crested and short crested sea, where the difference of the two cases is the expressions used to determine the parameters α_F and β_F. The parameters used for long crested sea are given from Eq. (4.3).

$$\begin{aligned} \alpha_F &= 0.3536 + 0.2892s_1 + 0.1060u_R \\ \beta_F &= 2 - 2.1597s_1 + 0.0968u_R^2 \end{aligned} \tag{4.3}$$

Where s_1 is the steepness parameter and u_R is the Ursell number found from Eq. (4.4).

$$\begin{aligned} s_1 &= \frac{2\pi h_s}{gt_1^2} \\ u_R &= \frac{h_s}{k_1^2 d^3} \end{aligned} \tag{4.4}$$

Here h_s is significant wave height, g is acceleration of gravity, t_1 is mean wave period, k_1 is the wave number related to t_1 and d is water depth. A JONSWAP spectrum is assumed to describe the total incoming sea, which means that t_1 can be approximated as $t_1 = 0.83T_p$, (Faltinsen, 1993). k_1 is found from the dispersion relationship for deep water, $k_1 = \frac{\omega^2}{g}$. The Troll-field has a water depth of 300 meters, which means that the wave length has to be 600 meters if the wave is going to affect the sea bottom. This corresponds to a wave period of 19.6 seconds, which is slightly higher than the critical steep sea state region. Therefore, the assumption of deep water is utilised. n_{3h} given in Eq. (4.2) represents the expected number of events occurring in a 3-hour period. This can be found by utilising the zero up-crossing period, T_2 as shown in Eq. (4.5). As a JONSWAP spectrum is assumed, the relation $T_2 = 0.78T_p$ is used, (Faltinsen, 1993). Both the approximation for t_1 and T_2 are utilized because a spectral analysis is not performed for the crest height problem. Alternatively, $\frac{t_1}{T_p}(\gamma)$ and $\frac{T_2}{T_p}(\gamma)$ as defined in DNVGL (2014) could be used.

$$n_{3h} = \frac{10800}{T_2} = \frac{13846}{T_p} \tag{4.5}$$

As the probability distribution for the 3-hour maximum crest height is established, the short term variability of the 3-hour maximum crest height for each sea state can be found.

4.1.2 Long term variability - marginal dist. $F_{H_s}(h)$

The joint distribution of H_s and T_p which represents the long term variability, can according to Bayes' rule be written as $f_{H_sT_p}(h,t) = f_{H_s}(h) \cdot f_{T_p|H_s}(t|h)$. As H_s often is considered as the most important weather characteristic for the problem at hand (which is certainly the case for the crest height), T_p is described conditionally on H_s.

The marginal distribution for H_s is found to be conveniently represented by a 3-parameter Weibull model given by Eq. (4.6), (Battjes, 1972).

$$F_{H_s}(h) = 1 - exp(-(\frac{h-\lambda_{H_s}}{\alpha_{H_s}})^{\beta_{H_s}}) \tag{4.6}$$

The parameters, α_{H_s}, β_{H_s} and λ_{H_s} are estimated using the method of moments as outlined in Haver (2016). This method requires that the moments of the distribution model are equal to the respective moments from the sample. Hence, the mean, the standard deviation and the skewness of the sample, are used to estimate the parameters in the 3-parameter Weibull model according to Eq. (4.7).

$$\begin{aligned}
\gamma_{H_s} &= \frac{\Gamma(1+\frac{3}{\beta_{H_s}}) - 3\Gamma(1+\frac{1}{\beta_{H_s}})\Gamma(1+\frac{2}{\beta_{H_s}}) + 2\Gamma^3(1+\frac{1}{\beta_{H_s}})}{[\Gamma(1+\frac{2}{\beta_{H_s}}) - \Gamma^2(1+\frac{1}{\beta_{H_s}})]^{\frac{3}{2}}} \\
\alpha_{H_s} &= \frac{\sigma_{H_s}}{\left[\Gamma(1+\frac{2}{\beta_{H_s}}) - \Gamma^2(1+\frac{1}{\beta_{H_s}})\right]} \\
\lambda_{H_s} &= \mu_{H_s} - \alpha_{H_s}\Gamma(1+\frac{1}{\beta_{H_s}})
\end{aligned} \tag{4.7}$$

β_{H_s} can be found from the first expression in Eq. (4.7) using a simple iteration process. When the estimate for β_{H_s} is found, α_{H_s} and λ_{H_s} can easily be calculated from the two remaining expressions in Eq. (4.7), respectively. The results obtained for the parameters are listed in Table 4.1.

Table 4.1: Estimates obtained for the parameters of the 3-parameter Weibull model for the marginal distribution of H_s.

Parameter	Estimate
α_{H_s}	2.080
β_{H_s}	1.304
λ_{H_s}	0.528

By sorting the H_s values in ascending order it is possible to plot the sample distribution in a 2-parameter Weibull probability paper. The established 3-parameter Weibull model can be plotted in the same probability paper, which will verifiy how the model represents the empirical observations. The comparison shows to be good in Figure 4.1.

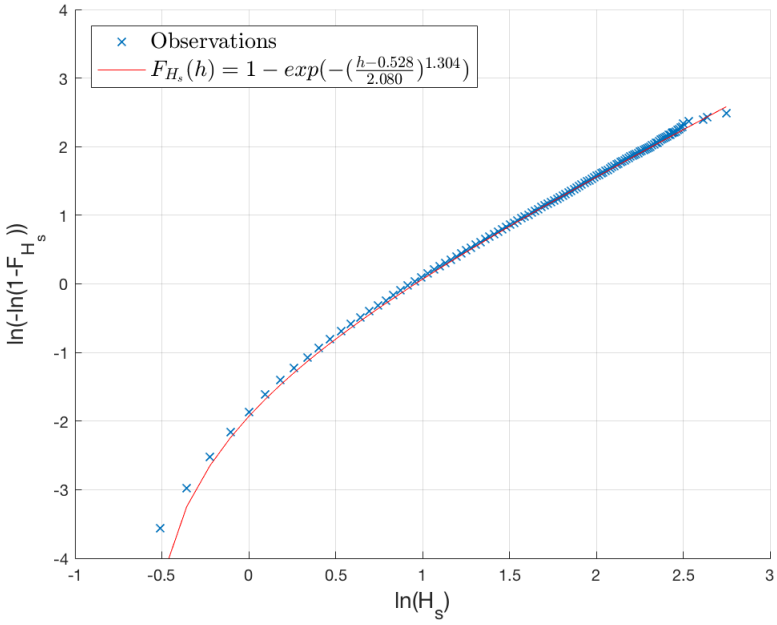

Figure 4.1: The 3-parameter Weibull model is plotted together with the empirical observations of H_s.

4.1.3 Long term variability - conditional dist. $F_{T_p-\epsilon|H_s}(t-\epsilon|h)$

The conditional distribution of T_p given H_s is normally assumed to follow the log-normal distribution. However, using the log-normal distribution as

a model for the conditional distribution of T_p given H_s gives problems for the environmental contour lines representing the critical sea states at ULS and ALS level. As seen from Figure 4.2 the contour lines violate the wave breaking limit. The suggested wave breaking limit is proposed by Haver and Nyhus (1986) to be $T_p = 3.2\sqrt{H_s}$ in combined sea.

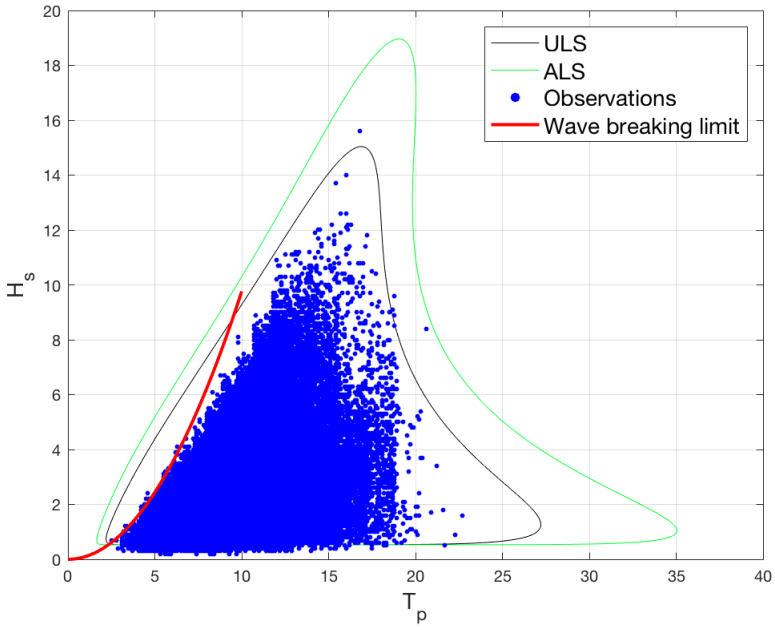

Figure 4.2: The ULS and ALS metocean contour lines shown for H_s and T_p using the log-normal distribution as the conditional distribution of T_p given H_s.

To make the contour lines follow the wave breaking limit in the steep area, a lower limit for T_p is introduced. The sea system is of a combined nature, including both wind and swell sea. When these two sea systems are merged to one total sea system describing the sea state, the sea state might be placed outside the wave breaking limit, (Haver, 1990). This gives contributions that are unphysical, because the waves will break. Therefore a lower limit $\epsilon = 3.2\sqrt{H_s}$ shall ensure that sea states will not be placed outside the wave breaking limit. Vikenes (2017) has shown that a 2-parameter Weibull distribution is a better model for the conditional distribution of T_p given H_s when the lower limit for T_p is used. The 2-parameter Weibull distribution for $T_p - \epsilon$ is given by Eq. (4.8).

$$F_{T_p-\epsilon|H_s}(t-\epsilon|h) = 1 - exp(-(\frac{t-\epsilon}{\alpha_{T_p-\epsilon|H_s}})^{\beta_{T_p-\epsilon|H_s}}) \tag{4.8}$$

For each class of H_s in the scatter diagram found in appendix A, the parameters $\alpha_{T_p-\epsilon|H_s}$ and $\beta_{T_p-\epsilon|H_s}$, are estimated using the method of moments. This means that the mean and standard deviation for each class of H_s has to be calculated using $T_p-\epsilon$ instead of T_p. According to Nielsen (2011) $\beta_{T_p-\epsilon|H_s}$ can be found from Eq. (4.9) by iteration using the bisection method.

$$\frac{M_2}{M_1^2} = \frac{\Gamma(1+\frac{2}{\beta_{T_p-\epsilon|H_s}})}{\Gamma^2(1+\frac{1}{\beta_{T_p-\epsilon|H_s}})} \tag{4.9}$$

M_1 and M_2 are the sample moments given by $M_k = \frac{1}{n}\sum_{i=1}^{n} t_i^k$ and Γ is the gamma function. When the estimate of $\beta_{T_p-\epsilon|H_s}$ is found, $\alpha_{T_p-\epsilon|H_s}$ can be found by setting the mean of the sample equal to the first moment of the 2-parameter Weibull model as shown in Eq. (4.10), (Haver, 2017).

$$\alpha_{T_p-\epsilon|H_s} = \frac{M_1}{\Gamma(1+\frac{1}{\beta_{T_p-\epsilon|H_s}})} \tag{4.10}$$

When estimates for $\alpha_{T_p-\epsilon|H_s}$ and $\beta_{T_p-\epsilon|H_s}$ are found for each H_s class, curves are fitted to the point estimates in order to get a continuous function describing the parameters. The fitted functions for $\alpha_{T_p-\epsilon|H_s}$ and $\beta_{T_p-\epsilon|H_s}$ are presented in Eq. (4.11).

$$\begin{aligned} \alpha_{T_p-\epsilon|H_s} &= \frac{p_1h^2+p_2h+p_3}{h^2+q_1h+q_2} = \frac{5.882h^2+14.150h+228.4}{h^2+7.952h+35.070} \\ \beta_{T_p-\epsilon|H_s} &= \frac{p_1h^2+p_2h+p_3}{h+q_1} = \frac{0.2791h^2-0.7732h+5.221}{h+1.912} \end{aligned} \tag{4.11}$$

Rational polynomials are used to describe the functions. They are chosen because they gave a satisfactory fit to the point estimates. Simpler functions could have been suggested to find standardized models for $\alpha_{T_p-\epsilon|H_s}$ and $\beta_{T_p-\epsilon|H_s}$, but a sensitivity study has not been performed. This is suggested as further work. The point estimates obtained will vary for different locations, because they are dependent on the hindcast data provided. The fitted functions are compared to the point estimates in Figure 4.3 and 4.4. The highest point estimates for $\beta_{T_p-\epsilon|H_s}$ has not been utilized in the fitting process, as it is important that the fitted line rises for the extrapolated

high values of H_s to minimize the variance at this level. Still, it can be questioned if the extrapolated line should have a flatter angle following the point estimates for the highest H_s values.

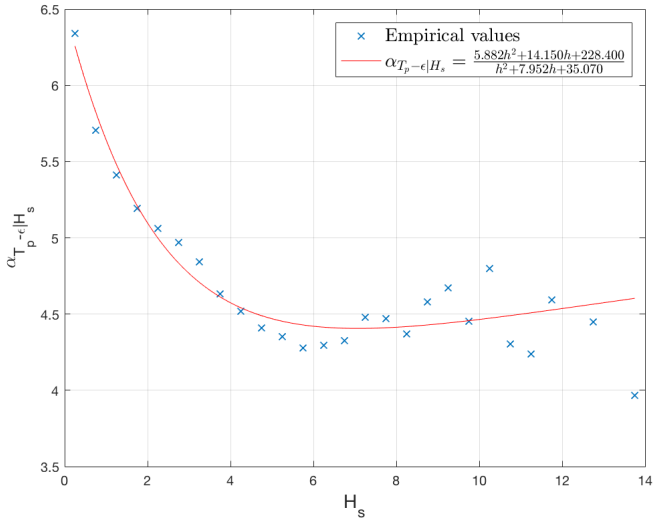

Figure 4.3: Point estimates of $\alpha_{T_p-\epsilon|H_s}$ are plotted together with the fitted function.

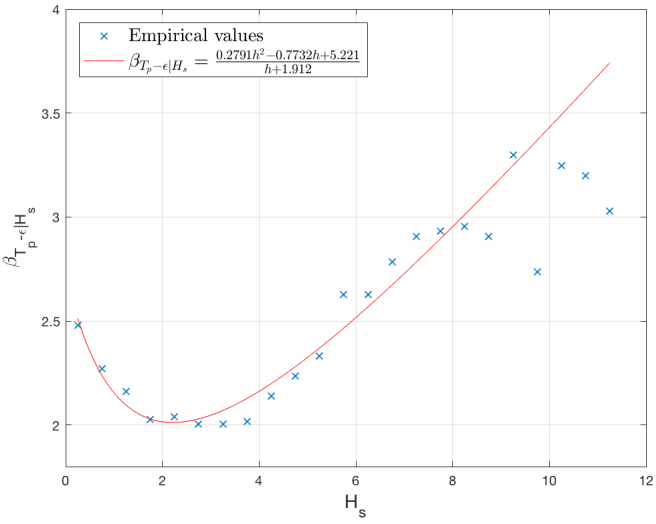

Figure 4.4: Point estimates of $\beta_{T_p-\epsilon|H_s}$ are plotted together with the fitted function.

The resulting ULS and ALS contour lines for these sea characteristics are shown in Figure 4.5. It is seen that when the lower limit for T_p is introduced, the contour lines do not violate the wave breaking limit. In addition, the long periodic swell sea states are of a realistic order with ALS periods around 25 seconds. The methodology of establishing the metocean contour lines are outlined more thoroughly in section 6.1.3 and chapter 7.

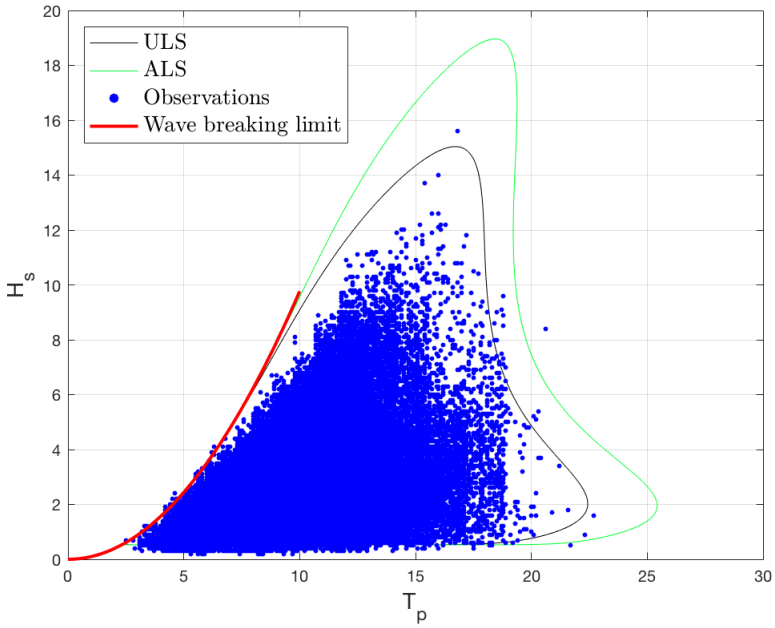

Figure 4.5: The ULS and ALS metocean contour lines are shown for H_s and T_p with a lower limit for T_p.

The long term variability, $f_{H_sT_p}(h,t)$, is established and the long term distribution can be found numerically according to Eq. (4.1).

4.1.4 ULS and ALS crest height

When the long term distribution of the 3-hour maximum crest height is calculated, the 3-hour maximum crest height can be estimated for specific return periods. The most relevant return periods used as limit states in design on the NCS are ULS and ALS, corresponding to a return period of 100 and 10000 years, respectively. The probability of exceeding these values correspond to $q_{ULS} = 10^{-2}/year$ and $q_{ALS} = 10^{-4}/year$. However, this is

the annual exceedance probability. Since the maximum crest height within a 3-hour time interval is considered, it is necessary to divide the annual probability of exceedance with the number of 3-hour sea states that occur annually, which is 2920. This means that the probability of exceeding a given return period value within a 3-hour sea state can be written according to Eq. (4.12).

$$Q_{C_{3h}}(c) = 1 - F_{C_{3h}}(c) = \frac{q}{2920} \tag{4.12}$$

The ULS and ALS probability levels are now given for the long term cumulative probability distribution as in Eq. (4.13).

$$F_{C_{3h}}(c) = 1 - \frac{q}{2920} \tag{4.13}$$

As the long term distribution and the relevant probability levels are known, the estimates of $C_{3h,ULS}$ and $C_{3h,ALS}$ can be determined. By plotting the long term distribution in a 2-parameter Weibull paper, the 3-hour maximum crest height for ULS and ALS are found where the long term distribution and the respective probability levels intersect, as shown in Figure 4.6. The results are provided in Table 4.2.

Table 4.2: Estimates obtained for the 3-hour maximum ULS and ALS crest height.

$C_{3h,ULS}$	17.2m
$C_{3h,ALS}$	22.4m

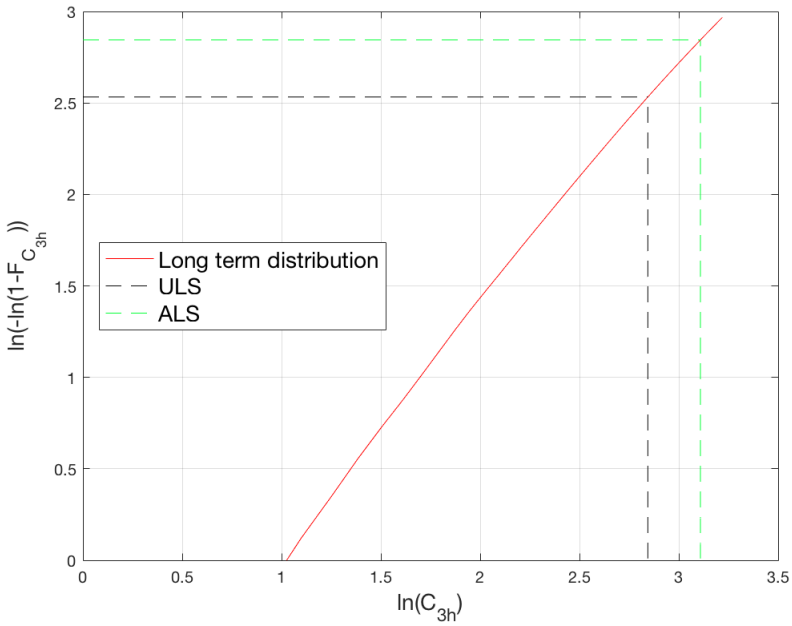

Figure 4.6: The long term distribution is plotted in Weibull scale together with the ULS and ALS probability levels. The intersection points determine $C_{3h,ULS}$ and $C_{3h,ALS}$.

An interesting quantity to investigate is the ratio between C_{3h} and $H_{s,3h}$. Ratios for different return periods are given in Table 4.3.

Table 4.3: Ratios $C_{3h}/H_{s,3h}$ obtained for different return periods.

Return period (year)	$H_{s,3h}$	C_{3h}	$C_{3h}/H_{s,3h}$
1	11.2m	12.5m	1.11
10	13.0m	14.6m	1.12
100	15.0m	17.2m	1.15
10000	19.0m	22.4m	1.18

The ratios for the return periods of 1 and 10 years are in compliance with the results reported by Gibson et al. (2014). For ULS and ALS the ratios seems to be somewhat lower compared to the results presented in Lian and Haver (2015). Several factors influence this ratio: wave steepness, spectral peak period, water depth, etc. Therefore the ratios obtained in Table 4.3 should only be used as an indication. The ratio between the ULS and ALS crest height is observed to be 1.3.

4.2 Modified all sea state approach

The modified all sea state approach (MASS) differs from the TASS approach in the way that a threshold for H_s is introduced, where the sea states below the threshold are neglected. This is reminiscent of the POT approach, where only the storms above a selected threshold are considered in the long term analysis. However, in a POT analysis several adjacent sea states are gathered in a storm event. In contrast to this MASS assumes that all sea states above the selected threshold are statistically independent. In this manner MASS takes advantage of all sea states above the threshold separately. The various approaches of MASS differs in how many sea states that are included in the analysis, hence where the threshold is set. The reason why the sea states below the threshold can be neglected is that it is assumed that they do not contribute to the ULS and ALS response values, (Haver, 2018). For the crest height case it is widely known that the crest height is closely connected to the significant wave height, and that the highest crest heights are found for the higher and steeper sea states. Hence, the lower sea states do not contribute to the exceedance probability values and can be neglected. For a different problem where the response is impacted by lower sea states, the threshold might be set so low that MASS approaches TASS in order to give reasonable results. Therefore, MASS is strictly speaking a method that should be used for response problems that have most of the contribution to the extreme values from higher sea states. It is evident that the choice of threshold is important for the problem at hand.

4.2.1 Short term analysis

All sea states above the given threshold are retrieved from the observations in the NORA10 hindcast. It is assumed that all sea states above the threshold are statistically independent. Since only total sea are considered for the crest height problem, the relevant data are $H_{s,tot}$ and $T_{p,tot}$. As for TASS, the Forristall 2^{nd} order distribution given in Eq. (4.2) is used to model the 3-hour maximum crest height. Monte Carlo simulations are used to find a possible realization of the 3-hour maximum crest height for each sea state above the threshold. This means that for each sea state $F_{C_{3h}|H_sT_p}(c|h,t)$ is a random variable between 0-1, giving a corresponding simulated C_{3h}. Together all C_{3h} forms a sample of short term extremes, which can be used to decide the long term distribution.

4.2.2 Long term analysis

The true long term distribution has to be modelled by a known empirical or theoretical distribution. In order to decide which distribution that give the best fit to the sample of short term extremes, the calculated extremes are plotted in probability papers for different distributions. The extreme value distribution that gives a linear fit to the data in the probability paper is a good model for the true long term distribution. Although only the short term extremes for the observations above the threshold are calculated, all available observations from NORA10 should be included in the analysis, to be consistent with the all sea state approach. The observations above the threshold need a corresponding cumulative probability in order to be plotted in the probability paper. Normally this is done by sorting the observations in ascending order, where observation number k has the cumulative probability $F = \frac{k}{N+1}$. N is the total number of observations in the sample. However, as only the values above a certain threshold are considered, this method has to be adjusted.

By assuming that there are N extremes in the sample, and that the values below the threshold has no probability of occurring, the method can be used for the K remaining extremes obtained from the sea states above the threshold, (Haver, 2018). By sorting the K extremes in descending order, the cumulative probability for the largest extreme in the sample is given by $F = \frac{N}{N+1}$. For the next extreme, $F = \frac{N-1}{N+1}$. Consequently, the smallest of the extremes in the sample of size K gets the cumulative probability $F = \frac{N-K}{N+1}$.

Normally all extremes plotted in the probability paper will be used in the curve fitting process. However, in this case only the 30-50 % of the highest extremes are used to fit the straight line. This is because the lowest extremes may have contributions from sea states below the threshold. Therefore they will not be representative for the process occurring at the highest levels. In Figure 4.7 and 4.8 the 40 % highest extremes are used in the fitting process. The lowest extremes do not follow the fitted linear line, which means that they are not well represented by the Gumbel nor the Weibull model.

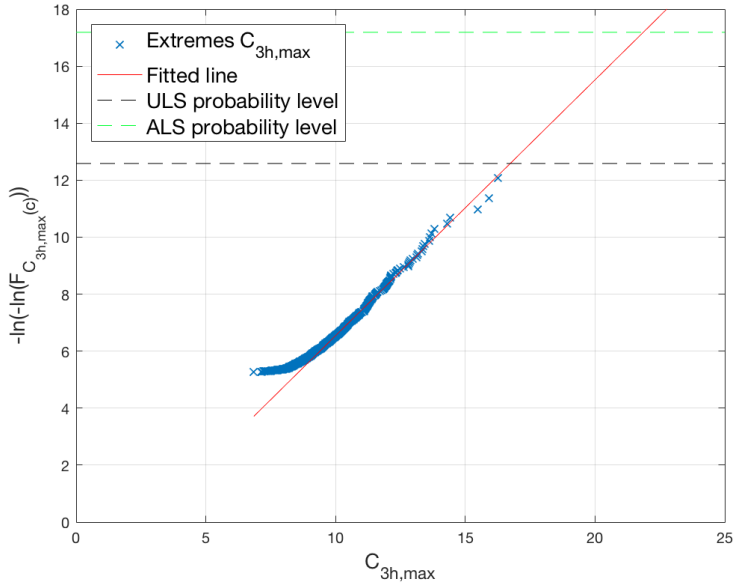

Figure 4.7: Gumbel fitted to the 40% highest extremes for a threshold $H_s = 8m$.

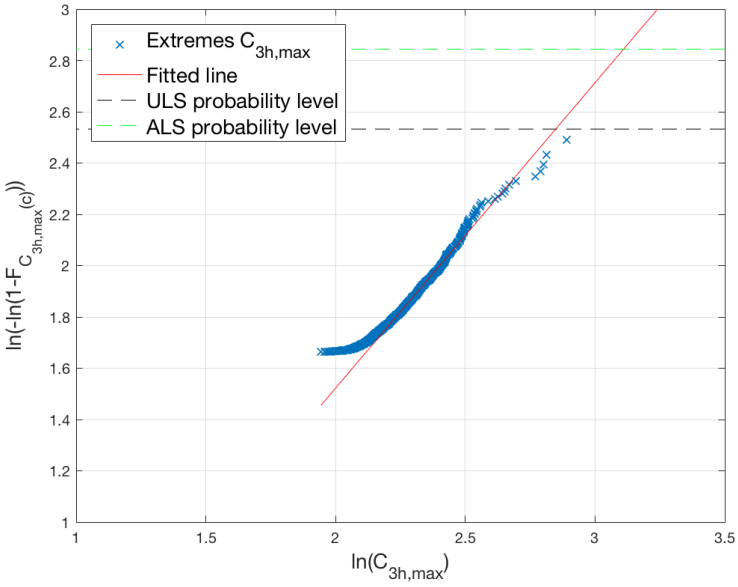

Figure 4.8: Weibull fitted to the 40% highest extremes for a threshold $H_s = 8m$.

When a good extreme value model is found and a proper curve is fitted to the highest extremes, the ULS and ALS crest heights are found by extrapolating the fitted line up to the respective probability levels. The probability of exceedance and the cumulative probability are given from Eq. (4.12) and (4.13), respectively. However, the probability values are changed when the long term distributions are plotted in Gumbel and Weibull scale. The cumulative probabability for ULS and ALS events are given in Table 4.4 together with the corresponding probability levels in Gumbel and Weibull scale.

Table 4.4: Probabilities for ULS and ALS events to occur within a 3-hour period.

	ULS	ALS
$F_{C_{3h}}(c)$	1 - 3.42 $\cdot 10^{-6}$	1 - 3.42 $\cdot 10^{-8}$
Gumbel scale	12.5859	17.1910
Weibull scale	2.5326	2.8444

The intersection point of the fitted line with the ULS value of the cumulative distribution corresponds to the ULS crest height along the horisontal axis. By doing the procedure of creating extremes, fitting the extreme distribution and calculating the ULS values 100 times, a good estimate for the ULS value is obtained by calculating the mean of this sample of long term extremes. In this way some of the uncertainties related to using the Monte Carlo simulation is reduced. The normal distribution of the 100 ULS crest heights obtained from the long term analysis is shown in Figure 4.9.

The Gumbel, exponential and Weibull distributions have been suggested as suitable models for the long term distribution. The ULS and ALS crest heights utilising a threshold of $H_s = 8$m are presented in Table 4.5.

Table 4.5: Estimates obtained for the 3-hour maximum ULS and ALS crest height from the MASS approach with a threshold at $H_s = 8$m.

	Gumbel	Exponential	Weibull
$C_{3h,ULS}$	17.0m	17.0m	16.7m
$C_{3h,ALS}$	22.3m	22.3m	21.3m

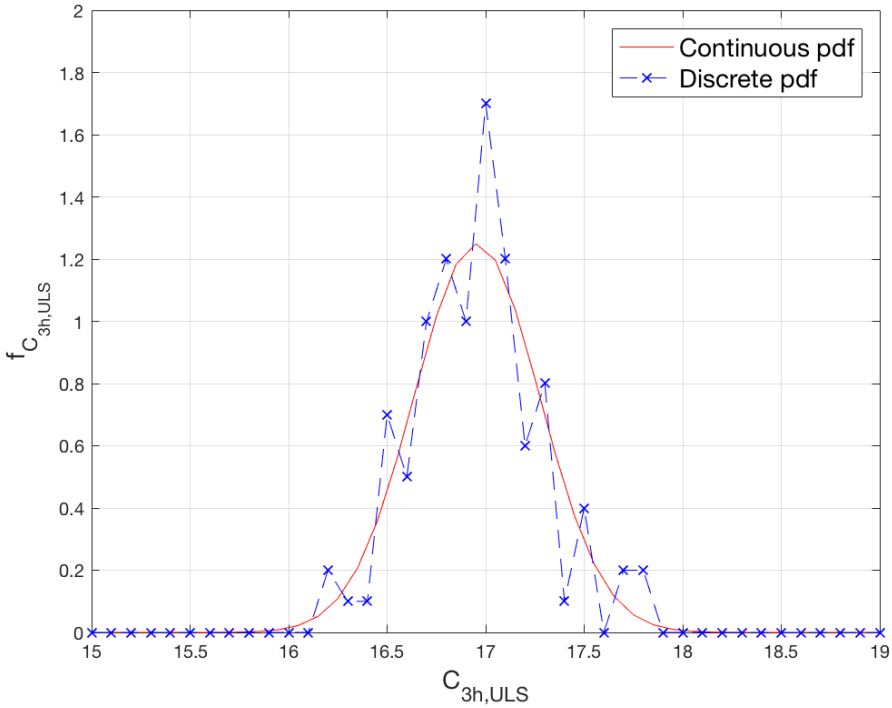

Figure 4.9: The discrete normal distribution is plotted versus the continuous normal distribution for the 100 long term estimates of $C_{3h,ULS}$.

4.3 Threshold sensitivity study

As for the POT approach, one of the most critical decisions in the MASS approach is where to set the threshold. If the threshold is set too high, there will be few observations available to fit the extreme value distribution. This leads to high variance and uncertainty in the obtained results. If, on the other hand, the threshold is set too low, sea states that do not contribute to the ULS and ALS level may influence the fitted extreme value distribution, leading to bias. In addition, it will for a complex response problem, like the upwell problem, be highly time consuming to consider too many events. Therefore, the threshold must be set at a level where all sea states that give contributions to the probability of exceeding the ULS and ALS values are placed above the threshold by balancing bias and variance in a satisfactory manner, (Coles et al., 2001).

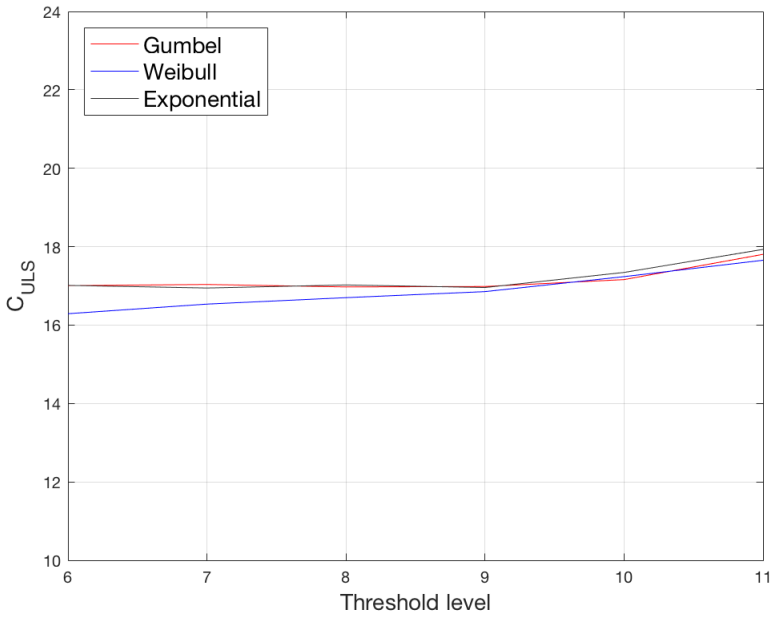

Figure 4.10: The 3-hour ULS crest height is plotted with Gumbel, exponential and Weibull distributions fitted to the 40% highest extremes for different thresholds.

From Figure 4.10 it can be seen that the Gumbel and exponential distributions give exactly the same results. This is not surprising, because the exponential distribution asymptotically approaches to the Gumbel distribution for extreme values. It is interesting to note that the ULS value stabilises for these two distributions for thresholds at $H_s = 9$m and lower. This seems to imply that sea states below 9m have negligible contribution to the exceedance of the ULS crest height, and that setting a threshold at 8-9m would be appropriate for this response problem. However, the Weibull model seems to not stabilise within this area. As the threshold decreases, the ULS results for the Weibull model decreases as well. The Forristall 2^{nd} order model for the crest height is built upon a 2-parameter Weibull model, which means that it should asymptotically approach the Gumbel distribution for extremes. Therefore, the Weibull model might not be suitable for modelling the long term distribution for the crest height problem, and the Gumbel model is used as the long term distribution in the further work.

Another question occurring from Figure 4.10 is why the ULS value is higher when the threshold is set high. Setting the threshold too high should lead

to loss of important contributions to the exceedance of the ULS value from the sea states just below the threshold. Theoretically this should give a lower ULS value for high thresholds, while the ULS value should stabilise at the correct value utilising lower thresholds that includes all sea states with important contributions. Figure 4.11 shows that it is the curve fitting procedure utilised in the MASS approach that gives higher $C_{3h,ULS}$ for the highest thresholds. As the threshold is set high, the extremes that are available in the fitting process brings the line to a flatter angle. This will again lead to higher ULS values for the crest height, as the ULS probability level remains the same. It should be remembered that the ULS and ALS probability levels are equal for the different thresholds because all observed hindcast sea states are considered when the cumulative distribution is decided.

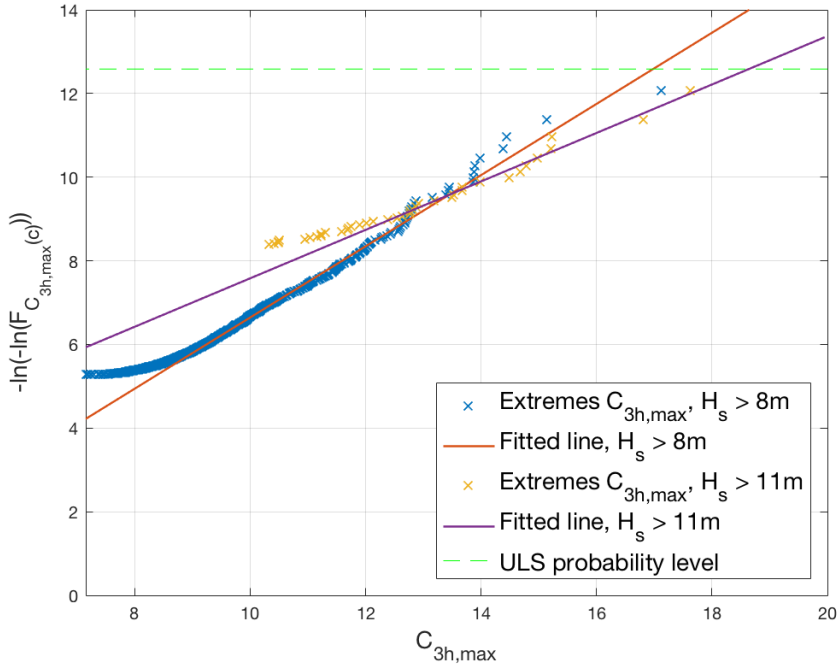

Figure 4.11: Both the empirical short term C_{3h} and the fitted line are shown for the thresholds $H_s = 8$m and $H_s = 11$m.

The threshold is set based on H_s because H_s is in general the most important weather characteristic for the response problem at hand. However, as shown in section 4.1.1 the crest height is especially dependent on the wave steepness, spectral peak period and water depth. A steeper sea state

will give a higher contribution to the ULS crest height than a flatter sea state (longer T_p), although they have the same H_s. As an example, steep sea states with $H_s = 9$m might give a higher 3-hour maximum crest height than a more gentle sea state with $H_s = 11$m and a large T_p. As seen from Figure 4.11 there are several of the sea states for a threshold at $H_s = 8$m that give higher C_{3h} than the lowest C_{3h} obtained at a threshold of $H_s = 11$m. Therefore, setting a too high threshold using the MASS approach will for the crest height problem give conservative results.

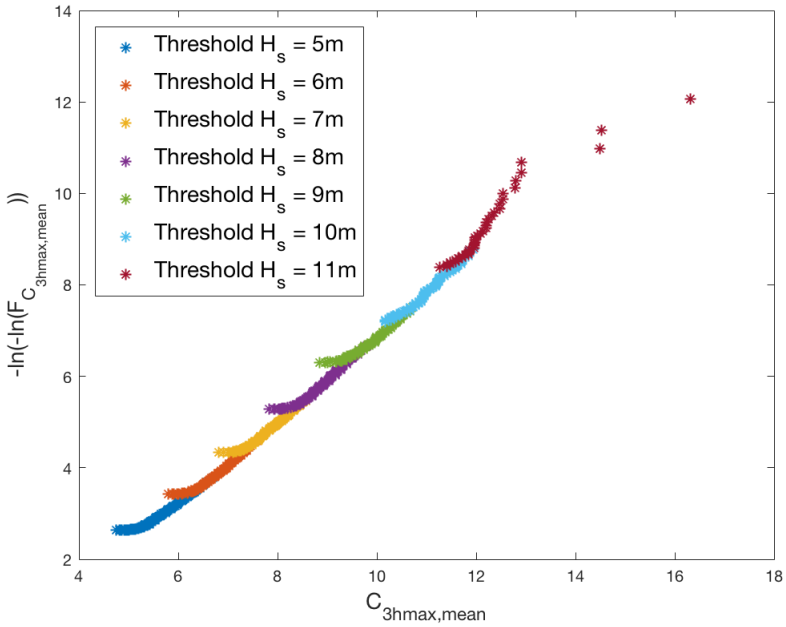

Figure 4.12: For different thresholds all response quantities above the different thresholds are plotted for the median, $F_{C_{3h}}(c) = 0.5$.

In Figure 4.12 the crest height for the median value, $C_{3hmax,mean}$ obtained for $F_{C_{3h}}(c) = 0.5$, is calculated for each sea state instead of using the Monte Carlo simulation. This is done for different thresholds in order to compare how C_{3hmax} behave. From the figure it is evident that it is the highest sea states that are most probable to provide the highest crest heights. Hence, it is the highest sea states that are most important regarding the estimation of $C_{3h,ULS}$. The observations shown for a threshold of $H_s = 11$m are plotted on top of the results obtained for the other thresholds, which means that the results shown for $H_s = 11$m are also part of the results obtained for the lower thresholds. It can also be seen that the Gumbel distribution is a good

model for C_{3h} as a linear line can be approximated for the extremes. The three points that stands out in Figure 4.12 are results of the higher sea states visualized in Figure 4.5. These sea states corresponds to approximately 50 and 200 year return periods, which means that they not necessarily fit the rest of the observations from the hindcast in the curve fitting process.

Still, as seen from Figure 4.7, 4.11 and 4.12 only the upper part of the extremes follow the linear fitted line. The lower extremes flattens out and should not be used in the fitting process. As Figure 4.13 show, fitting the curve to the 30-50% highest extremes gives the same results. This is in accordance with Figure 4.7 because the extremes forms a straight line in the upper range, giving the same fitted line using 30-50% of the highest extremes. However, when all values are included in the curve fitting, the estimate for $C_{3h,ULS}$ becomes higher, approximately 1m. Fitting the curve to the 40% highest extremes is used in the MASS approach for the crest height problem.

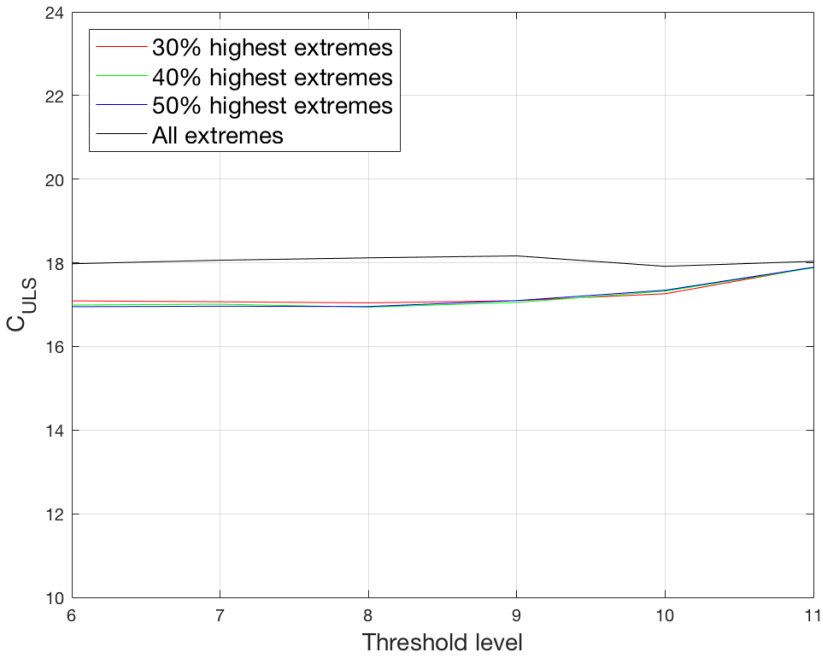

Figure 4.13: ULS crest height for the Gumbel model fitted to the 30%, 40%, 50% and 100 % highest extremes for different thresholds.

4.3.1 Contribution from important sea states

The main objective with the threshold sensitivity study is to decide how high the threshold can be placed without compromising the results. Therefore it is interesting to investigate which sea states that give the most contribution to the exceedance of $C_{3h,ULS}$. The expression for the ULS exceedance probability can be written as per Eq. (4.14).

$$\begin{aligned} 1 - F_{C_{3h}}(c_{3h,ULS}) &= Q_{C_{3h}}(c_{3h,ULS}) \\ &= \int_h \int_t Q_{C_{3h}|H_sT_p}(c_{3h,ULS}|h,t) f_{H_sT_p}(h,t) dh dt \\ &= \sum_{i=1}^{N} \sum_{j=1}^{M} Q_{C_{3h}|H_sT_p}(c_{3h,ULS}|h_i,tj) p_{i,j} \end{aligned} \tag{4.14}$$

$c_{3h,ULS}$ and $Q_{C_{3h}}(c_{3h,ULS})$ are known to be 17.2m and 3.42 $\cdot 10^{-6}$, respectively. $Q_{C_{3h}|H_sT_p}(c_{3h,ULS}|h_i,t_j)$ is the probability of exceeding $c_{3h,ULS}$ in sea state h_i, t_j, and $p_{i,j}$ is the probability for this sea state to occur. By calculating $Q_{C_{3h}|H_sT_p}(c_{3h,ULS}|h_i,tj)$ and $p_{i,j}$ for each sea state i,j in the scatter diagram, the probability contribution to $Q_{C_{3h}}(c_{3h,ULS})$ from each sea state can be found from Eq. (4.15).

$$K(h_i,t_j) = Q_{C_{3h}|H_sT_p}(c_{3h,ULS}|h_i,tj) \cdot p_{i,j} \tag{4.15}$$

To get a better feeling of how large the contribution from each sea state is, the contribution in percent can be found by utilising Eq. (4.16).

$$K(h_i,t_j) = \frac{Q_{C_{3h}|H_sT_p}(c_{3h,ULS}|h_i,tj) \cdot p_{i,j}}{Q_{C_{3h}}(c_{3h,ULS})} \cdot 100 \tag{4.16}$$

The results are plotted in Figure 4.14 and 4.15.

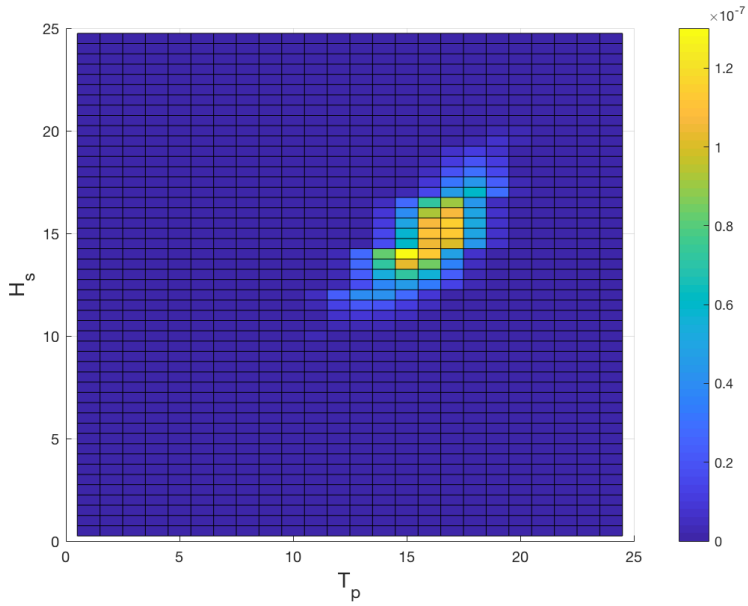

Figure 4.14: Contribution in probability from the sea states to the exceedance of the ULS crest height.

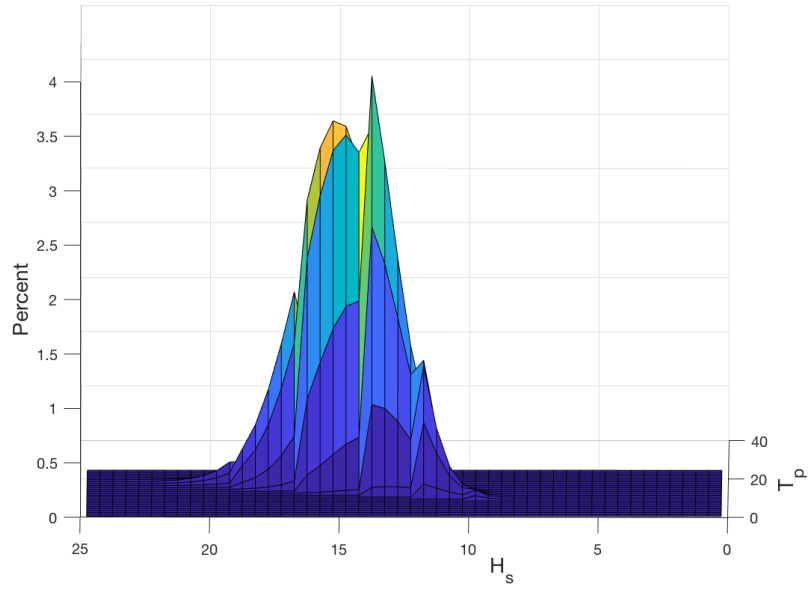

Figure 4.15: Contribution in percent from the sea states to the exceedance of the ULS crest height.

As indicated from Figure 4.14 and 4.15 most of the contribution to $Q_{C_{3h}}(c_{3h,ULS})$ comes from sea states with H_s above 10 meters. This implies that setting the threshold at H_s equal to 9-10 meters should be sufficient to include all sea states that provide contributions to $c_{3h,ULS}$. Figure 4.16 shows contours which include the sea states that give the n percent highest contribution to $Q_{C_{3h}}(c_{3h,ULS})$. The highest contributions to $Q_{C_{3h}}(c_{3h,ULS})$ are found inside the one percent contour. This corresponds to the highest and steepest sea states along the ULS metocean contour line. As the 99.9 percent contour includes only sea states larger than 8.5m, a threshold at 8m should include all important contributions to the ULS crest height. Figure 4.10 confirms that utilizing a threshold at H_s = 8-10m will give nearly the same ULS crest height. In general it can be seen that steep, high sea states give the largest contributions to $c_{3h,ULS}$.

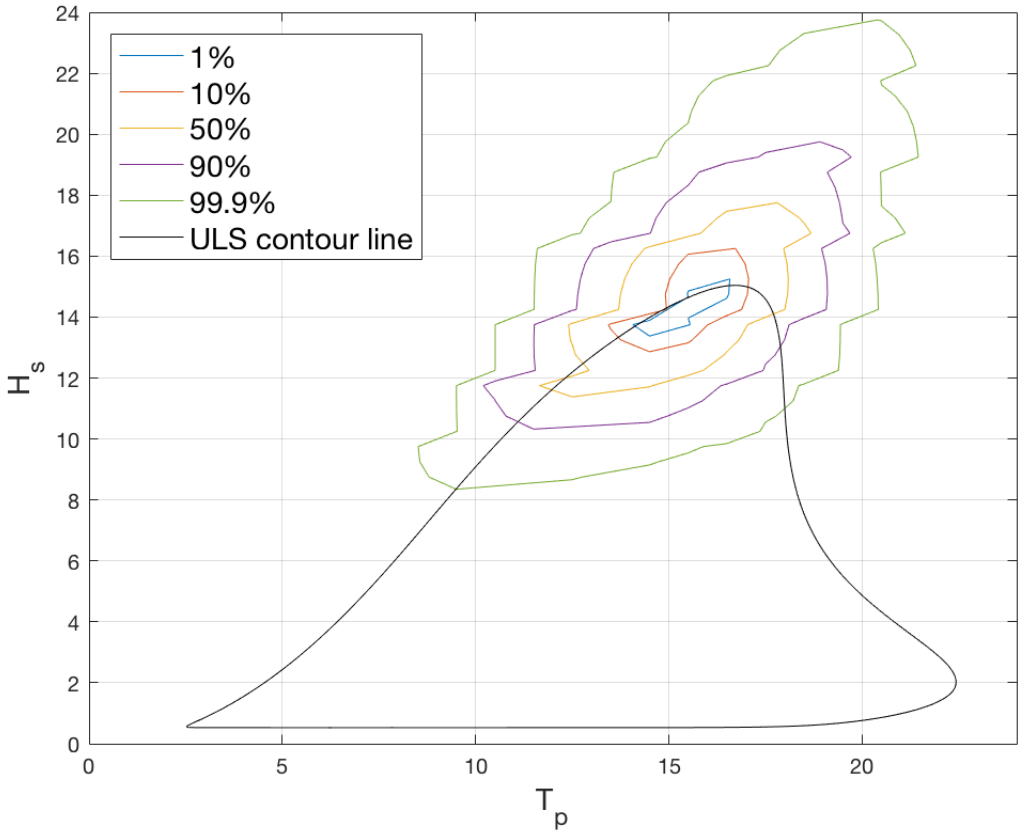

Figure 4.16: Contours showing what sea states that contributes to the exceedance probability of the ULS crest height.

4.4 Comparing $C_{3h,ULS}$ and $C_{3h,ALS}$ for TASS and MASS

The crest heights obtained for ULS and ALS performing the long term analysis using TASS and MASS, are listed in Table 4.6.

Table 4.6: Results obtained for the ULS and ALS crest height utilising the TASS and MASS approach, with a threshold at $H_s = 8$m utilized for MASS.

	TASS	MASS
$C_{3h,ULS}$	17.2m	17.0m
$C_{3h,ALS}$	22.4m	22.3m

The results show that the MASS approach is comparable to the TASS approach. The results obtained from MASS are slightly lower than the results from TASS, which is beneficial keeping in mind that the TASS approach gives conservative results.

Chapter 5

Upwell - Long term analysis only accounting for observed events

5.1 MASS

The upwell problem is, due to the simplified linear analysis given in DNVGL-OTG-13 in principle, suitable for applying TASS. However, the upwell problem requires an analysis where spectra and transfer functions are used to decide the upwell response for each sea state. Considering the large amount of data provided in NORA10 from 1957-2017, it becomes highly time consuming to perform a long term analysis using TASS. Therefore, MASS is suggested as an equally accurate and less time consuming approach to give long term estimates of the 3-hour maximum upwell in ULS, $U_{3h,ULS}$, and ALS, $U_{3h,ALS}$. As mentioned in chapter 3 only the wave frequency upwell, U_{WF}, is considered in this analysis.

The methodology for MASS is outlined for the crest height problem in section 4.2. Still, there are some important modifications performed for the MASS approach used in the upwell analysis. The crest height can be described by a statistical model given H_s and T_p as inputs, which makes it easy to calculate the response when the cumulative probability is known. Unfortunately, there are no statistical model describing the upwell problem. This means that wave spectra and transfer functions have to be utilised in order to calculate the response spectrum and the extreme responses. The procedure of establishing short term extreme upwell responses is outlined

in chapter 3, where U_{3h} can be found through a short term analysis of each sea state. As U_{3h} is found for each sea state above the selected threshold for H_s, a sample with 3-hour extremes are created as a foundation for the long term analysis.

5.1.1 Long term analysis

Since it is assumed that the upwell response is a Gaussian process with Rayleigh distributed local maxima, it follows that the extreme value distribution should asymptotically approach the Gumbel distribution. Local maxima is in this manner defined as the maxima obtained for each zero up-crossing of a narrow-banded process. The sample of the extremes are plotted in a Gumbel probability paper and a linear line is fitted to the 10-40 % of the highest extremes, depending on the chosen threshold. As seen from Figure 5.1 it is only the highest extremes that follow the Gumbel distributed straight line, hence the lower extremes should not be included in the fitting process. Compared to the crest height extremes plotted in Gumbel scale in Figure 4.7, it is seen that there are more upwell extremes that do not follow the linear line fitted to the highest upwell extremes. Therefore, fitting the curve to the 40 % highest extremes, as was done for the crest height problem, might not give correct results. For the upwell problem the percentage of the highest extremes that should be used in the fitting process are dependent on the threshold used in the analysis. When the threshold is set at $H_s = 11$m, a representative fit is obtained using the 30 % highest extremes, while at a threshold of $H_s = 8$m, the best fit is obtained using the 15 % highest extremes. Still, with a smaller percentage, it should be remembered that in this case a lot more extremes are included in the fitting process for $H_s = 8$m (178 extremes) than $H_s = 11$m (12 extremes).

$U_{3h,ULS}$ and $U_{3h,ALS}$ are found by extrapolating the fitted line up to the ULS and ALS probability levels in the Gumbel scale, as shown in Figure 5.1. By creating new samples of U_{3h} and performing the MASS long term analysis 100 times, a good estimate for $U_{3h,ULS}$ and $U_{3h,ALS}$ is obtained by calculating the mean of this sample as shown in Figure 5.2. In this way some of the uncertainties related to the Monte Carlo simulation are decreased.

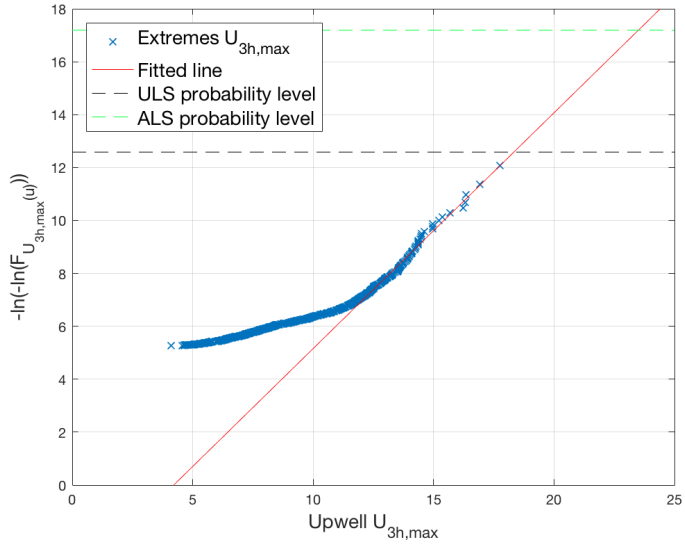

Figure 5.1: Gumbel is fitted to the 15% highest extremes for a threshold at $H_s = 8$m. In addition, extrapolation to the ULS and ALS probability levels is shown.

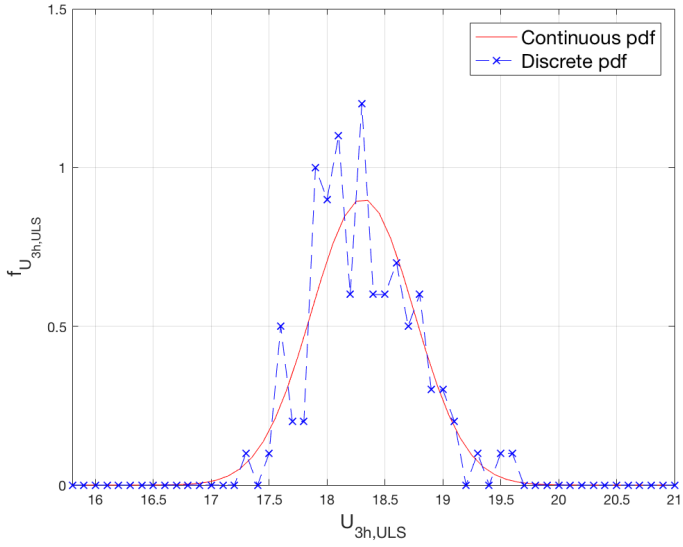

Figure 5.2: Probability density function for the normal distribution of the ULS results for the 100 long term analysis performed using a threshold of $H_s = 8$m. The Gumbel distribution is fitted to the 15% highest extremes.

A Monte Carlo simulation should include enough iterations for the result to converge towards a reliable final estimate. Figure 5.3 shows how many simulations that are needed for the different thresholds before $U_{3h,ULSmean}$ converge. It is seen that 100 simulations are needed to have a completely reliable estimate of $U_{3h,ULSmean}$. Still, if the plot were shown in a larger scale, the differences would be rather small for 20 simulations. However, 100 simulations are used in the further work.

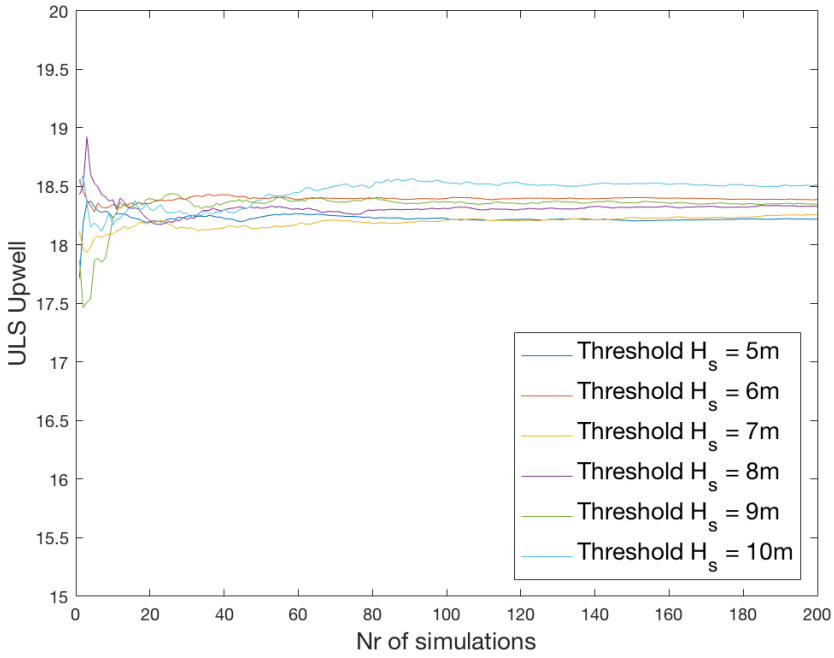

Figure 5.3: Number of simulations needed for the different thresholds for $U_{3h,ULSmean}$ to converge.

5.2 ULS and ALS upwell

Several different cases are used as input to the analysis. They are summarised in Table 5.1. Both the wave conditions, wave spectra and α-factor are changed to see what effect they have on $U_{3h,ULS}$ and $U_{3h,ALS}$.

Table 5.1: Different cases considered in the upwell long term analysis.

Case no.	Sea system	Wave spectrum	α
1	Combined sea	JONSWAP	1.2
2	Total sea	JONSWAP	1.2
3	Wind sea	JONSWAP	1.2
4	Total sea	Torsethaugen	1.2
5	Combined sea	JONSWAP	1.3
6	Total sea	JONSWAP	1.3
7	Wind sea	JONSWAP	1.3
8	Total sea	Torsethaugen	1.3

5.2.1 Case 1 - Combined sea

The main sea system used in this thesis is the combined sea as defined in section 2.2.1. $U_{3h,ULS}$ obtained in combined sea for the important field points under and around the platform are shown in Figure 5.4.

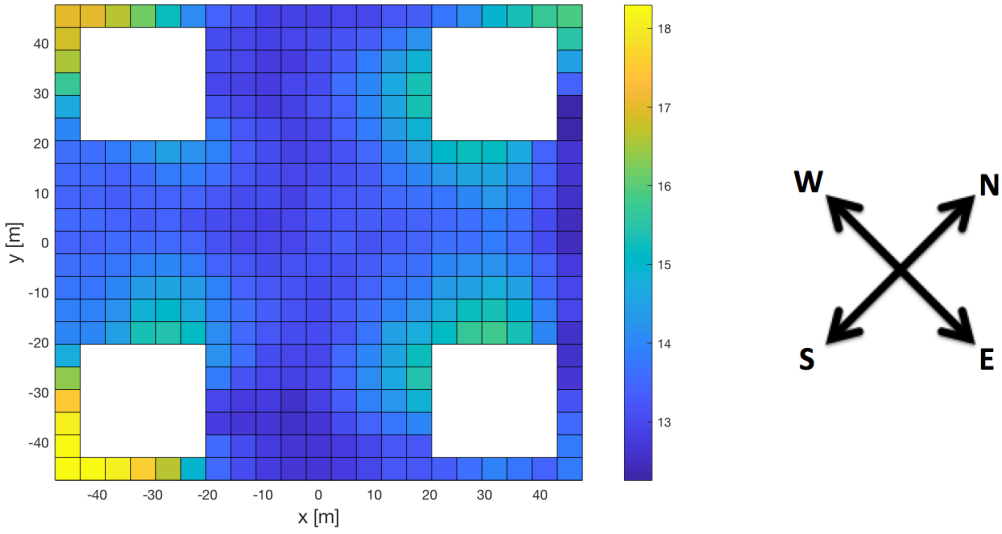

Figure 5.4: ULS upwell for the platform in combined sea with a threshold at $H_s = 8$m and $\alpha = 1.2$. The figure is shown in the platforms coordinate system and the heading compared to the geographical coordinate system is illustrated.

From Figure 5.4 it is obvious that the southwestern and northwestern corners of the platform are the most critical areas, retrieving the highest values for $U_{3h,ULS}$. This corresponds to the geographical south and west, respectively. The results for the northern, western and southern side of the platform are shown in Figure 5.5.

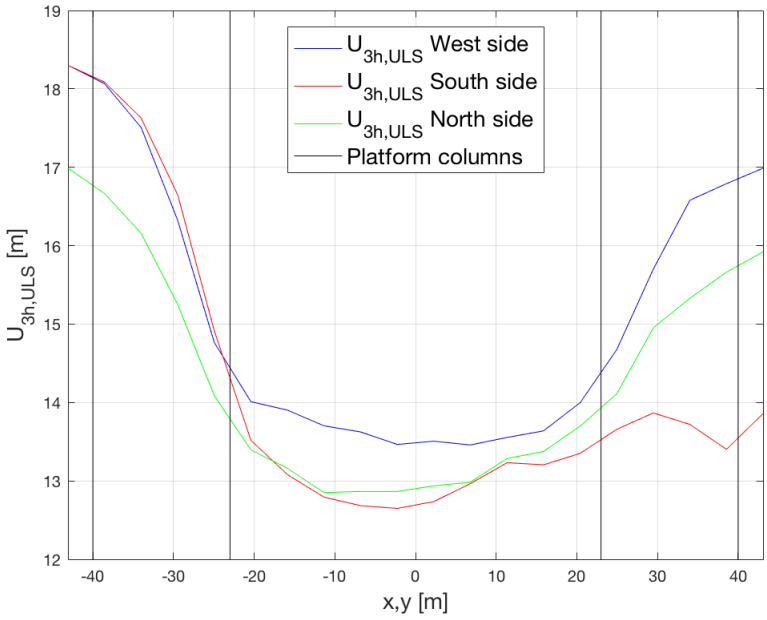

Figure 5.5: The ULS upwell results in combined sea are shown for the northern, western and southern side of the platform with a threshold at H_s = 8m and α = 1.2.

The most severe results are obtained for the field point at the southwest corner of the platform. As the most critical location under the platform will be governing for the design of the still water air gap, the southwestern corner is considered for $U_{3h,ULS}$ and $U_{3h,ALS}$. The results are shown in Table 5.2.

Table 5.2: Results for $U_{3h,ULS}$ and $U_{3h,ALS}$ obtained for the most critical location under the platform in combined sea with a threshold at H_s = 8m.

$U_{3h,ULS}$	18.30m
$U_{3h,ALS}$	23.43m

5.2.2 Case 2 - Total sea

Figure 5.6 shows the difference between $U_{3h,ULS}$ obtained for the different field points under and around the platform in total sea and combined sea. Positive residuals means that the results obtained in total sea are larger than the results obtained in combined sea. In general, utilising total sea in the analysis will give higher results than when combined sea is used. For most of the field points the difference is smaller than 1 meter, except for the points in the northwest corner of the platform, corresponding to the geographic west. In this area total sea gives results that are 1.5 meters larger than combined sea. For the most critical location under the platform located in the southwest corner of the platform, the residual is approximately zero.

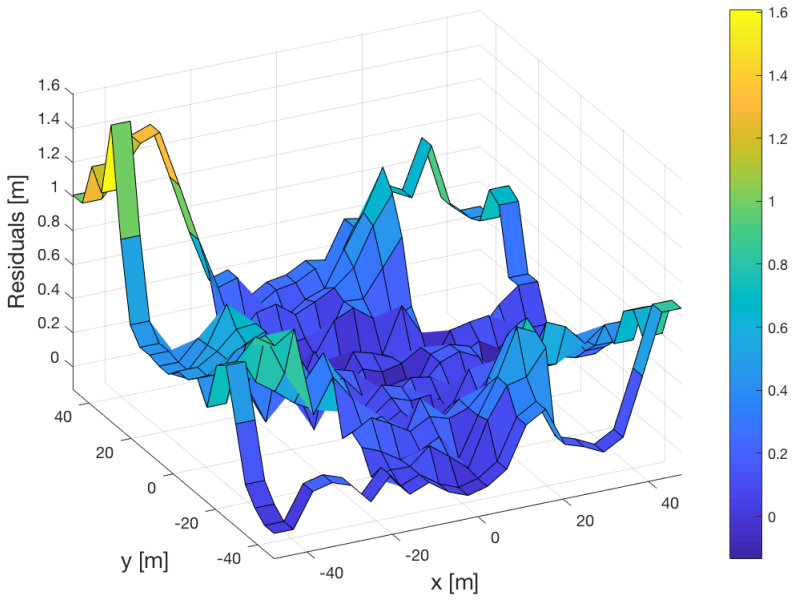

Figure 5.6: Difference between ULS upwell results for the total sea and combined sea with a threshold at $H_s = 8$m and $\alpha = 1.2$. Positive residuals means that the results obtained utilizing total sea are larger than the results obtained using combined sea. The figure is shown in the platforms coordinate system.

The results obtained for $U_{3h,ULS}$ and $U_{3h,ALS}$ for the most critical location under the platform in total sea are listed in Table 5.3.

Table 5.3: Results for $U_{3h,ULS}$ and $U_{3h,ALS}$ obtained for the most critical location under the platform in total sea.

$U_{3h,ULS}$	18.31m
$U_{3h,ALS}$	23.33m

5.2.3 Case 3 - Wind sea

Figure 5.7 shows the difference between $U_{3h,ULS}$ obtained for the different field points under and around the platform in combined sea and wind sea (swell neglected). Positive residuals means that the results obtained in combined sea are larger than the results obtained in pure wind sea. In general, the combined sea seems to give slightly larger results than pure wind sea. However, the difference is rather small, approaching 0.3m as the highest. This means that for the upwell analysis the swell contribution has a minor effect on $U_{3h,ULS}$, and it will give good results to perform the long term analysis in pure wind sea.

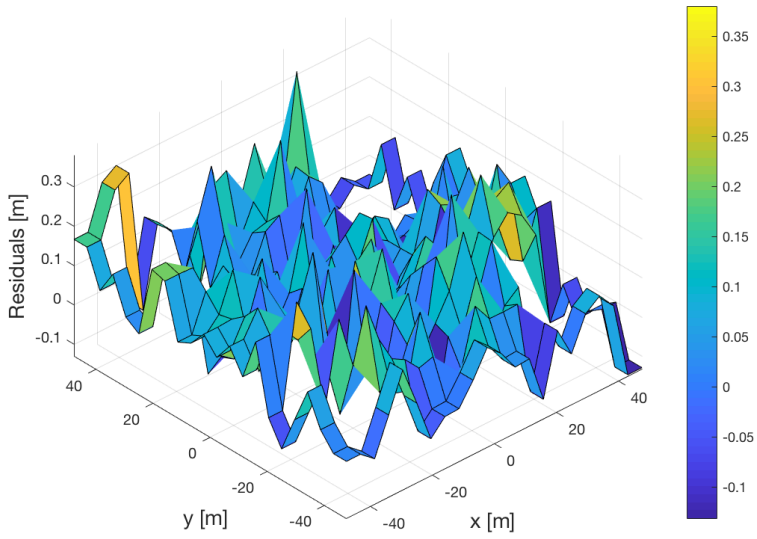

Figure 5.7: Difference between ULS upwell results for the combined sea and pure wind sea with a threshold at $H_s = 8$m and $\alpha = 1.2$. Positive residuals means that the results obtained utilizing the combined sea are larger than the results obtained using only wind sea. The figure is shown in the platforms coordinate system.

The results obtained for $U_{3h,ULS}$ and $U_{3h,ALS}$ for the most critical location under the platform in pure wind sea are listed in Table 5.4.

Table 5.4: Results for $U_{3h,ULS}$ and $U_{3h,ALS}$ obtained for the most critical location under the platform in wind sea.

$U_{3h,ULS}$	18.29m
$U_{3h,ALS}$	23.46m

5.2.4 Case 4 - Torsethaugen total sea

While the JONSWAP spectrum is a one-peaked spectrum, Torsethaugen involve two peaks, including the contributions from wind and swell sea into one spectrum. It is interesting to compare the upwell results when these two wave spectra are used in total sea. The results for $U_{3h,ULS}$ at the most critical location under the platform using the JONSWAP and the Torsethaugen spectra are shown in Table 5.5.

Table 5.5: Results for $U_{3h,ULS}$ and $U_{3h,ALS}$ obtained for the most critical location under the platform utilizing JONSWAP and Torsethaugen wave spectra. An α - factor of 1.2 is utilised.

Wave spectrum	ULS	ALS
JONSWAP	18.31m	23.33m
Torsethaugen	18.86m	23.91m

5.2.5 Case 5-8 - $\alpha = 1.3$

In DNVGL-OTG-13 it is recommended that in some cases a higher alpha factor, $\alpha = 1.3$, is used along the outer edged of the deck box in the up-wave direction, (DNVGL, 2017). As the most critical location under the platform is located at the outer edge in the southwest corner of the platform, the effect on the upwell when applying a higher alpha factor should be investigated. The results for $U_{3h,ULS}$ and $U_{3h,ALS}$ at the most critical location under the platform using $\alpha = 1.3$ are shown in Table 5.6 for the four cases analysed with $\alpha = 1.2$ earlier.

Table 5.6: Results for $U_{3h,ULS}$ and $U_{3h,ALS}$ obtained for the most critical location under the platform in combined, pure wind sea and total sea utilizing both JONSWAP and Torsethaugen spectrum. An α - factor of 1.3 is utilised.

Case no.	ULS	ALS
5	19.59m	25.08m
6	19.63m	25.00m
7	19.50m	24.97m
8	20.23m	25.66m

5.3 POT

The random storm approach, often referred to as the peak-over-threshold (POT) method, uses the observed storms above a given threshold to estimate the long term distribution. The POT approach used in Haver (2017) will be the method performed in this assignment. Due to its ability to capture extreme events based on few observations, the POT method is widely used in hurricane areas, where extreme storms with low frequency of occurring define the environmental conditions. As the ULS and ALS design is governed by the characteristics in the few storms, the POT method is useful because it neglects the sea states below the threshold. It is evident that the choice of threshold is of high importance. The weather on the NCS is characterised by a larger number of storms which are not in the extreme order of hurricanes, leading to less focus on POT approaches. Nevertheless, lately POT has shown to give good results also in the North sea, giving an important alternative to the other long term approaches.

5.3.1 Exact distribution of storm maximum upwell

The hindcast for the actual site is used to create the observed storms based on the definition of storms outlined in section 2.2.5. In order to decide the distribution of the storm maximum response, it is necessary to decide the distribution of the maximum response of each step within the storm. The storm is put together of one or several 3-hour stationary sea states (steps), depending on how many of the adjacent sea states that are above the threshold. It is assumed that the step maximum response follows a Gumbel distribution with parameters $\alpha_{m,k}$ and $\beta_{m,k}$. The distribution of the maximum upwell of step number m in storm k is given by Eq. (5.1).

$$F_{U_m|k}(u|k) = exp\Big(-exp\Big(-\Big[\frac{u-\alpha_{m,k}}{\beta_{m,k}}\Big]\Big)\Big) \tag{5.1}$$

When the distribution function for the 3-hour maximum upwell within each step is found, the storm maximum upwell can be determined. It is assumed that the extremes for the adjacent steps within the storm are statistically independent. According to Jahns et al. (1972) the distribution function of the maximum upwell for storm number k, with M number of steps, can be written as shown in Eq. (5.2).

$$\begin{aligned} F_{U_k|k}(u|k) &= \prod_{m=1}^{M} F_{U_m|k}(u|k) \\ &= \prod_{m=1}^{M} exp\Big(-exp\Big(-\Big[\frac{u-\alpha_{m,k}}{\beta_{m,k}}\Big]\Big)\Big) \\ &= exp\Big(-\sum_{m=1}^{M} exp\Big(-\Big[\frac{u-\alpha_{m,k}}{\beta_{m,k}}\Big]\Big)\Big) \end{aligned} \tag{5.2}$$

The parameters, $\alpha_{m,k}$ and $\beta_{m,k}$, are determined for each step within each storm by the method of moments. For the sea state describing the weather characteristics in a storm step, Monte Carlo simulations are used to derive the mean, $\mu_{m,k}$, and standard deviation, $\sigma_{m,k}$, of the 3-hour maximum upwell, following the short term analysis method outlined in section 3.5. By using Eq. (5.3) $\alpha_{m,k}$ and $\beta_{m,k}$ can be decided.

$$\begin{aligned} \beta_{m,k} &= \frac{\sqrt{6}}{\pi}\sigma_{m,k} \\ \alpha_{m,k} &= \mu_{m,k} - 0.5772\beta_{m,k} \end{aligned} \tag{5.3}$$

5.3.2 Largest value of an arbitrary storm

It is further assumed that every storm in the storm sample have the same probability of occurring. If the total number of observed storms are K, the distribution of the largest value of an arbitrary storm is given by Eq. (5.4).

$$F_{U_{max}}(u) = \frac{1}{K}\sum_{k=1}^{K} exp\Big(-\sum_{m=1}^{M} exp\Big(-\Big[\frac{u-\alpha_{m,k}}{\beta_{m,k}}\Big]\Big)\Big) \tag{5.4}$$

How many storms that occur within a year will vary randomly, hence this can be modelled as a random variable, denoted S. Due to its ability to describe the rate of occurrences within a time interval given the expected rate of occurrence, the Poisson distribution is assumed to be a good model for the random variable, S. The probability mass function is given by Eq. (5.5).

$$p_S(s) = \frac{\rho^s}{s!} exp(-\rho) \tag{5.5}$$

Where ρ is the annual expected number of storms. By assuming that the storm extremes are statistically independent, the distribution function for the annual extreme storm upwell is described by Eq. (5.6), (Haver, 2017).

$$\begin{aligned} F_{U_{annualmax}}(u) &= \sum_s (F_{U_{max}}(u))^s \cdot p_S(s) \\ &= exp(-\rho) \sum_{s=0}^{\infty} \frac{[\rho \cdot F_{U_{max}}(u)]^s}{s!} \\ &= exp(-\rho) exp(\rho \cdot F_{U_{max}}(u)) \\ &= exp(-\rho[1 - F_{U_{max}}(u)]) \\ &= exp\bigg(-\rho\bigg[1 - \frac{1}{K}\sum_{k=1}^{K} exp\bigg(-\sum_{m=1}^{M} exp\bigg(-\bigg[\frac{u-\alpha_{m,k}}{\beta_{m,k}}\bigg]\bigg)\bigg)\bigg]\bigg) \end{aligned} \tag{5.6}$$

5.3.3 ULS and ALS upwell

As the distribution for the annual extreme storm upwell is given, U_{ULS} and U_{ALS} can be found from Eq. (5.7).

$$1 - F_{U_{max}}(u_T) = \frac{1}{T_R} \tag{5.7}$$

Where T_R corresponds to 100 for ULS and 10000 for ALS. Figure 5.8 shows the variance in the results when 100 long term analysis are performed for a threshold at $H_s = 8$m in combined sea. Compared to the MASS approach, the variance in the calculated sample for the ULS values is much smaller for the POT approach.

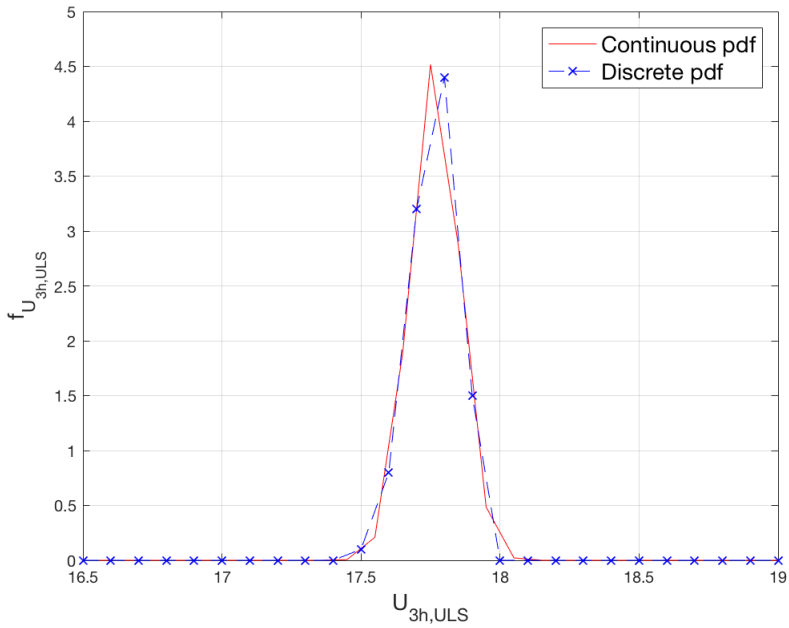

Figure 5.8: Probability density function for the normal distribution of the ULS results for 100 long term POT analysis performed using a threshold of $H_s = 8$m for combined sea.

The results for the most critical location under the platform utilising the different cases as shown in section 5.2 for the MASS approach, are shown in Table 5.7.

Table 5.7: U_{ULS} and U_{ALS} obtained from the POT approach accounting for observed events. A threshold $H_s = 8$m is utilised for the most critical location under the platform, which is the southwestern corner of the platform.

Case no.	ULS	ALS
1	17.79m	22.37m
2	17.92m	22.45m
3	17.72m	22.28m
4	18.42m	23.05m
5	19.01m	23.98m
6	19.17m	24.02m
7	19.01m	24.01m
8	19.75m	24.73m

5.4 Threshold sensitivity study

Extreme crest heights, as considered in chapter 4, are most likely to occur in high and steep sea states. This is not necessarily the case for the extreme upwell. Large sea states will produce large incoming waves, and hence large motions of the semi-submersible. Still, if T_p is sufficiently large, the semi-submersible will follow the waves, and the relative wave elevation, upwell, will not be extremely high. It is assumed that slightly lower, steep sea states are more likely to produce large upwell results, because the semi-submersible will not react fast enough to follow the waves. The inertia of the semi-submersible leads to a phase difference that might be critical, creating extreme upwell results as the wave crest hits the semi-submersible when the semi-submersible is at the lowest position of the oscillating cycle. The results for $U_{3h,ULS}$ from the MASS analysis at the most critical point under the platform are shown for different thresholds for H_s in Figure 5.9. It is clear that setting the threshold at $H_s = 11$m neglects important contributions to $U_{3h,ULS}$. For the lower thresholds, $U_{3h,ULS}$ have stabilised, which means that a threshold at $H_s = 10$m will give reasonable results, according to Figure 5.9.

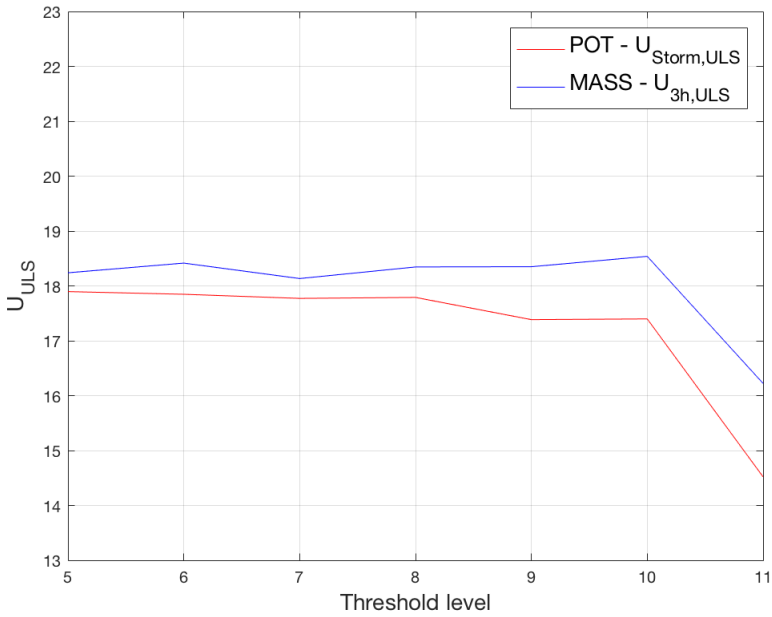

Figure 5.9: The results for $U_{3h,ULS}$ for the most critical location under the platform utilising different thresholds for H_s.

Figure 5.10 reveals why setting the threshold too high for the upwell problem will give non-conservative results. For the crest height problem (see Figure 4.11), the highest sea states in general produced the highest crest heights. This is not the case for the upwell problem, where many of the U_{3h} obtained at a threshold of $H_s = 8$m are larger than the U_{3h} obtained from sea states higher than $H_s = 11$m. In order to decide what threshold that should be used, it is convenient to locate what sea states that give the highest upwell responses. Remember that the ULS probability level is the same for the different thresholds because all sea states are included when the cumulative probability is decided.

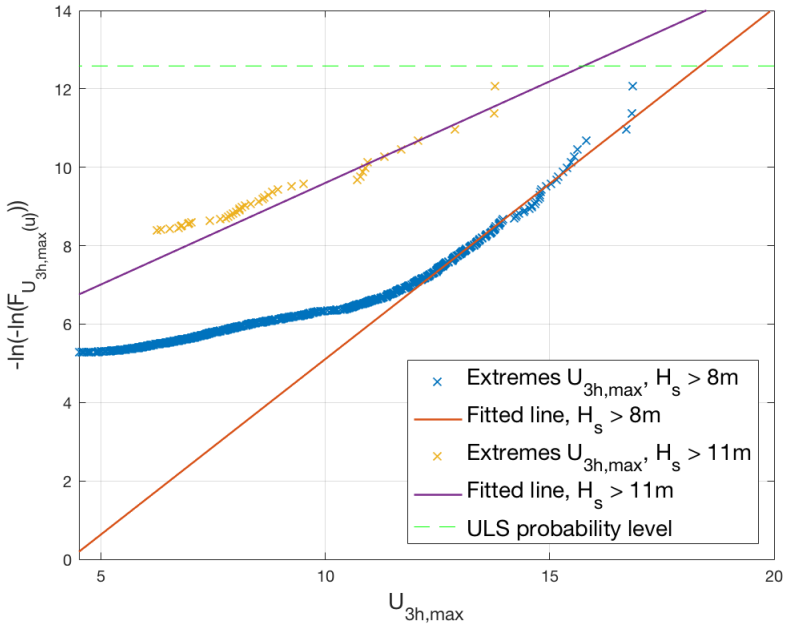

Figure 5.10: Both the empirical short term U_{3h} and the fitted line are shown for the thresholds $H_s = 8$m and $H_s = 11$m.

5.4.1 Finding which sea states that contribute most to the ULS upwell

The analysis is done in the same manner as for the crest height in section 4.3.1, utilising the $U_{3h,ULS}$ value obtained for the MASS approach at the most critical location under the platform with a threshold at $H_s = 8$m. However, as the sea states from the scatter diagram are used, the direction of the

incoming sea is fixed to come from the geographic south in order to compare the contributions to the ULS upwell value for the most critical location under the semi-submersible, which is placed in the southwest corner. This might be misleading because higher sea states that normally come from the geographic west will now be assumed to come from the geographic south. In other words, $U_{3h,ULS}$ which is used to decide $Q_{U_{3h}|H_sT_p}(u_{3h,ULS}|h_i, tj)$ might not be correct when all sea states are assumed to come from the geographic south. Nevertheless, it is assumed that the results will be a reliable pointer to which sea states that are important for the upwell extremes. Figure 5.11 shows contours which include the sea states that gives the n percent highest contribution to $Q_{U_{3h}}(u_{3h,ULS})$. To include the sea states that give the 90 % highest contributions to $Q_{U_{3h}}(u_{3h,ULS})$, sea states all the way down to H_s = 6m should be considered.

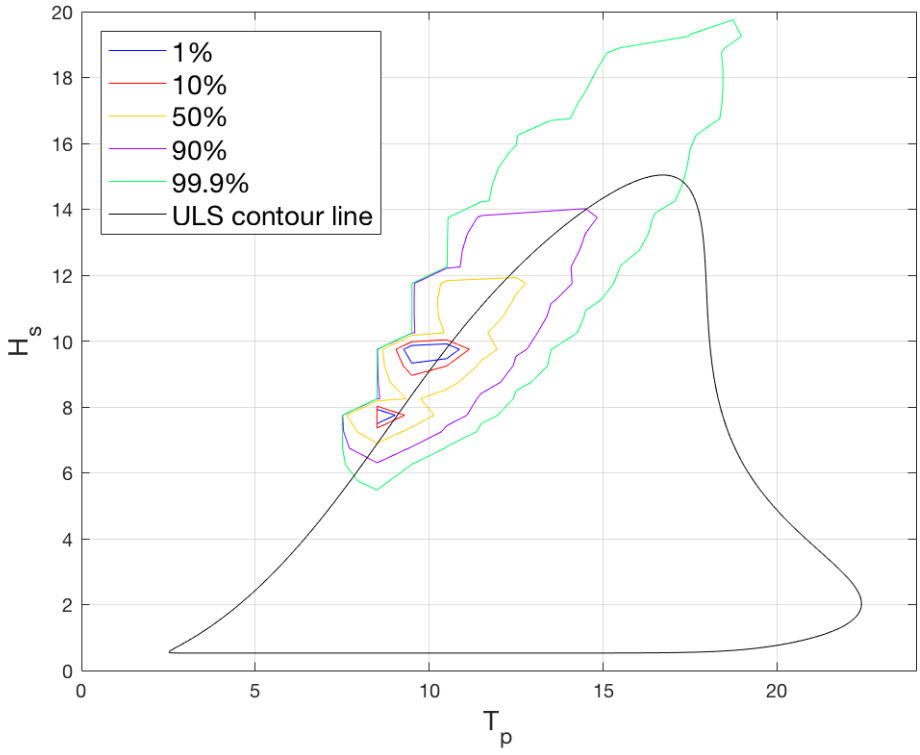

Figure 5.11: Contours showing what sea states that contribute to the exceedance probability of the ULS upwell for the southwestern corner of the platform. All sea states are assumed to come from the south.

The sea states that give the 10 % highest contributions to $Q_{U_{3h}}(u_{3h,ULS})$ are steep sea states with H_s from 7-10m. This means that the results obtained for a threshold $H_s = 10$m in Figure 5.9 should lack important contributions to $U_{3h,ULS}$ and in theory have a lower value. The high value found at a threshold of 10m is a consequence of the same phenomenon as shown for the crest height in Figure 4.11. The lack of sea states that give contributions to extreme 3-hour maximum upwell brings the sample of extremes to a flatter angle, leading to a higher $U_{3h,ULS}$ for the extrapolation of the fitted line. This is also visualised in Figure 5.12, where $U_{3hmax,mean}$ is plotted for all extremes above the different thresholds. It is seen that for thresholds of H_s = 7-8 m and lower, the extremes that create the basis for the curve fitting coincides to some extent and no higher upwell values come from these sea states. This might suggest that the threshold should be placed at $H_s = 8$m.

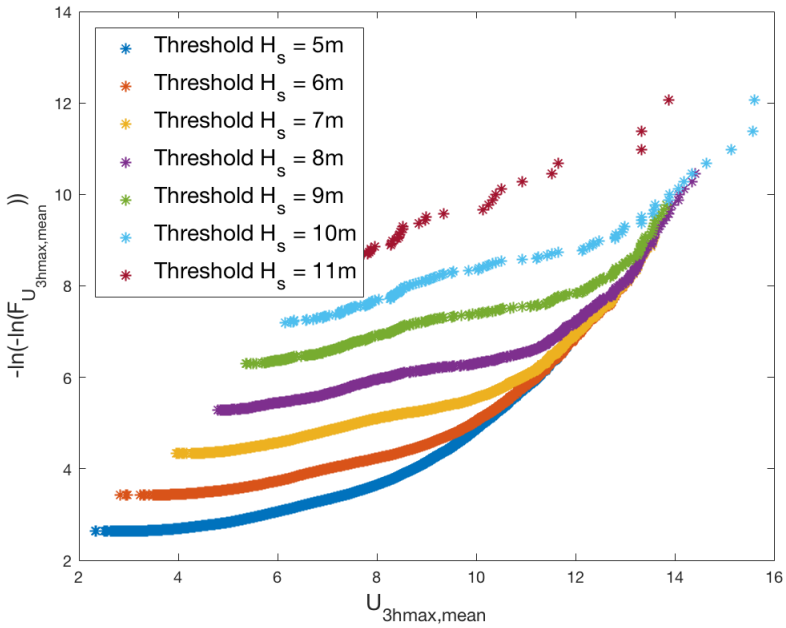

Figure 5.12: For different thresholds all response quantities above the thresholds are plotted for the median, $F_{U_{3h}} = 0.5$.

In Figure 5.13 the random values of U_{3h} utilizing the Monte Carlo simulation in the long term analysis are plotted for the different thresholds. It can be seen that if this long term analysis should be governing for the results, a threshold of $H_s = 7$m should be applied, because it provides the most conservative results.

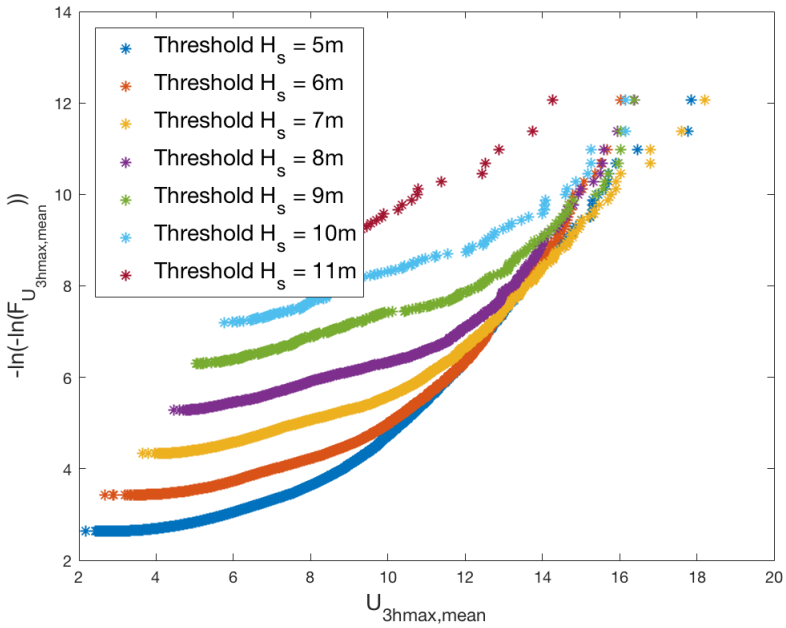

Figure 5.13: For different thresholds all response quantities above the thresholds are plotted for the random variable, $F_{U_{3h}}$ uniformly distributed between 0-1.

Another important aspect to remember is that Figure 5.11 is considering total sea based on $U_{3h,ULS}$ calculated for sea states with $H_{s,tot}$ higher or equal to 8m. The significant wave height of total sea is put together of wind sea and swell sea, $H_{s,tot} = \sqrt{H_{s,w}^2 + H_{s,sw}^2}$. This means that $H_{s,w}$ may be lower than 8m if $H_{s,sw}$ is of significance. The lowest $H_{s,w}$ obtained from the hindcast data with $H_{s,tot} \geq 8$m is 1.9m, combined with $H_{s,sw} = 7.8$m. In fact, 82% of the sea states with $H_{s,tot} \geq 8$m has $H_{s,w}$ between 7-10 meters, while 24% has $H_{s,w}$ between 7-8 meters. Therefore, the important contribution range shown in Figure 5.11 should be more or less covered by the sea states with a threshold of $H_{s,tot} = 8$m.

From Figure 5.11 it is obvious that the most critical sea states regarding upwell are the steepest sea states. It is not necessarily the highest sea states that give the largest upwell results, because the higher sea states are associated with larger T_p, which the platform can respond to and follow in a better way. T_p for the sea states with $H_{s,w}$ between 7-10 meters is low enough so that the platform does not have time to react before the wave has reached the front of the platform.

Figure 5.14 shows accumulated $U_{3h,mean}$ for the median value, $F_{U_{3h}} = 0.5$, for each class in the scatter diagram given in appendix A. However, to include how often the different sea states occur, the accumulated value is found by multiplying n_{3h} with the number of 3-hour sea states observed in each class. Total sea is considered to come from the south. Sea states all the way down to $H_s = 5$m are producing $U_{3h,mean}$ up to 13-14m. However, large upwell contributions to the extreme values from such low sea states are not in accordance with the results from Figure 5.11 and 5.12, and is probably a result of the large number of events observed for these low sea states. Based on the sensitivity study, a threshold of $H_s = 7$-8m should be used for the upwell problem. A threshold at $H_s = 8$m is used in the further work.

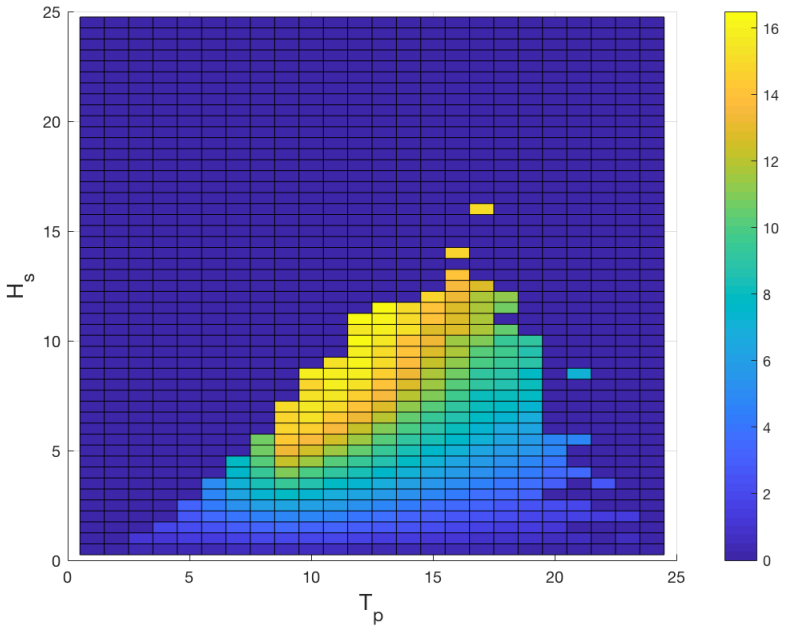

Figure 5.14: Accumulated $U_{3h,mean}$ for the median value, $F_{U_{3h}} = 0.5$, are shown for each class in the scatter diagram. The southwestern corner on the platform are considered. All sea states are assumed to come from the south.

Chapter 6

Upwell - Long term analysis accounting for non-observed events

In chapter 5, the long term analyses were performed based on the observed data from NORA10. The hindcast provided from NORA10 contains data from 1957-2017. This means that 60 years of data form the basis for the observed events. Hence, the 60 year return value can be decided completely based on observed events, if the long term variability of climatic conditions is neglected. For the 100 year return period there are 40 years left with no observations, where severe sea states may occur exceeding the extremes observed in the 60 years of hindcast data already obtained. On the other hand, the ULS value might have occurred in the 60 years already observed. Despite this uncertainty it is assumed that extrapolating to the 100 year return value (ULS) based on the 60 years of observed data will give non-conservative, but nearly reliable results. However, extrapolating to the ALS level (10000 years) based on 60 years of data, gives a rather uncertain ALS value. Most likely the ALS value obtained from the extrapolation will be non-conservative. Therefore, non-observed data has to be accounted for in order to get good estimates for the limit states, especially ALS.

6.1 POT

An important thing to remember is that by only considering the observed storms, important contributions from non-observed storms to the extreme

responses are neglected. A consequence of this is in most cases that the response value is underestimated, especially at ALS level. To account for non-observed storms, Tromans et al. (1995) have postulated that the distribution of the maximum storm response, U, converges to an asymptotic form when considered conditionally upon the most probable largest storm response, $\tilde{U}$. This means that the short term variability is made conditional on the most probable largest maximum upwell, $\tilde{U}$, within an arbitrary storm. By fitting a useful probability model to the observations of $\tilde{U}$, the long term variability of $\tilde{U}$ can be found. Together this forms the long term distribution of the storm maximum upwell as shown in Eq. (6.1).

$$F_U(u) = \int_{\tilde{U}} F_{U|\tilde{U}}(u|\tilde{u}) f_{\tilde{U}}(\tilde{u}) d\tilde{u} \tag{6.1}$$

Where $F_{U|\tilde{U}}(u|\tilde{u})$ represents the short term variability and $f_{\tilde{U}}(\tilde{u})$ is the long term variability. The POT approach as outlined in Haver (2017) and Sandbakken (2017), will be performed in the following accounting for non-observed events.

6.1.1 Short term variability $F_{U|\tilde{U}}(u|\tilde{u})$

The exact distribution of the storm maximum upwell found in Eq. (5.2) can be approximated to a Gumbel distribution, as seen in Eq. (6.2), (Haver, 2017).

$$F_{U_s|storm}(u|storm) \approx exp(-exp(-\left[\frac{u-\tilde{u}}{\beta_s}\right])) \tag{6.2}$$

$\tilde{u}$ is equal to the most probable largest value of the exact storm distribution and can be found for each storm. This is done by solving $\frac{d^2 F_{U_s|storm}(u|storm)}{dx^2} = 0$ numerically in MATLAB, which is the location where the pdf reaches its maximum. By plotting the exact storm distribution in Gumbel scale, β_s can be decided from the slope of the curve in the origin, (Sandbakken, 2017). Examples of the comparison between the exact and approximated storm distributions are shown in Figure 6.1.

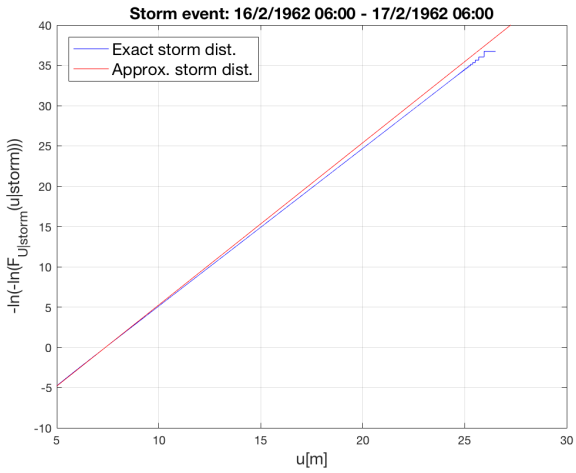

(a)

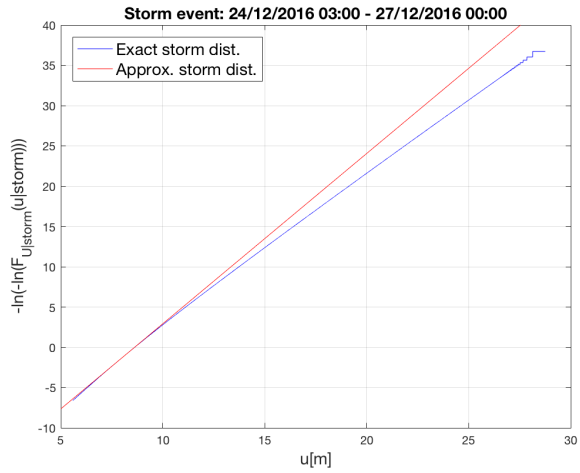

(b)

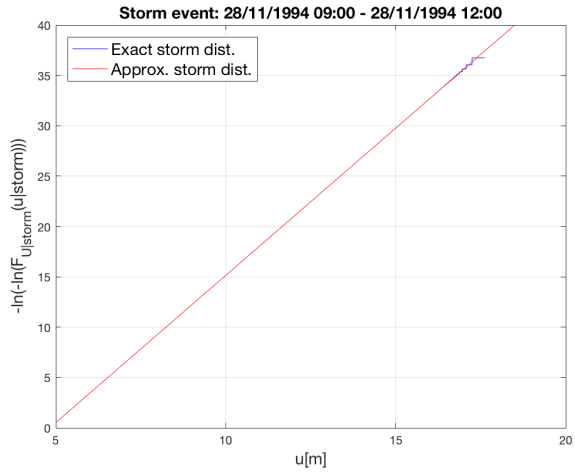

(c)

Figure 6.1: The exact storm distribution and the approximated Gumbel distribution is plotted for three storms.

For a normal storm as shown in (a) the approximated Gumbel distribution represents the exact storm distribution in a good way. However, for the longest storm found in the hindcast as shown in (b), the approximated Gumbel distribution deviates quite much from the exact storm distribution for large values. At ULS level the approximation seems to be acceptable, while the difference on ALS level corresponds to 1-2 meters. This is of concern as the approximated distribution gives non-conservative results.

In (c) the approximated Gumbel distribution replicates the exact storm distribution. This is because this storm is modelled as one stationary sea state.

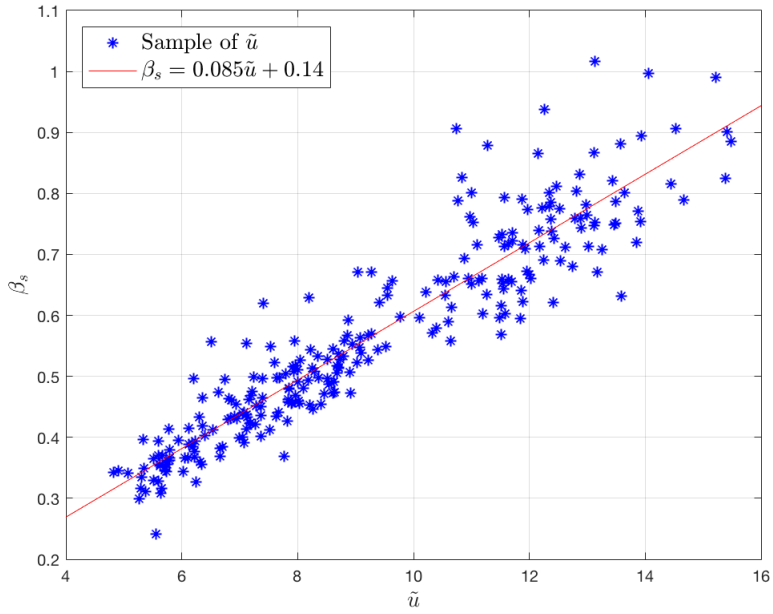

Figure 6.2: β_s is plotted against $\tilde{u}$ to show the linear relationship forming β_v.

As Eq. (6.2) is only valid for each storm, an expression has to be established that yields an arbitrary storm. This is done by the transformation $\beta_v = \frac{\beta_s}{\tilde{u}}$, where β_v is usable for an arbitrary storm. From Figure 6.2 it is evident that the relationship between β_s and $\tilde{u}$ is linear, which makes the expression for β_v valid. The final expression for the distribution of an arbitrary storm maximum upwell is as shown in Eq. (6.3).

$$F_{U|\tilde{U}}(u|\tilde{u}) = exp(-exp(-\left[\frac{u-\tilde{u}}{\beta_v \tilde{u}}\right])) \tag{6.3}$$

β_v is calculated for all storms. When plotted towards $\tilde{u}$ as in Figure 6.3, it is clearly seen that the scatter is large. According to Sandbakken (2017), the mean value of β_v should be used when no trend is observed in the data.

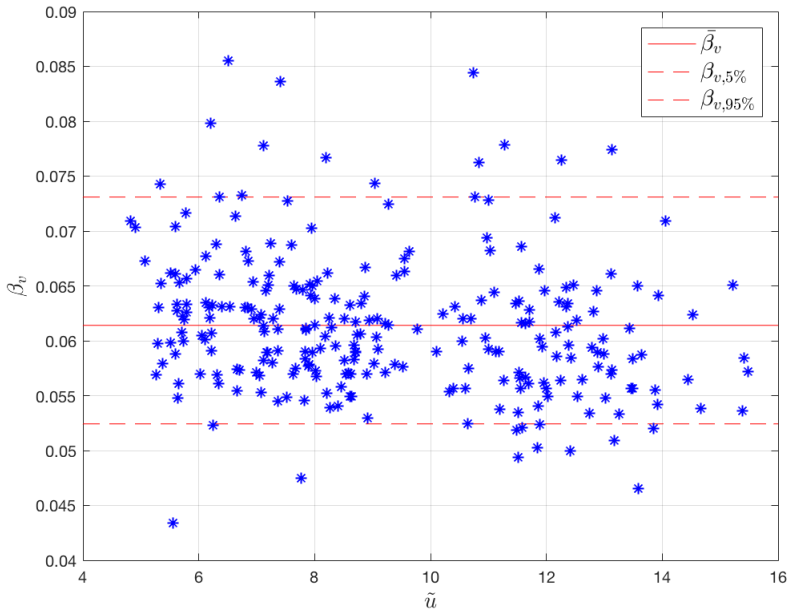

Figure 6.3: β_v is plotted against $\tilde{u}$ to find the mean value of β_v

The mean value is found together with the 90-percentiles in Table 6.1.

Table 6.1: Results obtained for $\bar{\beta}_v$ and the corresponding 90-percentiles.

$\bar{\beta}_v$	0.061
$\beta_{v,5\%}$	0.052
$\beta_{v,95\%}$	0.073

6.1.2 Long term variability $F_{\tilde{U}}(\tilde{u})$

In order to account for the long term variability, a probabilistic model can be fitted to the sample of $\tilde{u}$. According to Sandbakken (2017), a 3-parameter Weibull distribution should be a reasonable model for the long term distribution of the storm probable maximum. The parameters $\alpha_{\tilde{u}}$, $\beta_{\tilde{u}}$ and $\lambda_{\tilde{u}}$ are estimated by the method of moments, using the sample mean, variance and skewness. First $\beta_{\tilde{u}}$ is found by iteration of Eq. (6.4). Subsequently, $\alpha_{\tilde{u}}$ and $\lambda_{\tilde{u}}$ are found.

$$\begin{aligned}
\gamma_{\tilde{u}} &= \frac{\Gamma(1+\frac{3}{\beta_{\tilde{u}}}) - 3\Gamma(1+\frac{1}{\beta_{\tilde{u}}})\Gamma(1+\frac{2}{\beta_{\tilde{u}}}) + 2\Gamma^3(1+\frac{1}{\beta_{\tilde{u}}})}{[\Gamma(1+\frac{2}{\beta_{\tilde{u}}}) - \Gamma^2(1+\frac{1}{\beta_{\tilde{u}}})]^{\frac{3}{2}}} \\
\sigma_{\tilde{u}}^2 &= \alpha_{\tilde{u}}^2\left[\Gamma(1+\frac{2}{\beta_{\tilde{u}}}) - \Gamma^2(1+\frac{1}{\beta_{\tilde{u}}})\right] \\
\mu_{\tilde{u}} &= \lambda_{\tilde{u}} + \alpha_{\tilde{u}}\Gamma(1+\frac{1}{\beta_{\tilde{u}}})
\end{aligned} \tag{6.4}$$

The modelled 3-parameter Weibull distribution is plotted together with the sample values for the most probable largest storm upwell in Figure 6.4. It is seen from the figure that the 3-parameter Weibull distribution represents the true distribution well for higher values of $\tilde{u}$. The fit is rather poor for lower values of $\tilde{u}$, but since extremes are considered, this is not of concern.

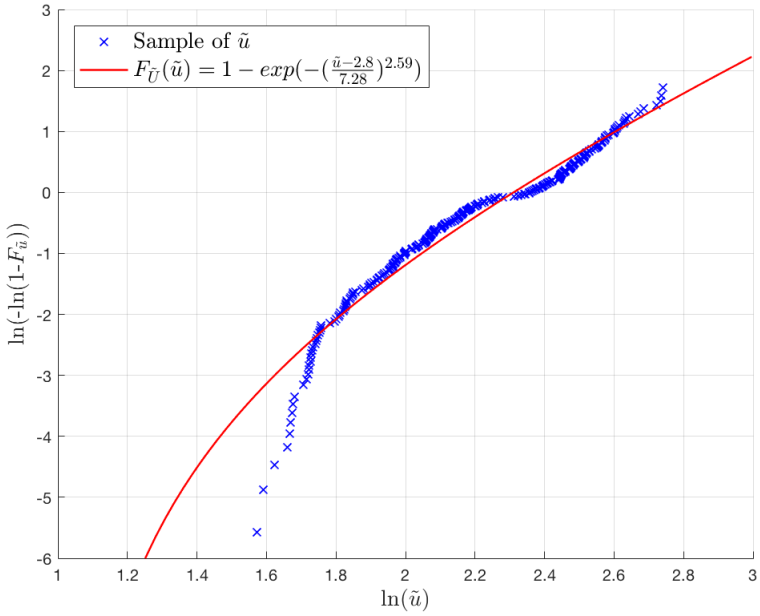

Figure 6.4: The fitted 3-parameter Weibull model is plotted together with the sample of most probable largest storm maxima.

6.1.3 Long term analysis

When the long term distribution, $F_U(u)$, in Eq. (6.1) is decided, extreme upwell values corresponding to given return values can be calculated. The

q-probability maximum upwell corresponding to the return period of T_R years, $q = \frac{1}{T_R}$, is decided from Eq. (6.5).

$$1 - F_U(u_q) = \frac{q}{N_s} \tag{6.5}$$

Where N_s is the expected number of storms above the selected threshold per year. Solving the long term integral numerically might be a rather cumbersome approach. Therefore, inverse first-order reliability method (IFORM), is used as an effective approach to perform the long term analysis.

IFORM

Reliability theory assumes that failure occurs when a limit state becomes negative, as per Eq. (6.6).

$$g(U, \tilde{U}, u_{crit}) = u_{crit} - U(\tilde{U}) < 0 \tag{6.6}$$

Where $\tilde{U}$ is included since U is made conditionally on $\tilde{U}$. The value u_{crit} separates the safe set from the failure set. Hence, the probability of failure can be expressed as in Eq. (6.7).

$$p_f(u_{crit}) = \iint_{g(U,\tilde{U},u_{crit})<0} F_{U|\tilde{U}}(u|\tilde{u}) f_{\tilde{U}}(\tilde{u}) du d\tilde{u} \tag{6.7}$$

By making u_{crit} the desired return value and $p_f(u_{crit})$ the probability of exceeding the return value, the ULS and ALS upwell results can be determined. As the probability of exceeding the ULS and ALS value, $p_f(u_{ULS})$ and $p_f(u_{ALS})$, is known, the IFORM approach presented in Winterstein et al. (1993) should be used to find u_{ULS} and u_{ALS}. It is convenient to transform the integral in Eq. (6.7) from the physical space to the standard Gaussian space. This is done using the transformations proposed by Rosenblatt (1952), which in this case means performing the transformations given in Eq. (6.8), (Madsen et al., 2006).

$$\begin{aligned} \Phi(u_1) &= F_{\tilde{U}}(\tilde{u}) \quad &\Longleftrightarrow \quad u_1 &= \Phi^{-1}[F_{\tilde{U}}(\tilde{u})] \\ \Phi(u_2) &= F_{U|\tilde{u}}(u|\tilde{u}) \quad &\Longleftrightarrow \quad u_2 &= \Phi^{-1}[F_{U|\tilde{U}}(u|\tilde{u})] \end{aligned} \tag{6.8}$$

The advantage of performing the transformations is that when the annual target probabilities are known, the radius, r, of the corresponding circles

with constant probability in the standard Gaussian space are known. This means that the exceedance probability for a given return period can be written as shown in Eq. (6.9).

$$p_r = 1 - \Phi(r) = \Phi(-r) \tag{6.9}$$

When the exceedance probability related to the q-probability maximum upwell is known, the radius of the circle showing constant probability of exceedance can be found from Eq. (6.10).

$$r = -\Phi^{-1}(p_r) = -\Phi^{-1}(\frac{q}{2920}) \tag{6.10}$$

When the radius of the circle is found, e.g. $r_{ULS} = -\Phi^{-1}(\frac{0.01}{2920}) = 4.5$, all combinations of u_1 and u_2 are defined for the given return period. To determine the q-probability maximum upwell, U, the circles must be transformed back to the physical space by using Eq. (6.8). A combination of U and $\tilde{U}$ is found for each combination of u_1 and u_2. This gives the foundation for the contours in the physical space.

6.1.4 ULS an ALS upwell

The ULS and ALS contour lines for combinations of U and $\tilde{U}$ are shown in Figure 6.5 utilizing $\bar{\beta}_v$ as listed in Table 6.1. To indicate the sensitivity of $\bar{\beta}_v$ on the results, the contours using the 90-percentiles for $\bar{\beta}_v$ are plotted. U_{ULS} and U_{ALS} are found as the highest values for U along the respective contours. The results are listed in Table 6.2.

Table 6.2: Results obtained for U_{ULS} and U_{ALS} utilizing the POT approach accounting for non-observed events. The results for $\tilde{U}$ (neglecting short term variability) are also indicated.

	U_{ULS}	U_{ALS}	$\tilde{U}_{ULS}$	$\tilde{U}_{ALS}$
$\bar{\beta}_v$	18.84m	24.35m	17.42m	20.96m
$\beta_{v,5\%}$	18.49m	23.49m		
$\beta_{v,95\%}$	19.35m	25.57m		

The results show that ALS is more sensitive to $\bar{\beta}_v$ than ULS. However, neither ULS nor ALS show large scatter in the results for the 90-percentile. In addition, the ULS and ALS results for $\tilde{u}$ (neglecting short term variability) are provided in Table 6.2. It is noticed that the short term variability is of

high importance for the results, contributing with 1.4m in ULS and 3.6m in ALS.

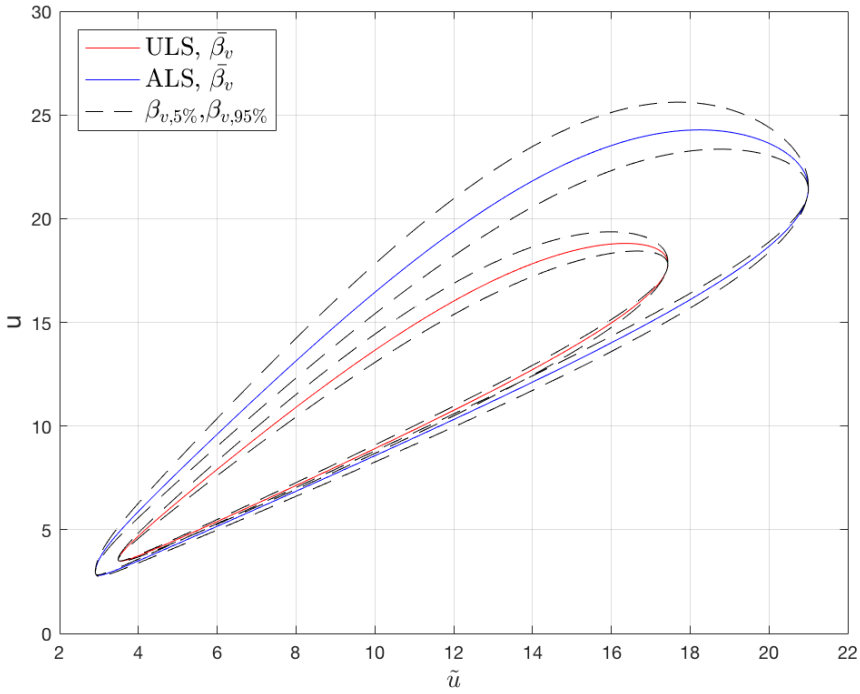

Figure 6.5: The ULS and ALS contour lines showing the relationship between U and $\tilde{U}$.

The results obtained for the most critical location under the platform for the different cases defined in section 5.2 are listed in Table 6.3. Compared to the results obtained for the POT method only accounting for observed sea states, the results are in general 1m higher (5-6 % increase) for ULS and 2m higher (8-9 % increase) for ALS. As expected accounting for non-observed events has the largest effect on ALS level.

Table 6.3: U_{ULS} and U_{ALS} obtained from the POT approach accounting for non-observed events. A threshold H_s = 8m is utilised for the most critical location under the platform, which is the southwestern corner of the platform.

Case no.	ULS	ALS
1	18.84m	24.35m
2	18.87m	24.21m
3	18.87m	24.43m
4	19.20m	24.48m
5	20.06m	25.87m
6	20.08m	25.72m
7	20.08m	25.93m
8	20.47m	26.04m

6.2 MASS

In general the ASS approach is a method that considers all sea states from a given hindcast, observed events. As discussed for the POT approach neglecting non-observed events will in most cases give a non-conservative result for ULS and ALS. Therefore, the method used for the POT approach in section 6.1 will be used for the MASS approach to see if it is a suitable method to account for non-observed events for the ASS approach as well.

MASS considers independent sea states instead of storms. Hence the distribution of the maximum 3-hour upwell, U, is assumed to converge to an asymptotic form when considered conditionally upon the most probable largest 3-hour upwell, $\tilde{U}$, (Tromans et al., 1995). The short term variability is made conditional on $\tilde{U}$ within an arbitrary sea state. The long term variability of $\tilde{U}$ is found by fitting a useful probability model to the observations of $\tilde{U}$. In the end this leads to solving the same long term distribution as found in Eq. 6.1, but accounting for 3-hour sea states instead of storms.

6.2.1 Short term variability $F_{U|\tilde{U}}(u|\tilde{u})$

The exact distribution of the 3-hour sea state maximum upwell found in Eq. (5.2) can be approximated to a Gumbel distribution, as seen in Eq. (6.11), (Haver, 2017).

$$F_{U_{ss}|seastate}(u|seastate) \approx exp(-exp(-\left[\frac{u-\tilde{u}}{\beta_s}\right])) \tag{6.11}$$

$\tilde{u}$ is equal to the most probable largest value of the exact 3-hour maximum distribution and can be found for each sea state. This is done by solving $\frac{d^2F_{U_s|seastate}(u|seastate)}{dx^2} = 0$ numerically in MATLAB, which is the location where the pdf reaches its maximum. However, as each $\tilde{u}$ is related to a 3-hour stationary sea state, the approximated Gumbel distribution will reproduce the exact 3-hour maximum distribution correctly as shown in Figure 6.6.

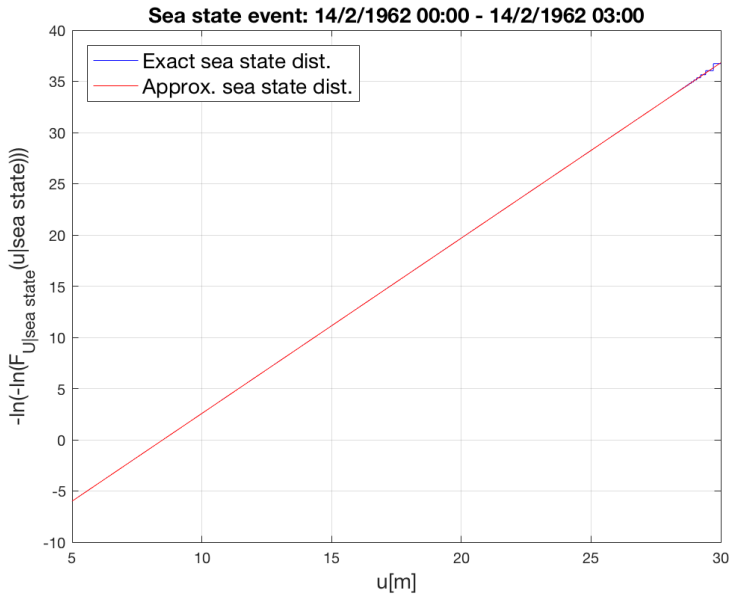

Figure 6.6: The exact sea state distribution and the approximated Gumbel distribution is plotted for a given sea state.

By plotting the exact storm distribution in Gumbel scale as shown in Figure 6.6, β_s can be decided from the slope of the curve in the origin. However, as Eq. (6.2) is only valid for each sea state, an expression has to be established that yields an arbitrary sea state. This is done by the transformation $\beta_v = \frac{\beta_s}{\tilde{u}}$, where β_v is usable for an arbitrary sea state. From Figure 6.7 it is evident that the relationship between β_s and $\tilde{u}$ is linear, which makes the expression for β_v valid. The final expression for the distribution of an arbitrary sea state maximum upwell is as shown in Eq. (6.12).

$$F_{U|\tilde{U}}(u|\tilde{u}) = exp(-exp(-\left[\frac{u-\tilde{u}}{\beta_v \tilde{u}}\right])) \tag{6.12}$$

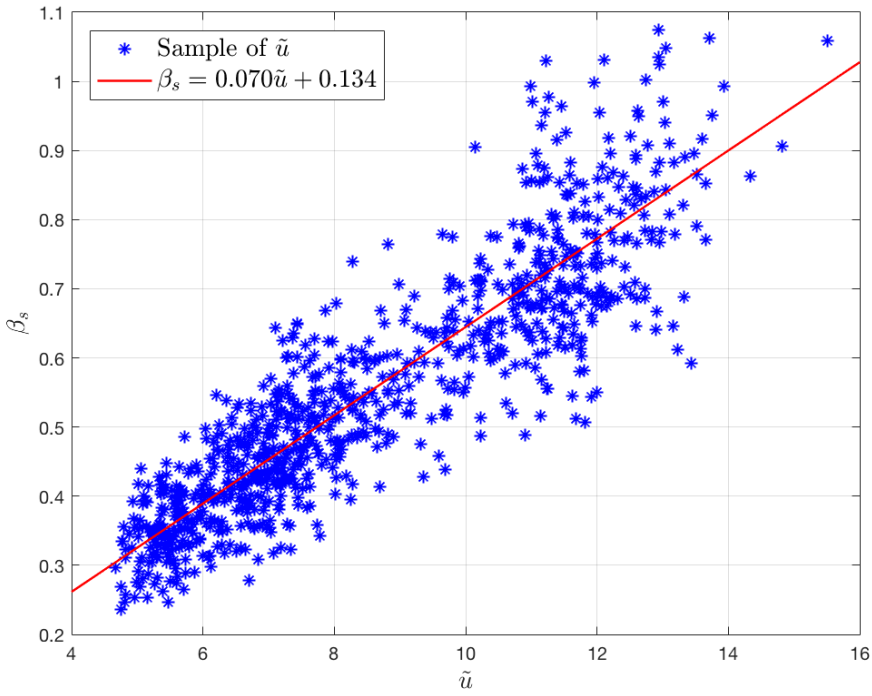

Figure 6.7: β_s is plotted against $\tilde{u}$ to show the linear relationship forming β_v.

β_v is calculated for all sea states. When plotted towards $\tilde{u}$ as in Figure 6.8, it is clearly seen that the scatter is large. According to Sandbakken (2017), the mean value of β_v should be used when no trend is observed in the data.

The mean value is found together with the 90-percentiles in Table 6.4.

Table 6.4: Results obtained for $\bar{\beta_v}$ and the corresponding 90-percentiles.

$\bar{\beta_v}$	0.065
$\beta_{v,5\%}$	0.050
$\beta_{v,95\%}$	0.080

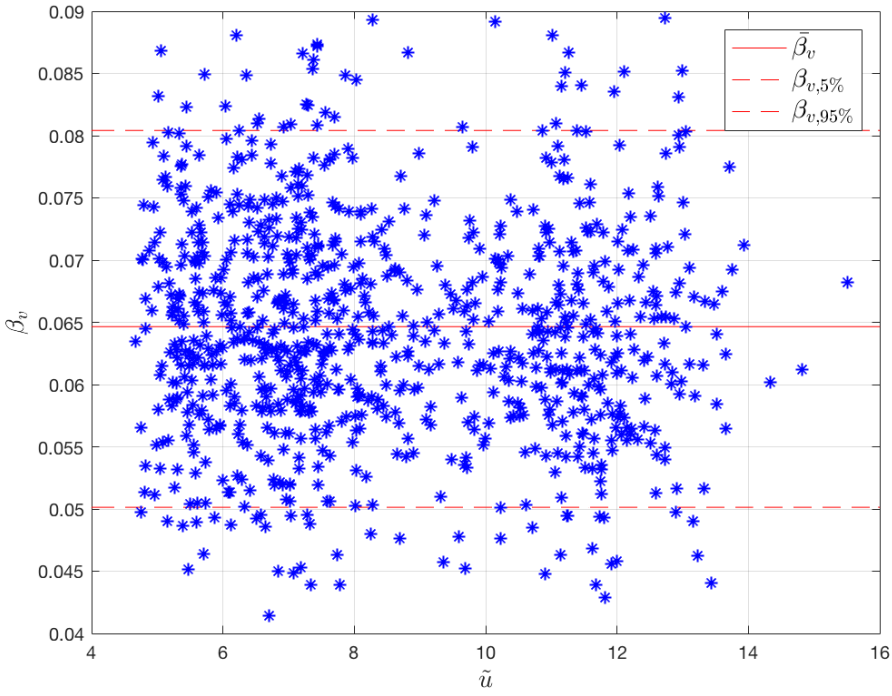

Figure 6.8: β_v is plotted against $\tilde{u}$ to find the mean value of β_v.

6.2.2 Long term variability $F_{\tilde{U}}(\tilde{u})$

In order to account for the long term variability, a probabilistic model can be fitted to the sample of $\tilde{u}$. It is assumed that a 3-parameter Weibull distribution is a reasonable model for the long term distribution of the 3-hour sea state probable maximum. The parameters $\alpha_{\tilde{u}}$, $\beta_{\tilde{u}}$ and $\lambda_{\tilde{u}}$ are estimated by the method of moments in the same way as for the POT approach in section 6.1.2. The modelled 3-parameter Weibull distribution is plotted together with the sample values for the most probable largest 3-hour sea state upwell in Figure 6.9. It is seen from the figure that the 3-parameter Weibull distribution represents the true distribution in a satisfactory manner for higher values of $\tilde{u}$. The fit is rather poor for lower values of $\tilde{u}$, but since extremes are considered, this is not of concern.

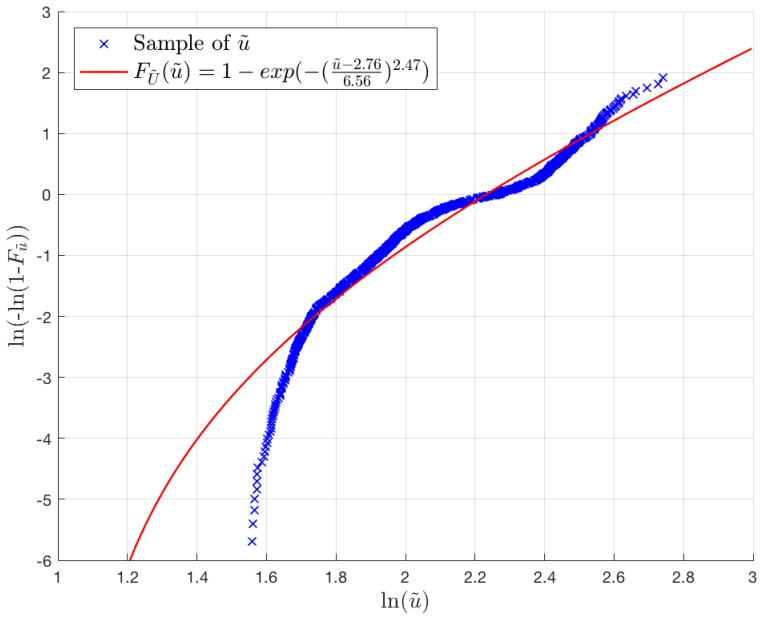

Figure 6.9: The fitted 3-parameter Weibull model is plotted together with the sample of most probable largest sea state maximum.

6.2.3 ULS an ALS upwell

The ULS and ALS contour lines for combinations of U and $\tilde{U}$ are shown in Figure 6.10 utilizing $\bar{\beta}_v$ as listed in Table 6.4. To indicate the sensitivity of $\bar{\beta}_v$ on the results, the contours using the 90-percentiles for $\bar{\beta}_v$ are plotted. U_{ULS} and U_{ALS} are found as the highest values for U along the respective contours. The results are listed in Table 6.5. The results show that ALS is more sensitive to $\bar{\beta}_v$ than ULS. However, neither ULS nor ALS show large scatter in the results for the 90-percentile. It is noticed that the short term variability is of high importance for the results, contributing with 2m in ULS and 4m in ALS.

Table 6.5: Results obtained for U_{ULS} and U_{ALS} utilizing the POT approach accounting for non-observed events. The results for $\tilde{U}$ are also indicated.

	U_{ULS}	U_{ALS}	$\tilde{U}_{ULS}$	$\tilde{U}_{ALS}$
$\bar{\beta}_v$	19.23m	24.64m	17.34m	20.53m
$\beta_{v,5\%}$	18.55m	23.11m		
$\beta_{v,95\%}$	20.10m	26.46m		

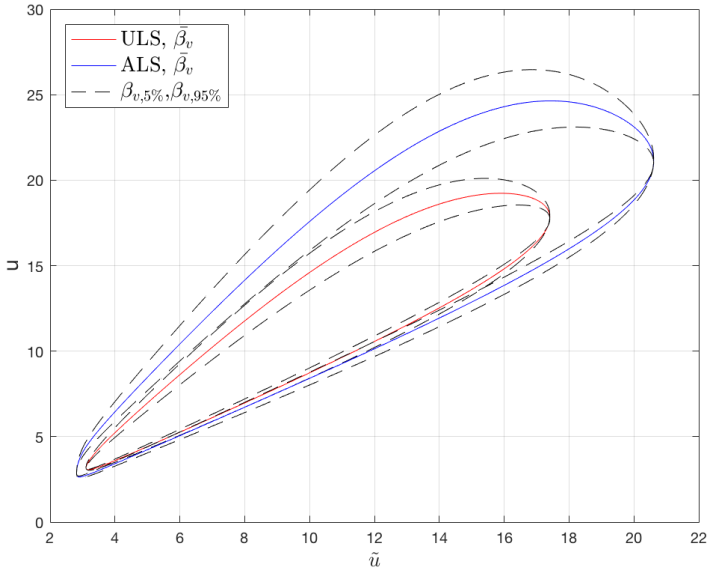

Figure 6.10: The ULS and ALS contour lines are shown for combinations of U and $\tilde{U}$.

The results obtained for the most critical location under the platform for the different cases defined in section 5.2 are listed in Table 6.6. Compared to the results obtained for the MASS approach only accounting for observed sea states, the results are in general 1m higher (5-6 % increase) for ULS and 1.2m higher (5-6 % increase) for ALS.

Table 6.6: U_{ULS} and U_{ALS} obtained from the MASS approach accounting for non-observed events. A threshold H_s = 8m is utilised for the most critical location under the platform, which is the southwestern corner of the platform.

Case no.	ULS	ALS
1	19.24m	24.65m
2	19.23m	24.53m
3	19.30m	24.75m
4	19.55m	24.73m
5	20.46m	26.17m
6	20.44m	26.02m
7	20.51m	26.25m
8	20.84m	26.31m

Chapter 7

Metocean contour lines - upwell

The metocean contour line method, MCL, is a simplified long term approach that reveals a possibility for estimating long term extremes without carrying out a full long term analysis. This is especially useful for complex response problems where time domain simulations or model tests are needed to establish the short term distribution of extremes. As a consequence of performing the simplified linear analysis approach, the upwell problem is described by spectra and transfer functions in the frequency domain. Hence, the short term distribution of extremes can be found relatively easily, and the upwell response problem may in this case not be characterised as a complex problem. Nevertheless, it is useful as a comparison and validation of the MCL to study how $U_{3h,ULS}$ and $U_{3h,ALS}$ become compared to the results from the MASS and POT.

The MCL method exploits that the environmental conditions corresponding to a return period of 100 and 10000 years can be established based on statistical models for the most important weather characteristics for the response problem at hand. For the simplified upwell analysis, H_s and T_p are the governing weather characteristics. By fitting statistical distributions to model the behaviour of H_s and $T_p - \epsilon|H_s$, the joint distribution of the two weather characteristics can be established. As outlined in section 4.1.2, the marginal distribution of H_s is well represented by a 3-parameter Weibull distribution. The conditional distribution of $T_p - \epsilon$ given H_s is modelled by a 2-parameter Weibull distribution as shown in section 4.1.3. As explained in section 4.1.3 the lower limit ϵ for T_p is introduced to avoid that the contour lines violate the wave breaking limit for steep sea states.

To establish the contour lines the procedure using IFORM as performed in section 6.1.3 is utilised. The only difference from what is done in section 6.1.3 is the statistical distributions used in the Rosenblatt transformation. Hence, Eq. (7.1) should be used instead of Eq. (6.8).

$$\begin{aligned} \Phi(u_1) &= F_{H_s}(h) &&\iff u_1 = \Phi^{-1}[F_{H_s}(h)] \\ \Phi(u_2) &= F_{T_p-\epsilon|H_s}(t-\epsilon|h) &&\iff u_2 = \Phi^{-1}[F_{T_p-\epsilon|H_s}(t-\epsilon|h)] \end{aligned} \tag{7.1}$$

The contour lines describing the weather characteristics for sea states with constant probability of exceedance corresponding to ULS and ALS level, respectively, are shown in Figure 7.1 together with the observed sea states from the NORA10 hindcast.

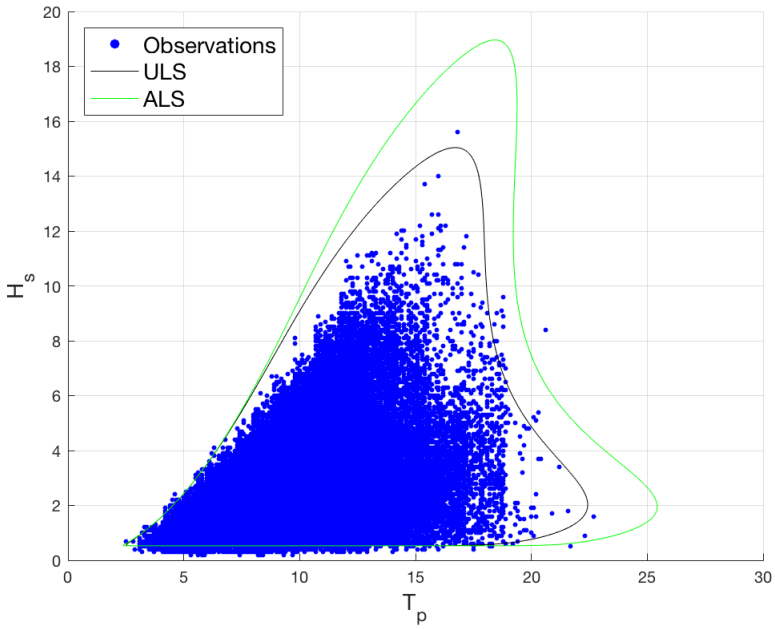

Figure 7.1: The ULS and ALS metocean contour lines shown for H_s and T_p with a lower limit ϵ for T_p.

7.1 ULS and ALS upwell

The contour lines represent the long term variability of the environmental conditions. To obtain estimates for $U_{3h,ULS}$ and $U_{3h,ALS}$, the most severe sea state along the contour lines has to be decided. The most severe sea

state is defined as the sea state along the contours that provides the largest response for the problem at hand. The main idea of the MCL is that as the weather characteristics for the most severe sea states in ULS and ALS condition is known, the short term distribution for U_{3h} will give a foundation for obtaining $U_{3h,ULS}$ and $U_{3h,ALS}$. As the short term distribution for U_{3h} is known, the remaining part is to decide what percentile levels ULS and ALS correspond to. In NORSOK (2017) it is recommended that ULS corresponds to the 90-percentile, while ALS corresponds to the 95-percentile. This is assumed to give conservative estimates.

As shown in section 5.4.1 the largest upwell response is obtained from steep sea states. Hence, sea states in the steepest area of the contours should be evaluated to find the most severe sea state. The region along the contours considered in the study of finding the most severe sea state is shown in Figure 7.2 together with the most severe sea states giving $U_{3h,ULS}$ and $U_{3h,ALS}$, respectively.

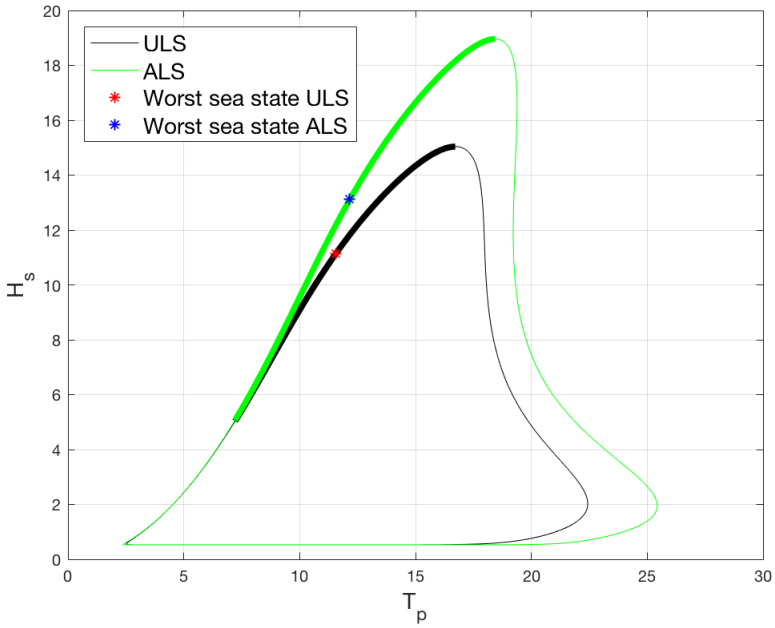

Figure 7.2: The ULS and ALS metocean contour lines showing the important region along with the actual most severe sea states.

The results for $U_{3h,ULS}$ and $U_{3h,ALS}$ utilising the MCL method for the southwestern corner of the platform, assuming that the total sea comes

from the geographical south, are listed in Table 7.1.

Table 7.1: Results obtained for $U_{3h,ULS}$ and $U_{3h,ALS}$ utilising the MCL method for the southwestern corner of the platform, assuming that the total sea comes from the geographical south.

	$U_{3h,ULS}$	$U_{3h,ALS}$
JONSWAP	18.67m	21.19m
Torsethaugen	19.39m	22.87m

As the direction of the incoming waves has shown to be important for the upwell problem, it is a weakness for the MCL method that the wave heading is disregarded. The MCL method should only be viewed as a method that can be used in the early design stage to get approximate estimates of ULS and ALS values for the problem at hand.

7.2 Compare percentile levels

The percentile levels given in NORSOK (2017) for ULS and ALS are only indicatives. As discussed in Haver and Winterstein (2009) appropriate percentiles for ULS and ALS depend on the response problem under consideration. In most cases the percentiles from NORSOK will give conservative ULS and ALS estimates, while some complex response cases (like e.g. slamming loads, (Suyuthi et al., 2009)) will require higher percentiles, especially with regard to ALS, to give reliable estimates. The percentiles found corresponding to the upwell estimates calculated from the MASS and POT approaches are listed in Table 7.2 and 7.3. The percentiles obtained for ULS only accounting for observed events shows that a 90-percentile for ULS will give conservative results. However, as non-observed events are accounted for in the analysis, the 90-percentile will give slightly non-conservative estimates, where 0.91-0.95 might be a more appropriate percentile level. The percentiles obtained for ALS are in general much higher than the recommended 95-percentile. Percentiles of 0.98-0.998 are related to high uncertainties, which means that a large number of short term analyses has to be performed in order to ensure that the estimated extremes are reliable. This is not always feasible with regard to time and cost. Therefore, the MCL method might not be suitable to decide reliable extremes at ALS level for some complex, non-linear response problems.

Table 7.2: The corresponding percentiles obtained for the upwell results from the MASS and POT approach are listed for the JONSWAP and Torsethaugen total sea (from the south) cases accounting for observed events. A threshold $H_s = 8$m is used for the most critical location under the platform, which is the most southern point in the geographical coordinate system.

Case no.	ULS_{MASS}	ULS_{POT}	ALS_{MASS}	ALS_{POT}
2	0.861	0.803	0.994	0.985
4	0.839	0.768	0.980	0.957

Table 7.3: The corresponding percentiles obtained for the upwell results from the MASS and POT approach are listed for the JONSWAP and Torsethaugen total sea (from the south) cases accounting for non-observed events. A threshold $H_s = 8$m is used for the most critical location under the platform, which is the most southern point in the geographical coordinate system.

Case no.	ULS_{MASS}	ULS_{POT}	ALS_{MASS}	ALS_{POT}
2	0.943	0.918	0.998	0.998
4	0.914	0.881	0.991	0.988

Chapter 8

Contribution from U_{LF} and U_{mean}

The wave frequency upwell, U_{WF}, considered in the long term analyses in this thesis is the most important contribution to the total upwell. However, U_{LF} and U_{mean} do also contribute to the total upwell. Both the size of the columns and the topside give large areas that absorb the mean and slowly varying loads. DNVGL-OTG-13 provides procedures for calculating the LF contributions from waves and wind, which involves quadratic transfer functions (QTFs) found from second-order difference frequency analysis. As only a linear analysis is performed in WAMIT, the QTFs are not available. Since different long term analyses of the U_{WF} is the main objective of this thesis, obtaining these QTFs has not been a priority. However, the contribution from U_{LF} and U_{mean} to the total upwell will be quantified based on guidelines provided in DNVGL-OTG-13 in order to give estimates for the total upwell utilized in the design of the still water air gap, a_0.

In lack of available model tests or numerical predictions of LF motions, each of the maximum LF roll angle and LF pitch angle can be taken as 5 degrees, (DNVGL, 2017). If the sea comes from an oblique direction, the rotation can be assumed to be around the axis normal to the wave direction, and the maximum angle should also for this case be set to 5 degrees. However, the model test results of the semi-submersible investigated in this thesis reveal that the LF contribution is found to be 6 degrees, (Bratland, 2018). Therefore this is used as a maximum angle, ϕ_{LF}, for the LF contribution, U_{LF}, in both ULS and ALS.

U_{mean} occurs as a result of the mean wind and wave induced loads. Normally this is opposed by ballasting to even keel. However, in ULS conditions

large motions might lead to inaccuracy in the ballasting process. Hence, a static mean heel angle, ϕ_{mean}, of 1 degree should be used to account for this inaccuracy in ULS conditions, (DNVGL, 2017). In ALS conditions ϕ_{mean} is set to 0 degrees with the argument that all bad luck is already achieved in this condition, (Bratland, 2018). According to DNVGL-OTG-13 the contributions to the total upwell from U_{WF}, U_{LF} and U_{mean} should be estimated as in Eq. (8.1).

$$U = U_{mean} + \sqrt{U_{WF}^2 + U_{LF}^2} \tag{8.1}$$

Where $U_{mean} = d_{hor} \cdot sin(\phi_{mean})$, $U_{LF} = d_{hor} \cdot sin(\phi_{LF})$ and d_{hor} is the horizontal distance from the center of the rotational axis out to the considered point on the semi-submersible. Considering $U_{3h,ULS}$ estimated for combined sea in section 5.1, the contributions to the total upwell are given in Table 9.3 for the southwestern corner of the platform ($d_{hor} = \sqrt{x^2 + y^2} = \sqrt{43.1^2 + 43.1^2} = 61m$).

Table 8.1: Results obtained for $U_{3h,ULS}$ and $U_{3h,ALS}$ along with the contributions from U_{WF} (from section 5.2.1), U_{LF}, $U_{LF,relative}$, U_{mean} and a with $d_{hor} = 61$m. The southwestern corner of the semi submersible is considered.

	ULS	ALS
U_{WF}	18.30m	23.33m
U_{LF}	6.38m	6.38m
$U_{LF,relative}$	1.08m	0.86m
U_{mean}	1.06m	0m
U	20.44m	24.19m
a	-0.44m	-4.19m

The results show that both U_{LF} and U_{mean} contribute with over 1m each to the total upwell in ULS. Since $a_0 = 20m$, considering only U_{WF} will give a positive air gap in ULS condition for the semi-submersible. However, including U_{LF} and U_{mean} result in negative air gap in ULS condition. The contribution from U_{LF} to the total upwell in ALS conditions is smaller than 1m.

Chapter 9

Discussion and comparison of results

9.1 U_{ULS}^{WF} and U_{ALS}^{WF} accounting for observed events

The results for the different cases defined in Table 5.1 obtained for MASS and POT accounting for observed events are listed in Table 9.1.

Table 9.1: U_{ULS}^{WF} and U_{ALS}^{WF} from the MASS and POT approach are listed for the different cases investigated accounting for observed events. A threshold $H_s = 8$m is used for the most critical location under the platform, which is the most southern point in the geographical coordinate system.

Case no.	ULS_{MASS}	ULS_{POT}	ALS_{MASS}	ALS_{POT}
1	18.30m	17.79m	23.43m	22.37m
2	18.31m	17.92m	23.33m	22.45m
3	18.29m	17.72m	23.46m	22.28m
4	18.86m	18.42m	23.91m	23.05m
5	19.59m	19.01m	25.08m	23.98m
6	19.63m	19.17m	25.00m	24.02m
7	19.50m	19.01m	24.97m	24.01m
8	20.23m	19.75m	25.66m	24.73m

The upwell results obtained for MASS are higher than the results obtained for POT for the most critical location under the platform when only observed events are considered in the long term analysis. The difference is approximately 0.5 m in ULS. TASS is assumed to give conservative results,

because the correlation of adjacent sea states are neglected. The results shows that in the same manner as TASS, MASS gives conservative results of about 2-3 % compared to POT. The ALS results are related to large uncertainties, keeping in mind that the 10000-year return period is estimated based on extrapolation from 60 years of data. Even though the results in ALS not can be taken as reliable, it can be noticed that the difference between the MASS and POT has grown to 1m.

The results for combined sea, total sea and wind sea are the same. This suggests that the contribution from swell sea has minor effect and can be neglected in the long term air gap analysis. The use of Torsethaugen spectrum gives higher results than the use of JONSWAP spectrum for total sea.

9.2 U_{ULS}^{WF} and U_{ALS}^{WF} accounting for non-observed events

The corresponding results obtained for MASS and POT accounting for non-observed events are listed in Table 9.2.

Table 9.2: U_{ULS}^{WF} and U_{ALS}^{WF} from the MASS and POT approach are listed for the different cases investigated accounting for non-observed events. A threshold $H_s = 8$m is used for the most critical location under the platform, which is the most southern point in the geographical coordinate system.

Case no.	ULS_{MASS}	ULS_{POT}	ALS_{MASS}	ALS_{POT}
1	19.24m	18.84m	24.65m	24.35m
2	19.23m	18.87m	24.53m	24.21m
3	19.30m	18.87m	24.75m	24.43m
4	19.55m	19.20m	24.73m	24.48m
5	20.46m	20.06m	26.17m	25.87m
6	20.44m	20.08m	26.02m	25.72m
7	20.51m	20.08m	26.25m	25.93m
8	20.84m	20.47m	26.31m	26.04m

It is found that MASS gives conservative results compared to POT in the same order for ULS as found when only observed events are considered. Worth to notice is that the more reliable ALS results obtained shows that the difference between MASS and POT is smaller at ALS level. MASS is still more conservative, but only with 1-1.5 %.

9.3 Final estimates for U_{ULS}, U_{ALS}, a_{ULS} and a_{ALS}

The final results for the total upwell, U_{ULS} and U_{ALS}, are listed in Table 9.3, where combined sea with JONSWAP wave spectrum and an α-factor of 1.2 are used as input, and non-observed events are accounted for in the long term analysis. Eq. 8.1 is used to calculate U. It is the relative contribution of U_{LF} to U that is listed in Table 9.3.

Table 9.3: Results obtained for U_{ULS} and U_{ALS} along with the contributions from U_{WF} (from chapter 6), $U_{LF,relative}$ and U_{mean}. The results are obtained from the long term analysis in combined sea accounting for non-observed events. The southwestern corner of the semi-submersible (most critical location) is considered.

	ULS_{MASS}	ULS_{POT}	ALS_{MASS}	ALS_{POT}
U_{WF}	19.24m	18.84m	24.65m	24.35m
$U_{LF,relative}$	0.72m	0.74m	0.57m	0.57m
U_{mean}	1.06m	1.06m	0m	0m
U	21.02m	20.64m	25.22m	24.92m

The results show that U_{mean} included in ULS gives a larger contribution to U than U_{LF}. This shows the importance of performing the ballasting process correctly in order to have the semi-submersible at even keel, or alternatively slightly higher in the direction of the incoming waves. With a static air gap, $a_0 = 20m$, the total upwell estimated from the long term analysis leads to negative air gap in ULS and ALS for the most critical location under the platform as listed in Table 9.4. However, the midpoint on the western side of the platform gives satisfying results, having sufficient air gap both in ULS and ALS. The two points considered in Table 9.4 are defined in Figure 9.1.

Table 9.4: Results obtained for upwell and air gap in ULS and ALS. The results are obtained from the long term analysis in combined sea accounting for non-observed events. The southwestern corner of the semi submersible is considered along with the midpoint at the western side of the platform.

	ULS_{MASS}	ULS_{POT}	ALS_{MASS}	ALS_{POT}
$U_{Southwest}$	21.02m	20.64m	25.22m	24.92m
$a_{Southwest}$	-1.02m	-0.64m	-5.22m	-4.92m
U_{West}	14.27m	14.43m	17.57m	17.71m
a_{West}	5.73m	5.57m	2.43m	2.29m

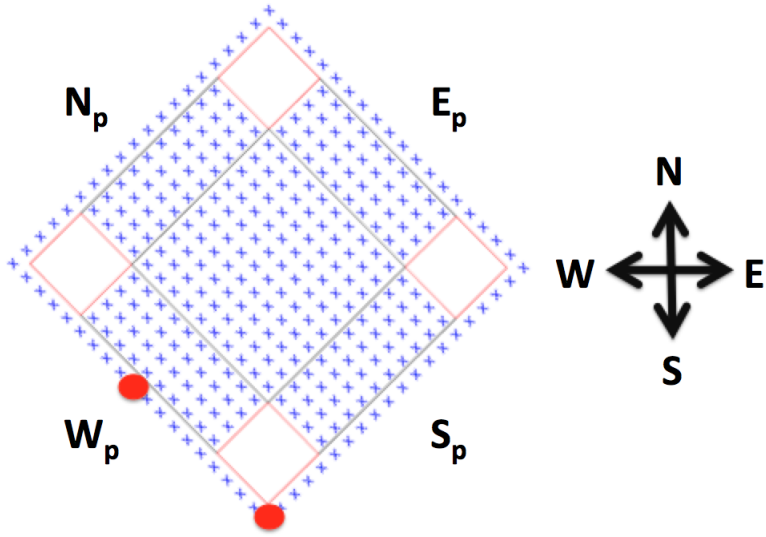

Figure 9.1: Location of the two points considered in the final results.

The negative air gap obtained in ULS is critical, and means that the semi-submersible has to be designed to withstand horizontal wave loads in deck. A negative air gap in the order of 5 meters in ALS means that large amounts of water will hit the semi-submersible high up on the superstructure.

9.4 Physical interpretation of the results

As shown in section 5.4.1, the most critical sea states regarding the upwell problem are the steepest sea states. The most severe observed sea state in the NORA 10 hindcast giving the largest upwell has a wind sea characterised by $H_{s,w} = 8m$ and $T_{p,w} = 11s$. The remaining particulars of the sea state are given in Table 9.5. Is this sea state able to create upwell all the way up to over 20 meters, or do the results accounting for non-observed events consider unphysical steep sea states that will brake?

Table 9.5: Characteristics for the most severe sea state regarding upwell for the most critical location under the platform, in the southwest corner.

$U_{3hmax,mean}$	16.82m
$H_{s,tot}$	8.4m
$H_{s,w}$	8m
$H_{s,sw}$	2.5m
$T_{p,w}$	11m
$T_{p,sw}$	13.6m
β_w	182°
β_{sw}	227°

The most severe sea state is characterised by a steep wind sea and a swell sea state with a short T_p. The wind sea comes from the south, while the swell sea comes from the southwest. Hence, they have large contributions in nearly the same direction. However, a wave with $H_s = 8$m will not alone be able to reach 20m above SWL. Diffraction effects will create extra height at certain locations under the platform. For the southwestern corner with an incoming wave from the south with $T_p = 11$s, the transfer function for the diffracted wave field adding the α-factor is 1.58. Hence, assuming a crest height, $c = 1.2 \cdot H_s = 9.6m$, the diffracted wave field leads to a wave elevation of 15.2m. Still, the semi-submersible will move along with the waves, which will in general have a positive effect on the air gap. But for steep waves the semi-submersible are not able to follow the waves, which leads to a phase difference between the incoming waves and the vertical motion of the semi-submersible. If this phase difference is sufficiently large, the crest will hit the corner of the semi-submersible when the semi-submersible is at its lowest point in the cycle. In this way a negative vertical motion of 5m combined with a wave elevation of 15.2m might produce a relative wave elevation of 20m, and a negative air gap.

The most severe sea states found utilising the MCL method has the characteristics $H_s = 11.1m, T_p = 11.6s$ and $H_s = 13.1m, T_p = 12.2s$ for ULS and ALS, respectively. Compared to the most severe sea state from NORA10, the H_s for these sea states are more convincing to obtain relative wave elevations of 20m. However, as H_s and T_p is of the same magnitude for ULS, and T_p is actually lower than H_s for ALS, it is more a question if these sea states are occurring in reality, or if they will break. Non of these sea states violate the proposed wave breaking limit, $\epsilon = 3.2\sqrt{H_s}$, but especially the most severe sea state in ALS might be unphysical because the wave breaking limit considers combined sea.

Chapter 10

Conclusion

The results from the long term analyses performed in this assignment accounting for non-observed events shows that the semi-submersible has negative air gap in the southwestern corner of the platform in both ULS and ALS conditions. This means that horizontal wave loads might hit the upper deck, which has to be taken into account in the design of the superstructure.

The suggested MASS approach seems to be a good alternative for the TASS approach, at least for the crest height problem. Due to the assumption of statistical independence between adjacent sea states, the ASS approaches are expected to give more conservative results than the POT approach. This is also the case for the upwell problem, where MASS gives higher upwell results than POT. Both MASS and POT are highly sensitive to the threshold set for H_s. The threshold for the upwell problem should not be set too high, because steep sea states all the way down to H_s = 7-8m are important for the extreme values.

Utilising combined sea as input to the long term analysis gives the same results as for total sea and pure wind sea. Hence, the swell contribution is of minor importance for the air gap result, and might be neglected in a long term analysis.

Steeper sea states are found to be most critical for the air gap. High sea states are related to longer wave periods, which the semi-submersible is able to respond to and follow in a good manner. However, steep sea states with H_s between 7-11m are related to shorter T_p, which the semi-submersible is not able to follow. Therefore the semi-submersible is out of phase with the incoming waves and a wave crest might hit the platform when the platform is on the lowest point in the cycle. As most of these steep sea states come from

the geographical south, the southwestern corner of the semi-submersible which faces the southern direction, is the most critical location under the platform with regard to air gap.

Chapter 11

Further work

Second-order analysis

A second order analysis for the upwell problem should be performed to get more accurate results. Alternatively the simplified linear analysis in OTG-13 could be used to find U_{WF}, and a second-order analysis could be performed to decide the LF contributions from wind and waves. Assuming a total LF contribution of 5 degrees is thought of as a conservative estimate, hence more realistic results might be obtained from a second-order analysis.

Compare model tests with WAMIT

It could be interesting to compare the model test results with the results obtained for the long term analysis using the transfer functions calculated in WAMIT. This would also confirm if sea states with $H_s = 8$m are able to produce upwell of 20m. Another aspect from the model tests is to find appropriate α-factors for each location under the platform. The α-factor is taken from OTG-13 to be 1.2 for the whole platform. This is probably conservative for many locations under the platform, while it might be non-conservative in the up-front area of the platform. Utilising the α-factors obtained from model tests will give more accurate results for the diffracted wave.

Both MASS, POT and MCL suggests that lower steep sea states are of importance for air gap. However, model tests suggest that it is the highest sea states that are the most critical. This difference should be investigated

further to see if the transfer functions obtained from WAMIT give too high contributions for lower wave periods.

Consider wind sea

The swell sea has little effect on the ULS and ALS results for the upwell in the wave frequency range. Therefore, performing the long term analysis using only the wind sea gives nearly the same results as when swell sea is included. Steep wind seas are considered most critical, and most of them come from the south. In this manner it would be relevant to perform the air gap analysis using only sea states that come from the southern direction, to see if only including these sea states will provide results that are comparable with the results obtained in this thesis.

Current

The effect of current is non-conservatively neglected in the long term analysis, and should be included to get more accurate results. For sites with a strong current, the wave-current interactions should be considered for steep waves, (DNVGL, 2017). However, the current contribution to the upwell is related to uncertainties and should be investigated.

All sea state approach

A traditional all sea state approach (TASS) could be used if the incoming direction of the waves is included in the joint distribution of H_s and T_p. Response surfaces for the upwell can then be established and a long term analysis utilising the TASS approach could be performed. The results can then be compared with the ones obtained for the MASS approach, to verify the validity of the MASS approach for the upwell problem.

Curve fitting - MASS

A sensitivity study on how many of the highest extremes that should be used in the fitting process of the Gumbel long term distribution for the MASS approach should be performed. The crest height and upwell problem

suggest that the percentage of the highest extremes that are used in the curve fitting process relies on the response problem at hand and where the threshold is placed. However, there might be some trends that can standardise the choice of percentage to be used in the fitting process.

Curve fitting - $\alpha_{T_p-\epsilon|H_s}$ and $\beta_{T_p-\epsilon|H_s}$

Normally the log-normal distribution is used to model the conditional distribution of T_p given H_s. The parameters used in the log-normal distribution has standardised fitting functions. As the lower limit for T_p is introduced, a 2-parameter Weibull distribution is found to be a better model for $T_p - \epsilon$ given H_s. Finding standardised fitting functions for the parameters in this case might be helpful making the 2-parameter Weibull distribution faster to use.

Bibliography

Aker Solutions (2018). *WAMIT output files*.

Andersen, O. J. (2009). Correction of spectral peak period of nora10 data base (statoil memo).

Battjes, J. A. (1972). Long-term wave height distributions at seven stations around the british isles. *Deutsche Hydrografische Zeitschrift*, 25(4):179–189.

Bratland, A. K. (2018). Private communication.

Coles, S., Bawa, J., Trenner, L., and Dorazio, P. (2001). *An introduction to statistical modeling of extreme values*, volume 208. Springer.

DNVGL (2014). DNVGL-RP-C205, Environmental conditions and environmental loads. Technical report.

DNVGL (2017). DNVGL-OTG-13, Prediction of air gap for coloumn stabilised units. Technical report.

Faltinsen, O. (1993). *Sea loads on ships and offshore structures*, volume 1. Cambridge university press.

Forristall, G. Z. (2000). Wave crest distributions: Observations and second-order theory. *Journal of physical oceanography*, 30(8):1931–1943.

Gibson, R., Christou, M., and Feld, G. (2014). The statistics of wave height and crest elevation during the december 2012 storm in the north sea. *Ocean Dynamics*, 64(9):1305–1317.

Haring, R., Heideman, J., et al. (1978). Gulf of mexico rare wave return periods. In *Offshore Technology Conference*. Offshore Technology Conference.

Hasselmann, K., Barnett, T., Bouws, E., Carlson, H., Cartwright, D., Enke, K., Ewing, J., Gienapp, H., Hasselmann, D., Kruseman, P., et al. (1973). Measurements of wind-wave growth and swell decay during the joint north sea wave project (jonswap). *Ergänzungsheft 8-12*.

Haver, S. (1990). On a possible lower limit for the spectral peak period. 90009, Statoil Report No. F&U-MT.

Haver, S. (2016). Stochastic description of ocean waves & response analysis and prediction of extremes. Technical report, NTNU, Lecture notes.

Haver, S. (2017). Metocean modelling and prediction of extreme response. NTNU, Lecture notes.

Haver, S. (2018). Private communication.

Haver, S. and Nyhus, K. (1986). A wave climate description for long term response calculations. In *5th International OMAE Symposium, Tokyo*, volume 4, pages 27–34.

Haver, S. and Winterstein, S. R. (2009). Environmental contour lines: A method for estimating long term extremes by a short term analysis. *Transactions of the Society of Naval Architects and Marine Engineers*, 116:116–127.

Jahns, H., Wheeler, J., et al. (1972). Long-term wave probabilities based on hindcasting of severe storms. In *Offshore Technology Conference*. Offshore Technology Conference.

Jasper, N. (1956). Statistical distribution patterns of ocean waves and wave induced ship stresses and motions with engineering applications. *SNAME*, 64.

Lian, G. and Haver, S. K. (2015). Measured crest height distribution compared to second order distribution. In *14th International Workshop on Wave Hindcasting and Forecasting*.

Madsen, H. O., Krenk, S., and Lind, N. C. (2006). *Methods of structural safety*. Courier Corporation.

Nielsen, M. A. (2011). Parameter estimation for the two-parameter weibull distribution.

Nordenstrøm, N. (1971). Part 1: environmental conditions and short term response, volume 71-2-s of methods for predicting long term distributions of wave loads and probability of failure for ships. Technical report, Det norske Veritas, Oslo.

NORSOK (2017). N-003. *Actions and Action Effects*.

Price, W. G. and Bishop, R. E. D. (1974). *Probabilistic theory of ship dynamics*. Halsted Press.

Reistad, M., Breivik, O., and Haakenstad, H. (2007). A high-resolution hindcast study for the north sea, the norwegian sea and the barents sea, paper presented at 10th international workshop on wave hindcasting and forecasting and coastal hazard symposium, coastal and hydraul. lab. *Eng. Res. and Dev. Cent., US Army Corps of Eng., North Shore, Hawaii*.

Rosenblatt, M. (1952). Remarks on a multivariate transformation. *The annals of mathematical statistics*, 23(3):470–472.

Sandbakken, S. (2016). Long term analysis of semi submersible offset. Master's thesis, NTNU, Department of Marine Technology.

Sandbakken, S. S. (2017). Long term analysis of semi submersible offset. *OMAE*.

Suyuthi, A., Haver, S. K., et al. (2009). Extreme loads due to wave breaking against platform column. In *The Nineteenth International Offshore and Polar Engineering Conference*. International Society of Offshore and Polar Engineers.

Torsethaugen, K., Haver, S., et al. (2004). Simplified double peak spectral model for ocean waves. In *The Fourteenth International Offshore and Polar Engineering Conference*. International Society of Offshore and Polar Engineers.

Tromans, P. S., Vandersohuren, L., et al. (1995). Response based design conditions in the north sea: Application of a new method. In *Offshore Technology Conference*. Offshore Technology Conference.

Vestbøstad, T. M., Haver, S., Andersen, O. J., and Albert, A. (2002). Prediction of extreme roll motion on an fpso using long term statistics. In *ASME 2002 21st International Conference on Offshore Mechanics and Arctic Engineering*, pages 129–136. American Society of Mechanical Engineers.

Vikenes, O. K. (2017). Assessing air gap of semi-submersibles in the northern north sea. Technical report, NTNU, project work.

WAMIT (2016). WAMIT user manual. `http://www.wamit.com/index.htm`. [Online; accessed 11-December-2017].

Winterstein, S. R., Ude, T. C., Cornell, C. A., Bjerager, P., and Haver, S. (1993). Environmental parameters for extreme response: Inverse form with omission factors. *Proceedings of the ICOSSAR-93, Innsbruck, Austria*, pages 551–557.

Appendix A

Scatter diagram

		0<Tp≤1																							
		1	2	3	4	5	6	7	8	9	10	11	12	13	14	15	16	17	18	19	20	21	22	23	24	25
0<Hs≤0,5	0,5	0	0	1	31	361	593	301	213	303	197	104	72	75	10	14	9	1	2	2	0	0	1	0	0	0
	1	0	0	2	269	1472	3467	5002	3903	2708	2124	1539	1006	614	299	164	133	62	20	18	5	1	0	1	0	0
	1,5	0	0	0	26	1231	3674	5066	6016	5561	3737	2230	1649	1295	706	361	160	92	36	20	5	0	0	0	0	0
	2	0	0	0	0	248	2271	4845	4585	4466	4283	2795	1745	1256	770	448	271	122	38	25	6	3	1	1	0	0
	2,5	0	0	0	0	19	600	3476	4496	3561	3254	3043	2165	1189	780	424	280	105	43	21	2	1	0	0	0	0
	3	0	0	0	0	0	77	1401	3579	3401	2602	2259	1840	1210	659	485	289	139	44	32	0	0	0	0	0	0
	3,5	0	0	0	0	0	10	377	1948	3271	2503	1686	1362	1122	586	382	261	164	47	24	1	0	1	0	0	0
	4	0	0	0	0	0	0	70	742	2525	2427	1522	980	829	469	299	188	123	61	20	2	2	0	0	0	0
	4,5	0	0	0	0	0	0	8	172	1343	2091	1561	872	609	370	205	145	86	48	24	2	0	0	0	0	0
	5	0	0	0	0	0	0	0	28	545	1356	1477	767	413	267	139	102	65	27	25	4	0	0	0	0	0
	5,5	0	0	0	0	0	0	0	4	161	739	1109	767	327	176	106	71	45	25	17	1	3	0	0	0	0
	6	0	0	0	0	0	0	0	0	41	334	760	702	367	156	76	40	27	8	13	0	0	0	0	0	0
	6,5	0	0	0	0	0	0	0	0	6	135	474	565	309	132	71	39	16	16	10	0	0	0	0	0	0
	7	0	0	0	0	0	0	0	0	2	36	259	409	325	125	66	33	10	14	9	0	0	0	0	0	0
	7,5	0	0	0	0	0	0	0	0	0	5	95	208	239	121	67	23	3	8	11	0	0	0	0	0	0
	8	0	0	0	0	0	0	0	0	0	1	32	123	140	107	48	18	10	7	4	0	0	0	0	0	0
	8,5	0	0	0	0	0	0	0	0	0	1	8	65	101	79	31	17	3	5	1	0	1	0	0	0	0
	9	0	0	0	0	0	0	0	0	0	0	2	29	51	63	26	15	6	4	4	0	0	0	0	0	0
	9,5	0	0	0	0	0	0	0	0	0	0	0	8	20	30	24	13	3	3	1	0	0	0	0	0	0
	10	0	0	0	0	0	0	0	0	0	0	0	6	15	12	18	4	6	1	1	0	0	0	0	0	0
	10,5	0	0	0	0	0	0	0	0	0	0	0	1	7	21	4	12	9	2	0	0	0	0	0	0	0
	11	0	0	0	0	0	0	0	0	0	0	0	1	4	8	9	6	4	0	0	0	0	0	0	0	0
	11,5	0	0	0	0	0	0	0	0	0	0	0	0	3	4	4	3	2	1	0	0	0	0	0	0	0
	12	0	0	0	0	0	0	0	0	0	0	0	0	0	0	5	3	1	1	0	0	0	0	0	0	0
	12,5	0	0	0	0	0	0	0	0	0	0	0	0	0	0	0	2	2	0	0	0	0	0	0	0	0
	13	0	0	0	0	0	0	0	0	0	0	0	0	0	0	0	2	0	0	0	0	0	0	0	0	0
	13,5	0	0	0	0	0	0	0	0	0	0	0	0	0	0	0	0	0	0	0	0	0	0	0	0	0
	14	0	0	0	0	0	0	0	0	0	0	0	0	0	0	0	2	0	0	0	0	0	0	0	0	0
	14,5	0	0	0	0	0	0	0	0	0	0	0	0	0	0	0	0	0	0	0	0	0	0	0	0	0
	15	0	0	0	0	0	0	0	0	0	0	0	0	0	0	0	0	0	0	0	0	0	0	0	0	0
	15,5	0	0	0	0	0	0	0	0	0	0	0	0	0	0	0	0	0	0	0	0	0	0	0	0	0
	16	0	0	0	0	0	0	0	0	0	0	0	0	0	0	0	0	1	0	0	0	0	0	0	0	0
	16,5	0	0	0	0	0	0	0	0	0	0	0	0	0	0	0	0	0	0	0	0	0	0	0	0	0
	17	0	0	0	0	0	0	0	0	0	0	0	0	0	0	0	0	0	0	0	0	0	0	0	0	0
	17,5	0	0	0	0	0	0	0	0	0	0	0	0	0	0	0	0	0	0	0	0	0	0	0	0	0
	18	0	0	0	0	0	0	0	0	0	0	0	0	0	0	0	0	0	0	0	0	0	0	0	0	0
	18,5	0	0	0	0	0	0	0	0	0	0	0	0	0	0	0	0	0	0	0	0	0	0	0	0	0
	19	0	0	0	0	0	0	0	0	0	0	0	0	0	0	0	0	0	0	0	0	0	0	0	0	0
	19,5	0	0	0	0	0	0	0	0	0	0	0	0	0	0	0	0	0	0	0	0	0	0	0	0	0
	20	0	0	0	0	0	0	0	0	0	0	0	0	0	0	0	0	0	0	0	0	0	0	0	0	0
	20,5	0	0	0	0	0	0	0	0	0	0	0	0	0	0	0	0	0	0	0	0	0	0	0	0	0
	21	0	0	0	0	0	0	0	0	0	0	0	0	0	0	0	0	0	0	0	0	0	0	0	0	0
	21,5	0	0	0	0	0	0	0	0	0	0	0	0	0	0	0	0	0	0	0	0	0	0	0	0	0
	22	0	0	0	0	0	0	0	0	0	0	0	0	0	0	0	0	0	0	0	0	0	0	0	0	0
	22,5	0	0	0	0	0	0	0	0	0	0	0	0	0	0	0	0	0	0	0	0	0	0	0	0	0
	23	0	0	0	0	0	0	0	0	0	0	0	0	0	0	0	0	0	0	0	0	0	0	0	0	0
	23,5	0	0	0	0	0	0	0	0	0	0	0	0	0	0	0	0	0	0	0	0	0	0	0	0	0
	24	0	0	0	0	0	0	0	0	0	0	0	0	0	0	0	0	0	0	0	0	0	0	0	0	0
	24,5	0	0	0	0	0	0	0	0	0	0	0	0	0	0	0	0	0	0	0	0	0	0	0	0	0
	25	0	0	0	0	0	0	0	0	0	0	0	0	0	0	0	0	0	0	0	0	0	0	0	0	0

Scatter diagram (Troll hindcast 1957-2017)

Appendix B

U_{WF} - MASS

JONSWAP
$\alpha = 1.2$
$H_s = 8\text{m}$

B.1 Combined sea

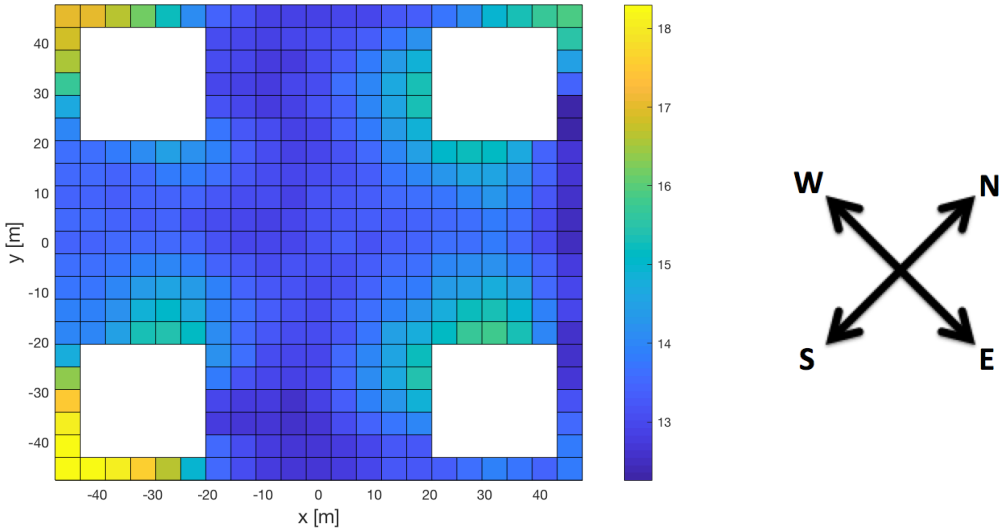

ULS

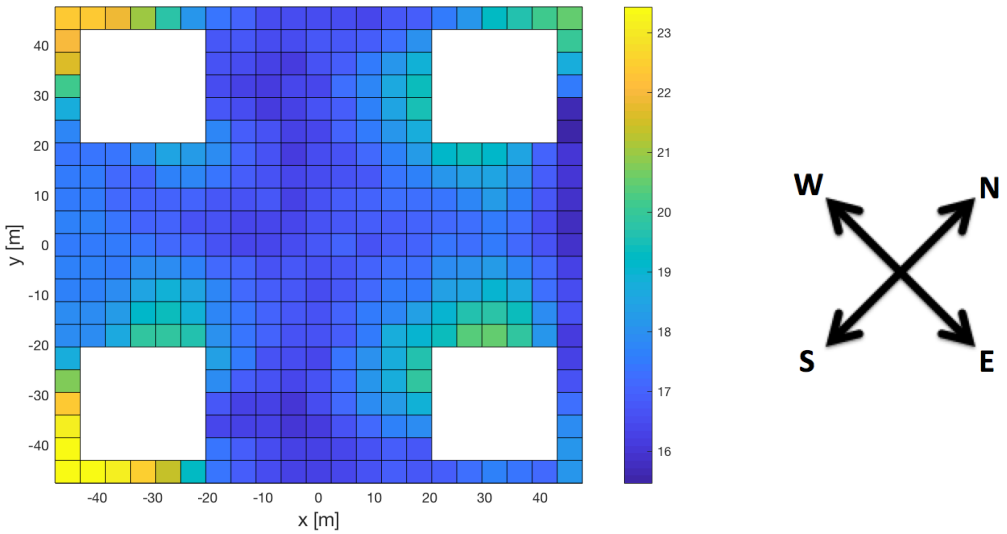

ALS

B.2 Total sea

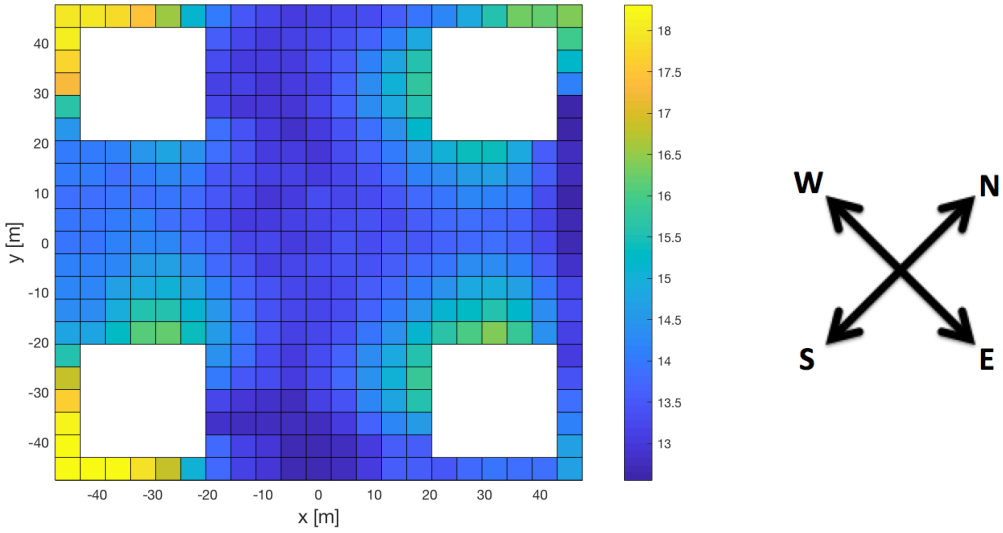

ULS

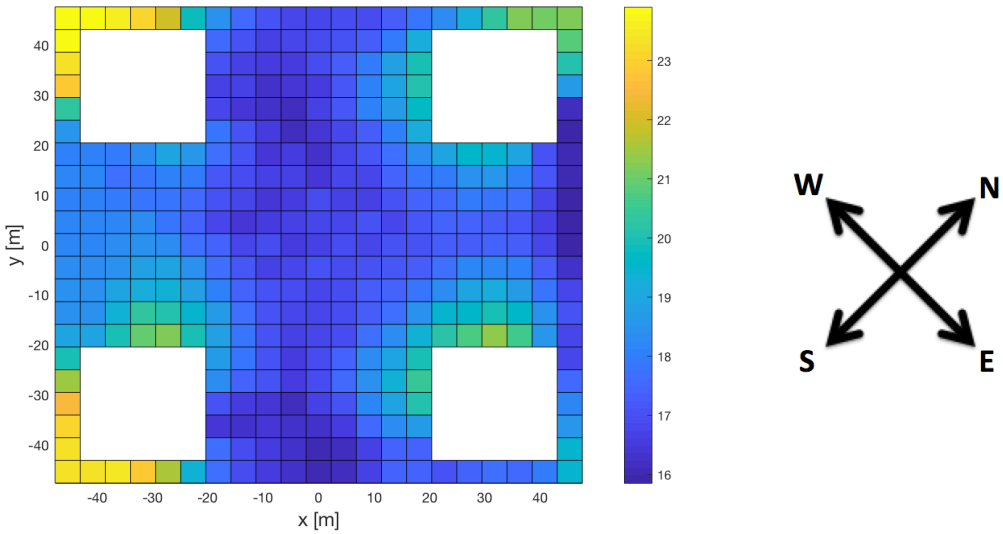

ALS

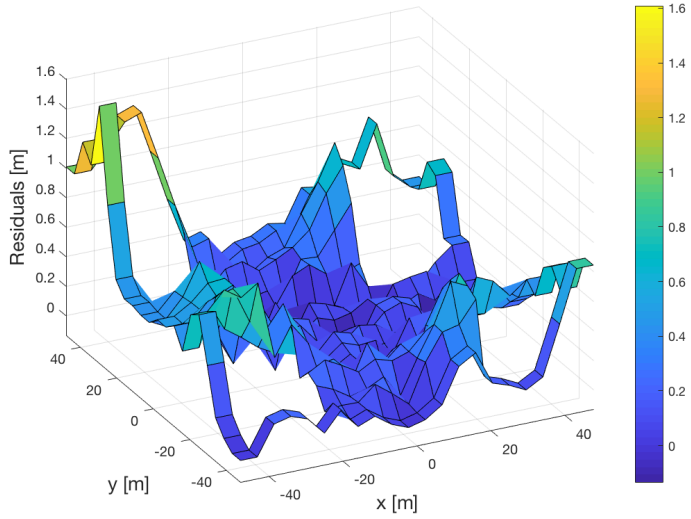

Difference between ULS upwell for the total sea and combined sea. Positive residuals means that the results obtained utilizing total sea are larger than the results obtained using combined sea.

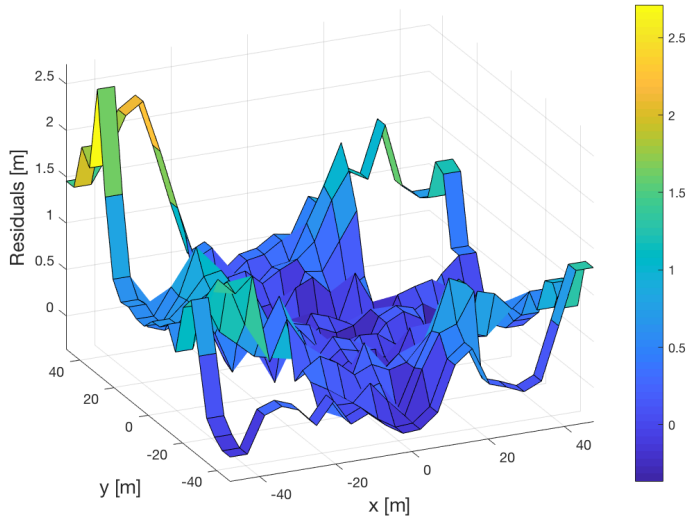

Difference between ALS upwell for the total sea and combined sea. Positive residuals means that the results obtained utilizing total sea are larger than the results obtained using combined sea.

B.3 Wind sea

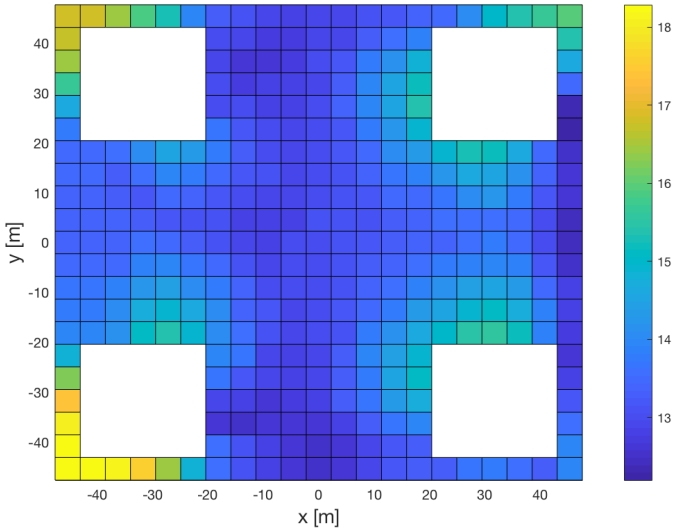

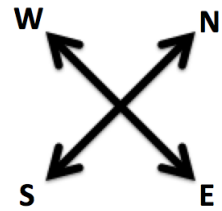

ULS

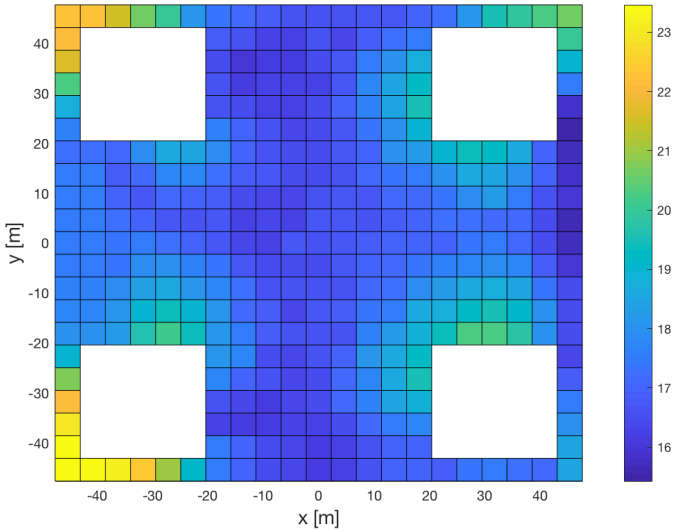

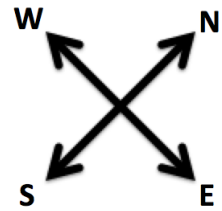

ALS

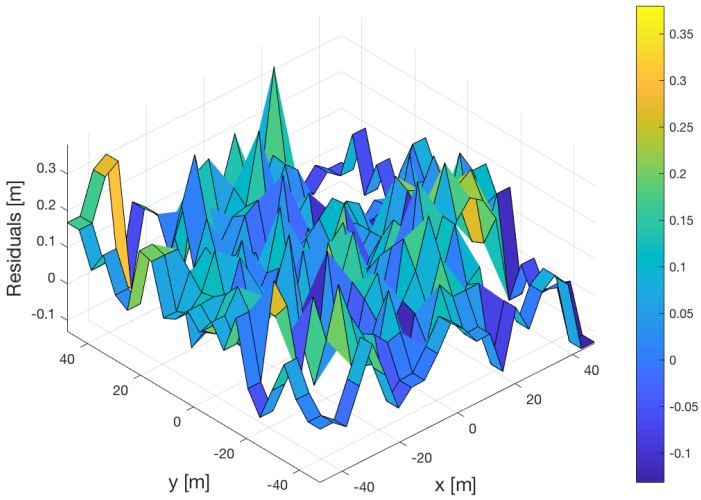

Difference between ULS upwell for total sea and combined sea. Positive residuals means that the results obtained utilizing the combined sea are larger than the results obtained using only wind sea.

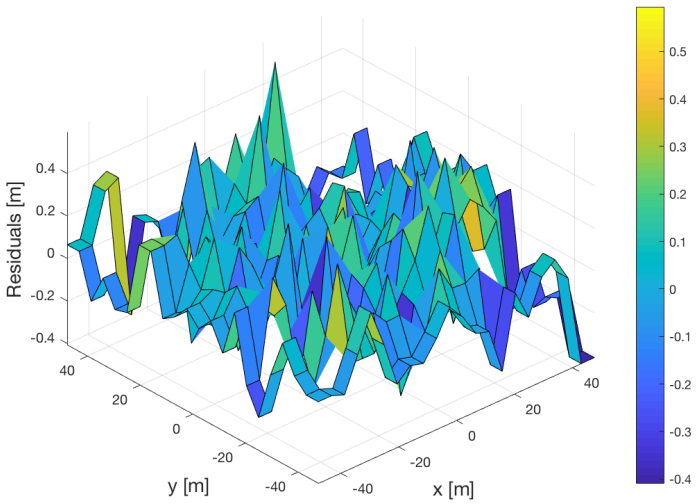

Difference between ALS upwell for wind sea and combined sea. Positive residuals means that the results obtained utilizing the combined sea are larger than the results obtained using only wind sea.

Appendix C

U_{WF} - MASS

JONSWAP
$\alpha = 1.3$
$H_s = 8\text{m}$

C.1 Combined sea

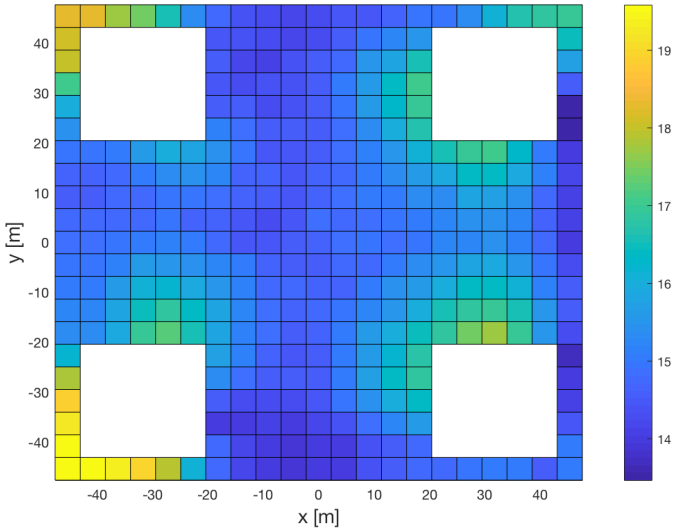

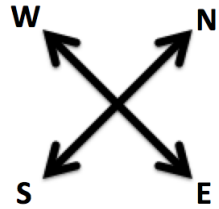

ULS

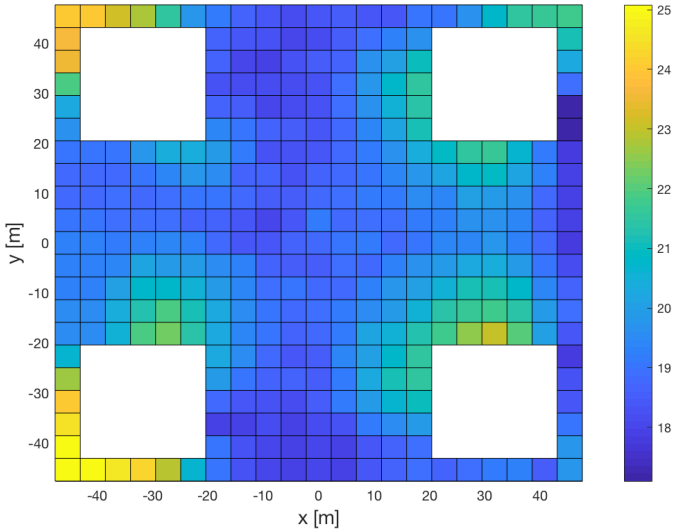

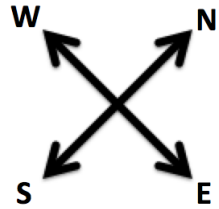

ALS

C.2 Total sea

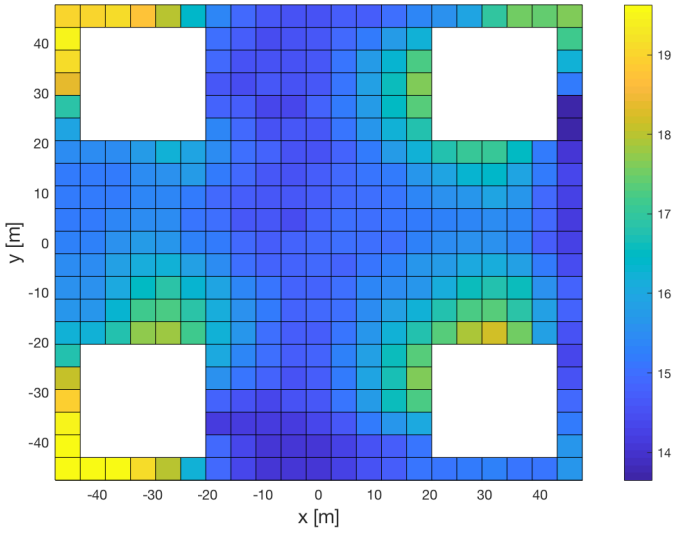

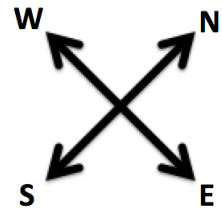

ULS

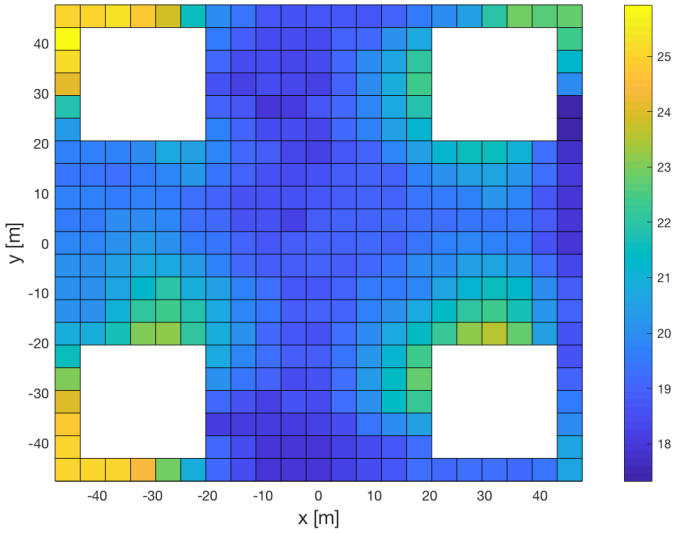

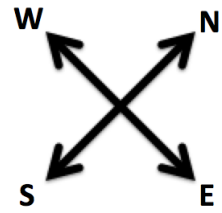

ALS

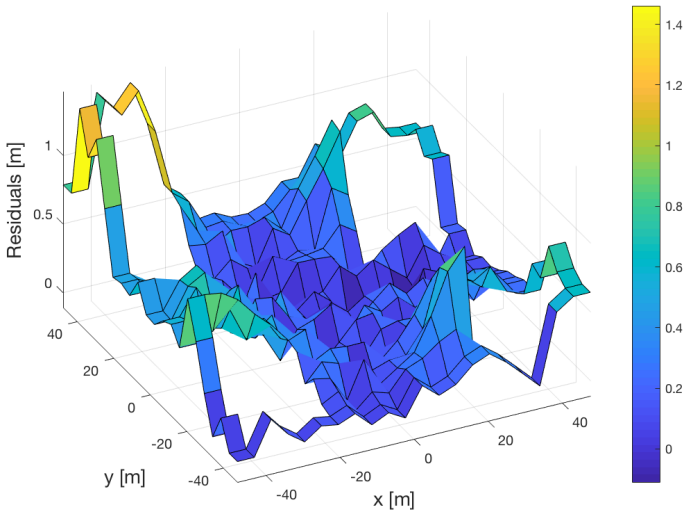

Difference between ULS upwell for the total sea and combined sea. Positive residuals means that the results obtained utilizing total sea are larger than the results obtained using combined sea.

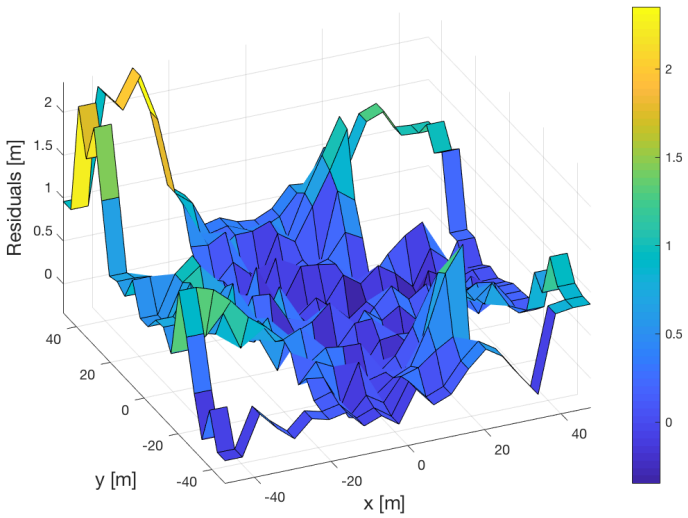

Difference between ALS upwell for the total sea and combined sea. Positive residuals means that the results obtained utilizing total sea are larger than the results obtained using combined sea.

C.3 Wind sea

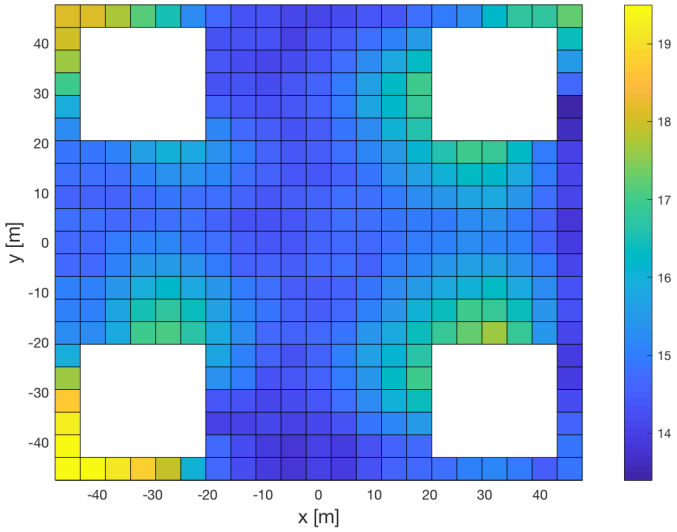

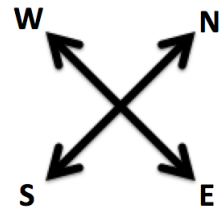

ULS

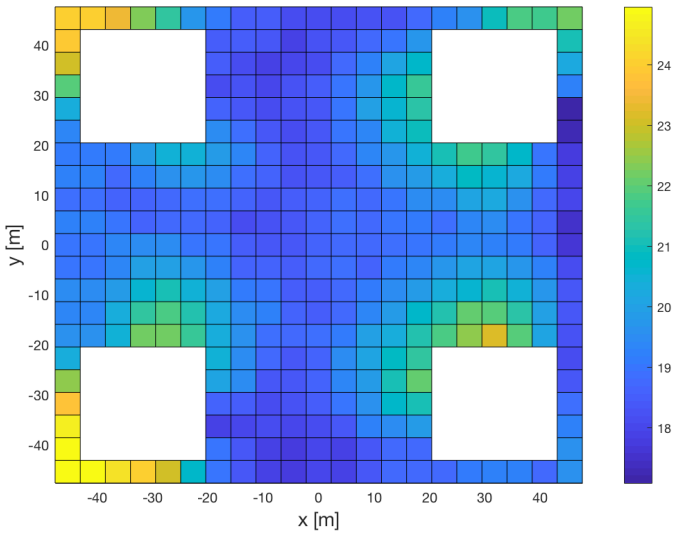

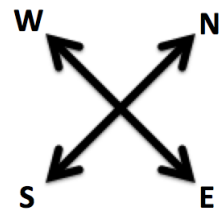

ALS

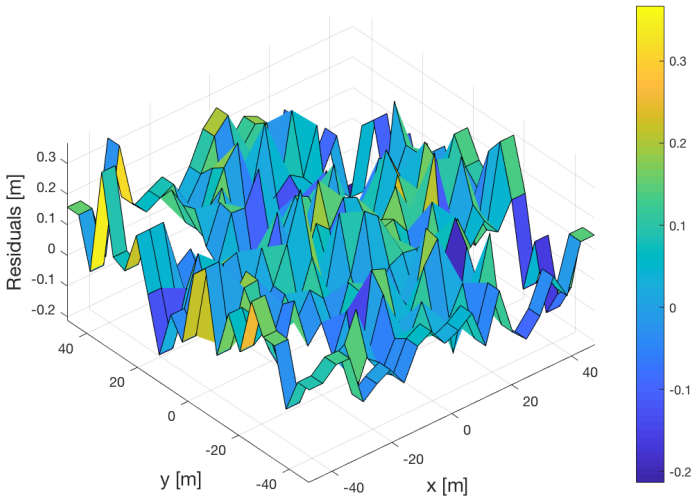

Difference between ULS upwell for the total sea and combined sea. Positive residuals means that the results obtained utilizing the combined sea are larger than the results obtained using only wind sea.

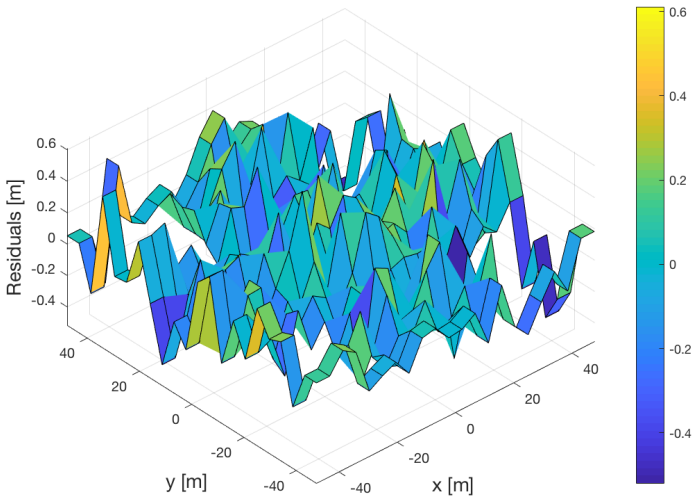

Difference between ALS upwell for the wind sea and combined sea. Positive residuals means that the results obtained utilizing the combined sea are larger than the results obtained using only wind sea.

Appendix D

U_{WF} - MASS

Torsethaugen
$\alpha = 1.2$
$H_s = 8\text{m}$

D.1 Total sea

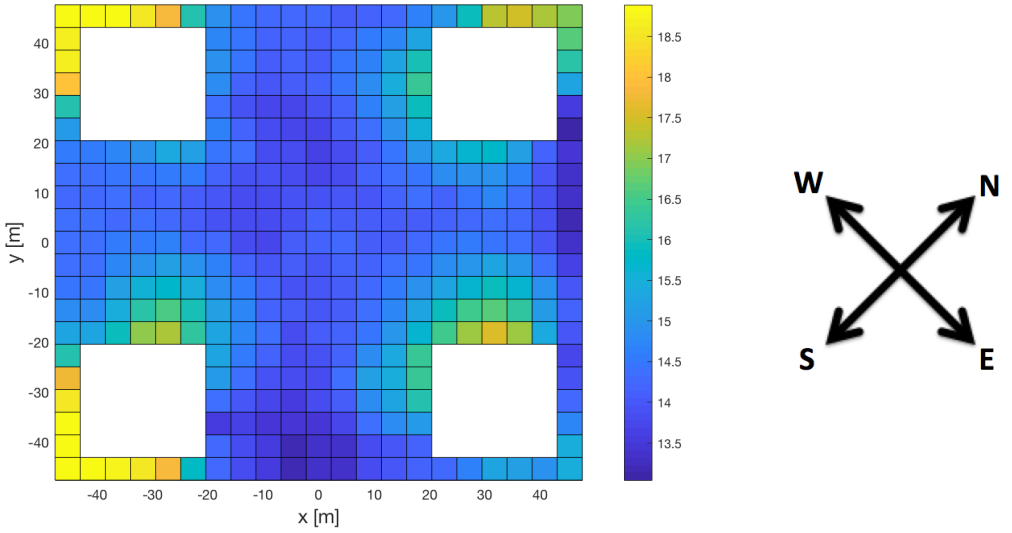

ULS

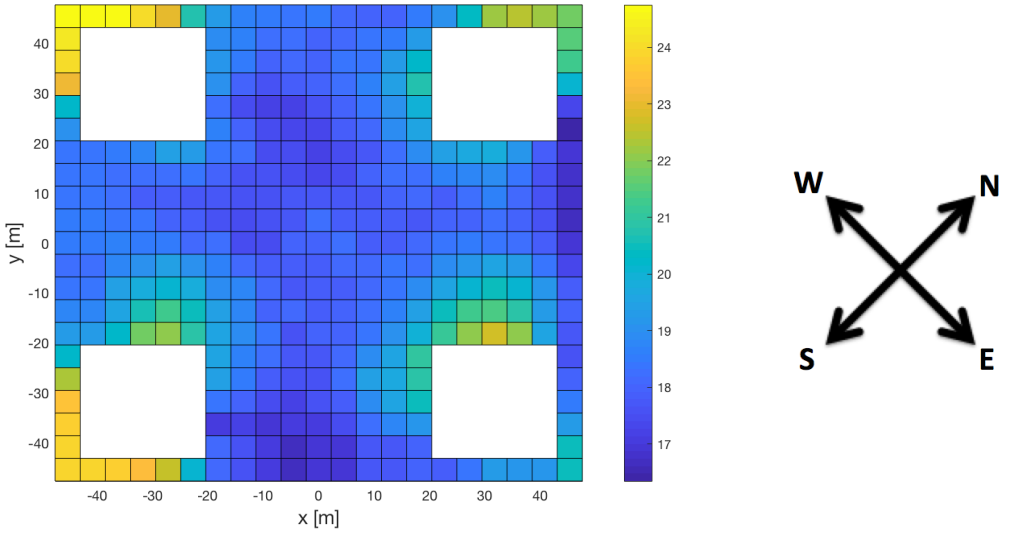

ALS

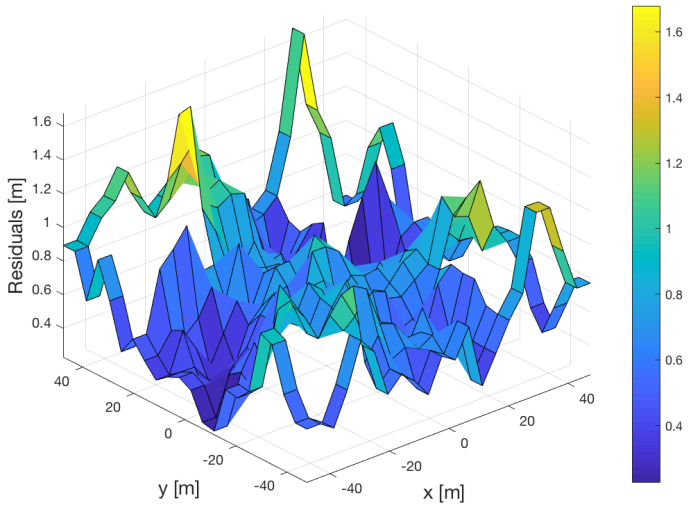

Difference between ULS upwell for total sea using Torsethaugen vs JONSWAP. Positive residuals means that the results obtained utilizing Torsethaugen are larger than the results obtained using JONSWAP.

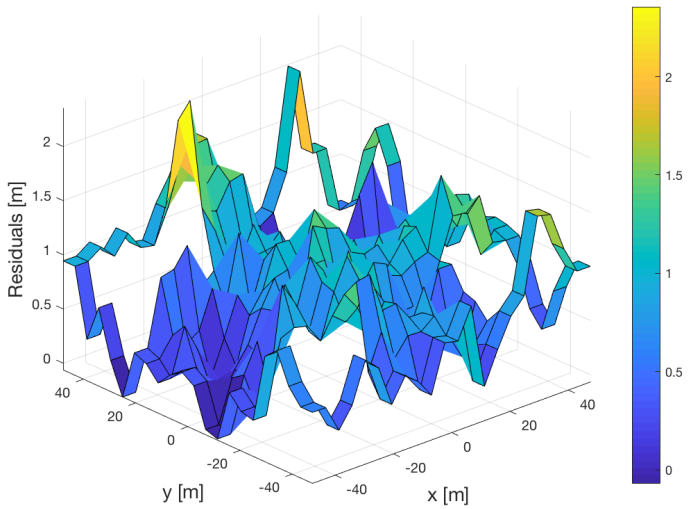

Difference between ALS upwell for total sea using Torsethaugen vs JONSWAP. Positive residuals means that the results obtained utilizing Torsethaugen are larger than the results obtained using JONSWAP.

Appendix E

U_{WF} - MASS

Torsethaugen
$\alpha = 1.3$
$H_s = 8\text{m}$

E.1 Total sea

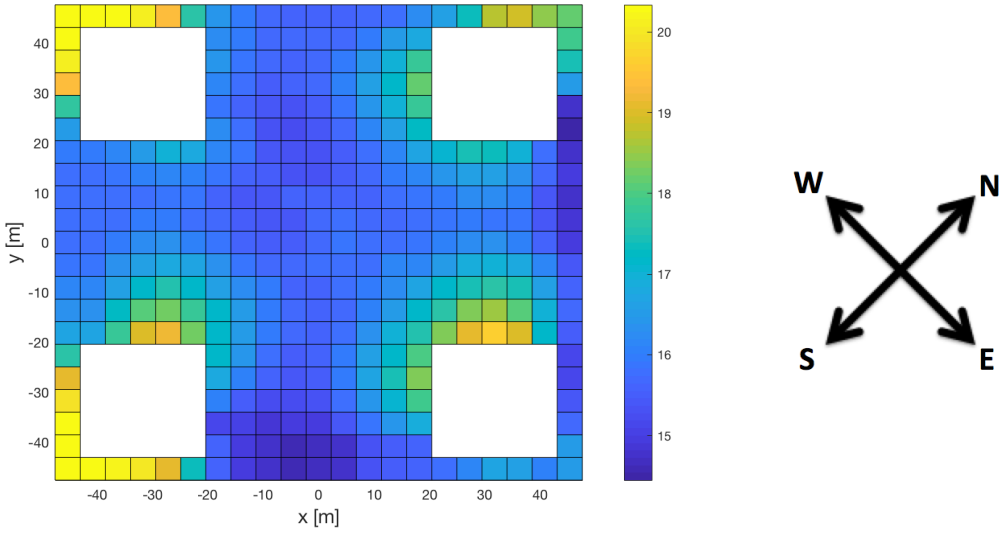

ULS

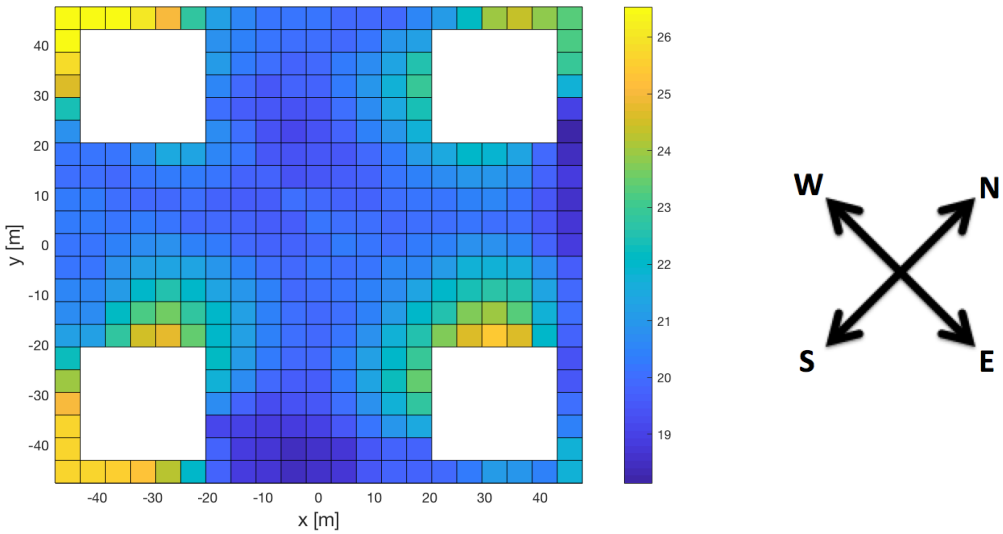

ALS

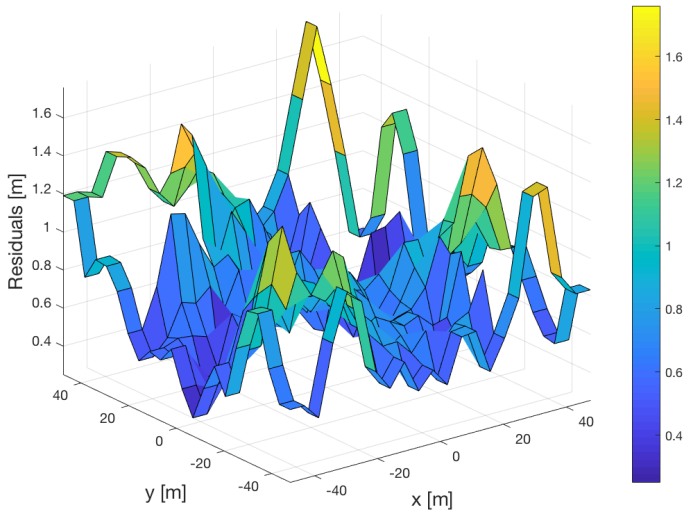

Difference between ULS upwell for total sea using Torsethaugen vs JONSWAP. Positive residuals means that the results obtained utilizing Torsethaugen are larger than the results obtained using JONSWAP.

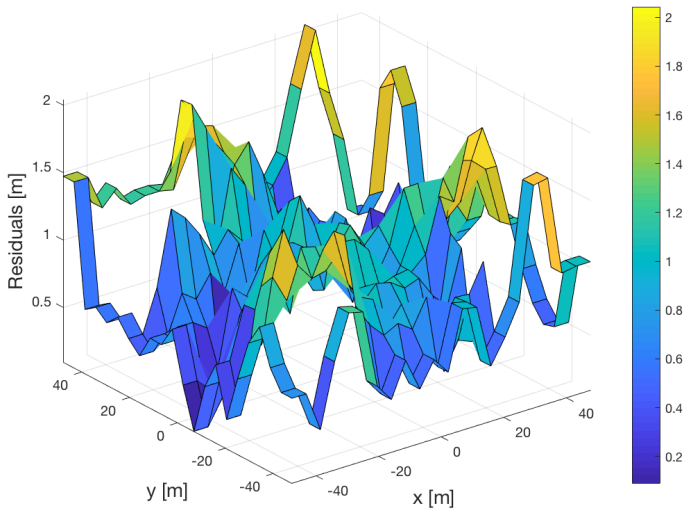

Difference between ALS upwell for total sea using Torsethaugen vs JONSWAP. Positive residuals means that the results obtained utilizing Torsethaugen are larger than the results obtained using JONSWAP.